

Development and Applications of Instrumental Chemical Analysis

David P A Kilgour

A thesis presented for the degree of
Doctor of Philosophy in the
School of Chemistry at the
University of Edinburgh, 2002



“The voice of science is not only muted within its jargon, but it is often solemn as well....To a scientist, “the literature” has come to mean, not great thoughts stretching out in search of the truth, but a tortured text, laboriously phrased to pass the scrutiny of dried-up referees selected by the editors of scientific journals.”

Magnus Pike
“There and Back”
Pan Books Ltd
1978

Acknowledgements

Look Mum, I've finished!

A PhD is a funny beast. I spent nearly 4 years training this one to jump through hoops while it made spirited bids for freedom over the fence. Fortunately, I was not left completely to my own devices and I would like to thank all those other members of the circus who have helped me along the way.

Firstly, I would like to thank my parents for supporting me in the roundabout route that led me here.

I certainly wouldn't have come to this point without the experience offered to me by Professor Colin Graham, Dr Steven Elphick, Dr Ian Main and Dr Bryne Ngwenya; who gave me my first taste of research and the freedom to enjoy it.

Professor Chris Hall has my eternal gratitude for his support and the opportunity provided by the cement project. Without him, this would be a slim volume.

Dr Johannes Barth (SURRC) and John Morrison (Micromass) deserve huge thanks for their assistance in the stable isotope measurements and I will be forever in the debt of Dr Robert Lewis and the Lothian and Border Police Forensic Laboratory for their invaluable help with the cannabis project.

I would like to thank the marvellous professorial triumvirate; Baxter, Harrison and Monaghan, for their advice and support throughout the latter half of my PhD.

I would like to thank those wonderful people as the EMSG for making it fun to come into work. Of course I would also like to thank Savoy and especially Helen for making it just as much fun to leave work!

Finally, I would like to thank the Ringmaster of the EMSG, Dr Pat Langridge-Smith for giving me the motive and the opportunity to commit this crime.

Now, the rest of this page contains a prototype, wafer-thin explosive and a sensitive wireless polygraph. If you attempt to put this thesis down without reading it all the way through, it'll blow your eyebrows off.



Abstract

This thesis reports on two research projects into the applications of instrumental chemical analysis.

The first describes research into elucidating a new and more cost-effective method of measuring the setting rate of cement than time resolved X-ray diffraction detection of cement mineralogy. The solution arrived at was to monitor the composition of the fluid phase by ICP-AES and applied thermodynamic modelling. By using this method, it was possible to detect the Ettringite to Monosulphate phase shift, an important kinetic point in the setting of cement.

The second section describes a project where the aim was to find a method of determining the source region of a group of cannabis resin samples ranging from 20 to 1 year old. The resin was analysed by stable isotope mass spectrometry for its $\delta^2\text{H}$, $\delta^{13}\text{C}$ and $\delta^{15}\text{N}$ isotope ratios, which revealed that in all likelihood, the samples came from a single country. Additionally, the relative abundances of cannabinoids extracted from the resin were analysed by GC-MS and showed that there may have been some change in the biosynthesis pathway of the main psychoactive cannabinoid, tetrahydrocannabinol, in this growth area sometime in the last 4 years.

These projects cover an extremely large analytical range: the first project used spectroscopy to answer a physical/inorganic chemistry question for an engineering application, whereas the second project used mass spectrometry to answer a geographic/biochemical question for forensic scientists. Combined, these projects

have shown some of the breadth of skills that an instrumental analytical chemist must have in the modern world.

As both projects were self-contained, they have been presented as such in this thesis, as individual and independent sections.

Additionally, work on both the projects required bespoke computer software to handle the volume of data produced. There is therefore an additional section on the development of software for chemical analysis.

Contents

Thesis Introduction.	1 - 2
Section 1: A New Method of Measuring the Setting of Cement.	3-88
Section 2:Determining the Origin of Cannabis Resin.	89-208
Section 3: Software.	209-223
Courses Attended.	224

Thesis Introduction

Chemical analysis is a subject that is all too rarely seen as a discipline in its own right. A lack of understanding about the chemistry of the system that is to be investigated, or the appropriate method for analysing that system and its changes, can easily lead a naïve or unwary investigator into difficulties.

This thesis describes two projects where there was a requirement for an investigation into the most pertinent method of extracting useful data from systems that are chemically complicated.

The first project, “A New Method of Measuring the Setting of Cement”, was carried out collaboratively with the Centre for Materials Science and Engineering at the University of Edinburgh. Its aim was to develop an alternative method for measuring the progressive setting of cement after the addition of water, to x-ray diffraction. It had been decided that the most promising direction would be to analyse fluid taken from cement as it set.

Cement is a complex mixture of hydrous silicates, sulphates, oxides and hydroxides, containing a large array of elements. As little was known about the fluid phase in a setting cement, many of these had to be measured simultaneously, and their effects on the changing stabilities of significant minerals modelled, before any sense could be made of the system.

The second project, “Determining the Origin of Cannabis Resin”, was a response to a request from the Lothian and Borders Police Forensic Laboratories. They had asked if it would be possible to group different seizures of cannabis resin back into the original batches that it was imported in.

Again, cannabis resin, or hashish, is a complex mixture, although this time it comprised a wide variety of biochemical compounds. To add to the complexity, the number of samples available for analysis was restricted for legal reasons, and therefore as much information had to be extracted from each sample as possible. Many of the drug compounds in the resin degrade over time.

In order to complete both of these projects, a large number of techniques had to be appraised and refined and novel analytical procedures had to be developed and employed holistically.

In both projects, the complexity and size of the respective data matrices required specialised software to streamline the post-processing stages. Without this facility, it is unlikely that either project would have been successful. As modern analytical techniques allow more information to be extracted from any system, the importance of the ability to handle, understand and visualise the data produced will increase proportionately.



Section 1:

A New Method of Measuring the Setting of Cement.



Table of Contents of Schlumberger Cement Project

Table of Contents of Schlumberger Cement Project	4
Table of Figures	5
Project Introduction	7
1. Introduction	8
1.1 Manufacture of Cement	12
1.2 Cement in Oil Wells	14
1.3 The Setting of Cement	15
2. Fluid Analysis Method	20
2.1 Experimental Method. – Ambient Pressure and Temperature	20
2.2 Fluid Analysis	21
2.3 Emission vs. Absorption	24
2.4 Use of the ICP-AES	26
2.4 Analysis Procedure Standards	31
3. Results	32
4. Discussion of Raw Concentration Results	42
5. Thermodynamic Modelling of the Data	43
6. Modelled Data	46
6.1 Average Supamix Trials	46
6.2 Dykerhoff Trials	50
7. Future Work	52
8. Conclusions	54
Appendix 1	55
Appendix 2 – SCRAM97 PC Interface	62
Example of Input file –	80
Example of Output File -	82
Reference List	87



Table of Figures

Figure 1 - Clockwise from top left. Excavated villa floor from Lepenski Vir. Artist's impression of the settlement during the Neolithic Age. Photograph of the site today. [2].....	8
Figure 2 - Pictures of the interior and exterior of the Pantheon in Rome.	9
Figure 3 - Comparison of Portland stone, as used in St Paul's Cathedral and actual Portland Cement.	11
Figure 4 - Diagram showing principal details of cement manufacture. The Virtual Visit project, developed by Edinburgh University and Heriot-Watt University.©1996 [10].....	13
Figure 5 - Impression of cement grains after the final grinding. Note the larger multi-mineralic grains of clinker and the smaller mono-mineralic grains of gypsum...	13
Figure 6 - Hoover Dam. 3,250,000 cubic yards of cement and aggregate.	19
Figure 7 - Showing the difference between absorption (top) and an emission (bottom) spectra.	24
Figure 8 - Comparison of excited population across a flame and a plasma. Notice the higher excited population towards the edge of the plasma which limits auto-absorption.	26
Figure 9 - Diagrammatic representation of the sample input apparatus on the Thermo-Jarrell Ash ICP-AES.	27
Figure 10 - Main features of an ICP torch.	28
Figure 11 - Diagram displaying optical elements used to analyse emitted light in the Thermo-Jarrell Ash IRIS ICP-AES.	29
Figure 12 - Left - Photograph of optics within new model of Thermo-Jarrell Ash IRIS ICP-AES. Right - An example of an ICP plasma. The RF coil can be clearly seen around the top of the torch.	30
Figure 13 - Graph displaying the Calcium results from this study. Note the oscillation of the concentration on many of the lines. The reasons behind this are to be investigated.	35
Figure 14 - Sulphate concentrations of trials. Trial 3 registers as zero as sulphate was not measured for this trial. Notice that the minima for the oilwell cements is shifted to later time, reflecting slowing of the setting reaction.	36
Figure 15 - Sodium concentrations vs. time. Notice the similarity between these and the potassium concentrations (next figure).	37
Figure 16 - Potassium concentrations vs. time. Notice the similarity between these and the sodium concentrations (prev. figure).	38
Figure 17 - Silicic acid concentrations vs. time. Trials 3, 4 and 5 are not plotted as the standardisation regime was being refined during these analyses.	39
Figure 18 - Aluminium concentrations vs. time.	40
Figure 19 - Sample time, vs. value of calculated pH, ($[K^+] \times 30$), ($[Na^+] \times 150$) and ($[SO_4^{2-}] \times 500$) for the average Supamix trial.	47
Figure 20 - Sample time, vs. value of calculated pH, (monosulphate saturation product $\times 12$) and (gypsum saturation product $\times 12$) for the Average Supamix Trial.	47
Figure 21 - XRD data. Displays 11 XRD traces of the same cement during setting, from early time at the bottom to later time at the top.	50
Figure 22 - Data from the Dykerhoff Trials. Time (minutes) vs. value.	51
Figure 23 - Data from the Dykerhoff Trials. Time (minutes) vs. value.	52
Figure 24 - SCRAM97 PC Interface main window.	65

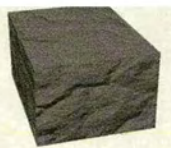
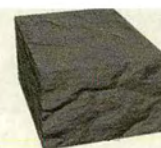


Figure 25 - SCRAM97 PC Interface Fluid Definition window.....67
Figure 26 - SCRAM97 PC Interface Single Fluid Output window69
Figure 27 - SCRAM97 PC Interface dialog box.....70
Figure 28 - SCRAM97 PC Interface Graph Output window.71
Figure 29 - SCRAM97 PC Interface Graph Output window, axes selection listbox...71
Figure 30 - SCRAM97 PC Interface Import Spreadsheet Template.....73
Figure 31 - SCRAM97 PC Interface Import window.74



Project Introduction

This section of the thesis reports on work done in collaboration with the Centre for Materials Science and Engineering, at the University of Edinburgh, on a project sponsored by Schlumberger Cambridge Research.

The aim of the project was to attempt to identify, by means other than X-ray diffraction, significant indicators in the setting of cements, that can be used to determine bulk setting kinetics, to allow work on the development of cement setting retarders.



1. Introduction

Cement, derived from the Latin “caementum”, has been used in one form or another for at least 7600 years. The most ancient example was used to bind the floors of a Neolithic building in Lepenski Vir, in Serbia (see Figure 1) [1].



Figure 1 - Clockwise from top left. Excavated villa floor from Lepenski Vir.

Artist's impression of the settlement during the Neolithic Age. Photograph of the site today. [2]

Lime cement, manufactured by burning (calcining) chalk or limestone, is the simplest example, and was extensively used in construction in the ancient world. It is,



however, not a particularly good binding agent. This property can be improved by the addition of silica and alumina to the cement, e.g. in the form of volcanic soils – pozzolano, santorin soil and trass.

This improvement in cement technology was discovered by the Romans, around the time of Christ. The strength and longevity of Roman cements, of this type, are illustrated by the Pantheon, built by the Emperor Hadrian in Rome around 126 AD, and still in use today. Figure 2 gives an impression of the impressive size of the building (the top of the dome is 44m above the floor and the dome is 56m across).

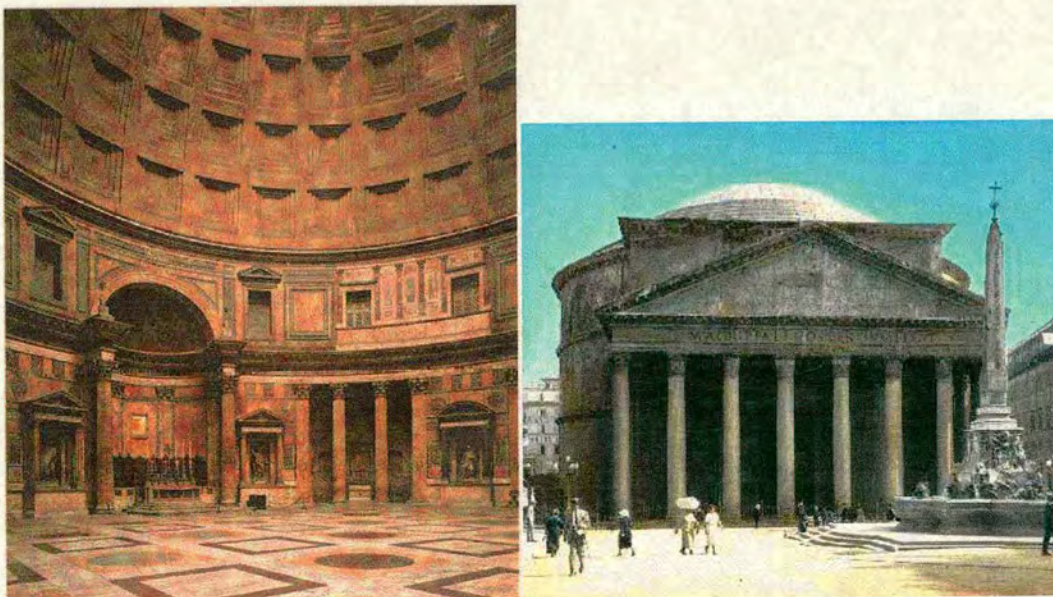


Figure 2 - Pictures of the interior and exterior of the Pantheon in Rome.

Little improvement in cement technology happened between the time of the Romans and the late 18th century, when the incorrectly named “Roman” cement appeared in Britain. This cement, a forerunner of Portland cement, was made by calcining



argillaceous limestone, where the lime, silica and alumina were supplied by the same rock.

Modern Portland cement, developed by Joseph Aspdin, and his son, first appeared in 1824, and was named thus because the end product resembled Portland stone (See Figure 3) [3;4]. Portland stone, mined on the Isle of Portland in Dorset, is a thick bedded Jurassic oolitic limestone, and was the principal stone used for the construction of the City of London after the Great Fire (St Paul's Cathedral, the British Museum etc). The ability to produce a cheap, mouldable facsimile was therefore very profitable.

Aspdin initially made his cement on his kitchen stove, by heating chalk and clay together, and pulverising the result with a mortar and pestle. Once he had been granted a patent on this process, he built his first cement works at Wakefield in Yorkshire, where the calcining process was carried out in beehive shaped kilns. Modern re-analyses of his early cements show that clinkering (the product of calcining) was very incomplete*, but that enough had occurred to make his product better than contemporary competitors' cements. With his son, he built newer and larger works with bigger kilns more capable of reaching the 1250° C required for adequate clinkering.

Later, in the 1870s, the use of blast furnace slag, as an additive to supply the silica and alumina to the cements, appeared in the USA and Continental Europe but did not become common in Britain.

* i.e. only a small proportion of minerals have been calcined.

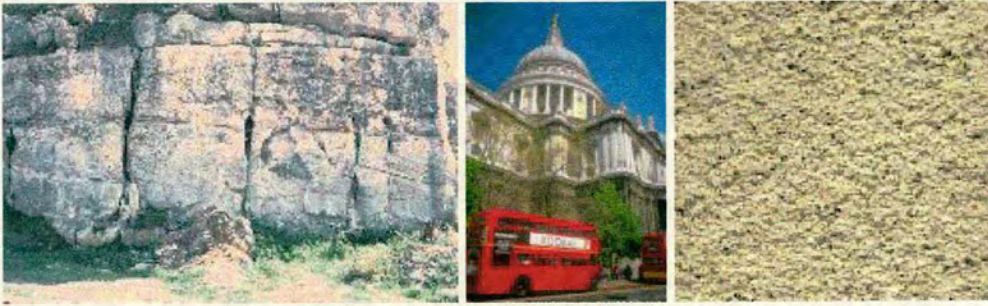


Figure 3 - Comparison of Portland stone, as used in St Paul's Cathedral and actual Portland Cement.

In the 1880s and 1990s, much work was done, in particular by Michaëlis[5], Le Chatelier [6;7] (in fact, it was while Le Chatelier was working on this project that he discovered the theory on equilibrium now known as Le Chatelier's Principle.) and Törnebohm [8] on discovering the mineralogy of Portland cement.

Their work, along with that of others, revealed that Portland cement largely comprised 5 phases [3;9] [4]:

Phase	Mineral Name	Formula	Approx. wt %	Cement Nomenclature
tricalcium silicate	alite	Ca_3SiO_5	50+	C_3S
β -dicalcium silicate	belite	Ca_2SiO_4	10	$\beta\text{-C}_2\text{S}$
tricalcium aluminate	aluminate	$\text{Ca}_3\text{Al}_2\text{O}_6$	5	C_3A
tetracalcium aluminoferrite	ferrite	$\text{Ca}_2\text{AlFeO}_5$	20	C_4AF
calcium sulphate	gypsum	$\text{CaSO}_4 \cdot 2\text{H}_2\text{O}$	5	CSH_2
alkalis		Na_2O equiv.	0.5	

Gypsum is added to slow initial setting, to allow time for working of the cement in practice. i.e. mortaring, moulding etc. [4;9]



1.1 Manufacture of Cement

Modern cement is manufactured from either limestone and shale or chalk and clay [4]. This section describes the process used at Blue Circle Cement Scotland's Dunbar plant, where limestone and shale are used as the raw materials.

The raw materials are both quarried near Dunbar, and are crushed and milled before being transported to the cement works by conveyor belt.

Once in the plant, the limestone and shale are ground to a fine powder in the *raw mill* and sand is added to increase the silica content. The fine powder is separated from the coarse grindings by a gas flow. The coarse grindings fall back into the *raw mill* to be reground, while the gas flow, carrying the fine particles, passes on to the *electrostatic precipitator*, where the particles are recovered. These are then stored in silos before continuing through a preheating and precalcining phase and entering the *kiln*.

The *kiln*, heated by combustion of coal dust to 1450°C, calcines the raw material to produce clinker, which is cooled and mixed with a small amount of gypsum. This final mixture is reground and stored as cement (See Figure 4). Cement, when viewed under the microscope, appears as two sets of intermixed grain types: larger multi-mineralic grains of clinker and much smaller mono-mineralic grains of gypsum (a consequence of the lower mechanical strength of gypsum). (See Figure 5).

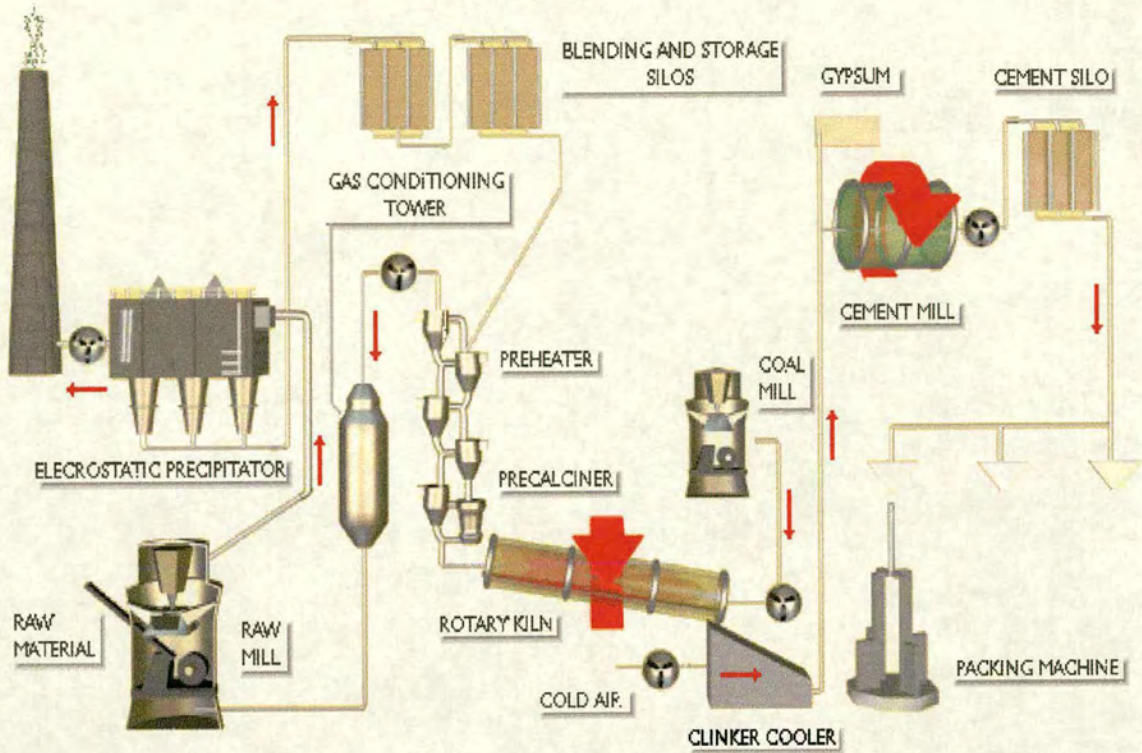


Figure 4 - Diagram showing principal details of cement manufacture. The Virtual Visit project, developed by Edinburgh University and Heriot-Watt University.©1996 [10]

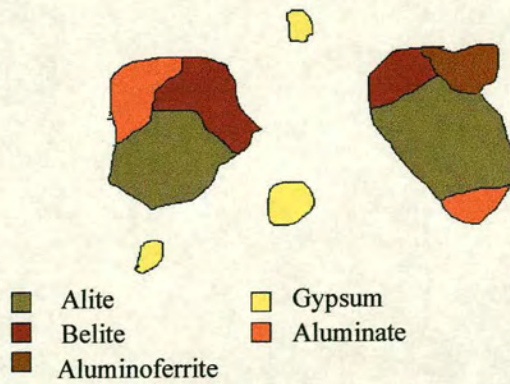


Figure 5 - Impression of cement grains after the final grinding. Note the larger multi-mineralic grains of clinker and the smaller mono-mineralic grains of gypsum.

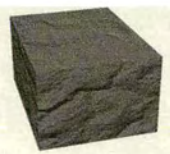


1.2 Cement in Oil Wells

The first recorded use of cement in the oil industry occurred in 1903 in California, when a consignment of cement was “dumped” down a well to stop bore water intrusion [3]. However, the first premeditated use of cement in strengthening a well was by A.A Perkins, of the Perkins Cementing Company, again in California, in 1910 [3]. Ordinary Portland cements were used in both these cases. However, as oil and gas wells have grown deeper, special cements have had to be developed, where the setting of the slurry is delayed to allow for the pumping time required to get the cement into position, several kilometres underground.

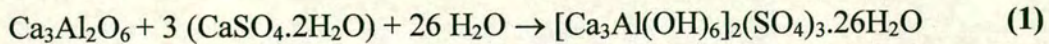
These oil well cements are manufactured by a relatively small number of companies around the world to produce high batch to batch consistency, and their factories are not necessarily conveniently placed for the oil industry. This, obviously, raises the cost of drilling, as this special cement must be transported significant distances to the drilling site in large quantities. It would, therefore, be of use to the industry if, by better understanding of the process by which ordinary Portland cement (OPC) sets, it could design additives which would control the rates and perhaps the manner of setting.

The purpose of this project was to analyse fluids withdrawn from setting cements under ambient conditions, to allow study of the conditions and timings of hydration and correlation of these with known events in the solid phase evolution detected by synchrotron X-ray diffraction (XRD) analysis; further, to use these results to better understand the method of setting, and the effect and design of different additives.



1.3 The Setting of Cement

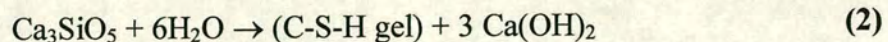
The most reactive phase in Portland cement is tricalcium aluminate or C_3A ($Ca_3Al_2O_6$). The first reaction after cement is mixed with water is:



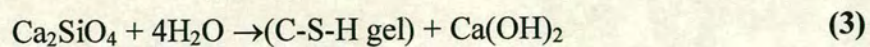
Here, C_3A reacts with gypsum to form ettringite. Ettringite forms in an impermeable gel like phase on the surface of the cement grains, protecting them from further hydration, thus slowing the hydration rate.

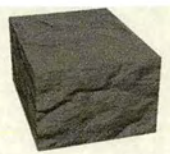
Other major hydration reactions which, occur during this process, are as follows:

Hydration of Alite

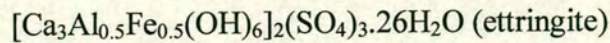
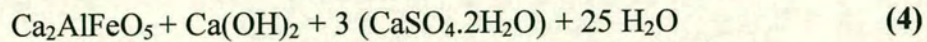


Hydration of Belite





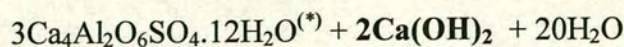
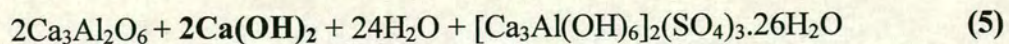
Hydration of Ferrite



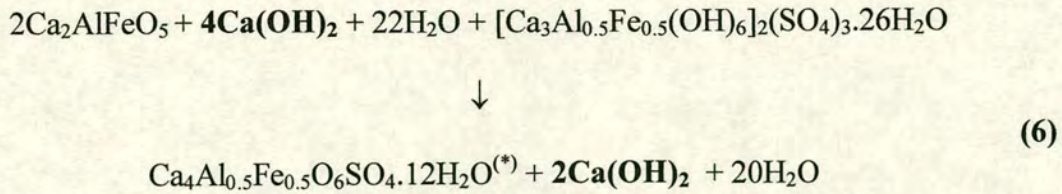
The (C-S-H gel) product from reactions (2) and (3) above has an approximate formula of $3\text{Ca}_2\text{SiO}_7 \cdot 3\text{H}_2\text{O}$, but it is strongly non-stoichiometric. It forms the major component of set cement. [9]

It should be noted that ettringite exists as a complete solid solution series from the pure aluminium end member to the pure Fe (III) end member [11]: i.e. the equations above (1 and 4) are idealised. In reality, observed ettringite is a continuous mixture of that produced by both sources.

Once the available gypsum has been used up, aluminate and ferrite change reaction paths, reacting with the ettringite, they created before, and dissolved calcium hydroxide (**portlandite**):



and



(*) monosulphate series members

Note that in (5), the pH is not buffered as the portlandite reactant and product stoichiometries balance, whereas in (6), 2 moles of portlandite are consumed.

As none of the ettringite in real cement systems is the pure aluminium end member, in all real cases, this reaction would have a pH buffering effect, which would increase with iron content; the beginning of this process should coincide with the loss of gypsum and the detection of monosulphate by XRD.

Once all ettringite is transformed to monosulphate, the pH buffering from this reaction is lost, and the pH will begin to rise again as the hydration of alite and belite (reactions (2) and (3)) continues [9]. As the hydration fronts move into the clinker grains, the gel products swell and begin to grow together, and the cement begins to set. A great deal of water is consumed in this step, raising the pH still more, until the system becomes saturated in portlandite ($\text{Ca}(\text{OH})_2$). The precipitation of portlandite then buffers the pH at a new, higher level. These, “massive”, portlandite crystals form in the remaining interstitial spaces.



At this time, under normal water to cement ratios, the amount of free water in the system becomes so low the system is practically impermeable, and the conventional ideas of bulk dissolution, leading to saturation and precipitation of crystals, no longer holds. There are no free water paths for ions to migrate away from dissolution sites to “distant” crystallisation fronts.

By this point, as the cement has now become so viscous as to render it extremely difficult to pump, it is often considered as set. The remaining, unhydrated, clinker grains are slowly consumed, but the reaction is kinetically hindered because the products are no longer being removed from the aqueous system by crystallisation. The nucleation of crystals has to overcome an energy barrier, after which crystal growth continues easily. This process tends to favour the formation of a small number of large crystals. In this case, however, this is not possible, as the system is not locally connected to other parts. Therefore it must attempt to form a large number of small crystals, demanding a large number of nucleation sites, each of which requires an energy input to pass the energy barrier. There is no excess of energy available to overcome this barrier, so the rate of reaction is low. This is why although the Hoover Dam (See Figure 6) has been completed in 1935, the concrete within will not set completely for some considerable time to come.

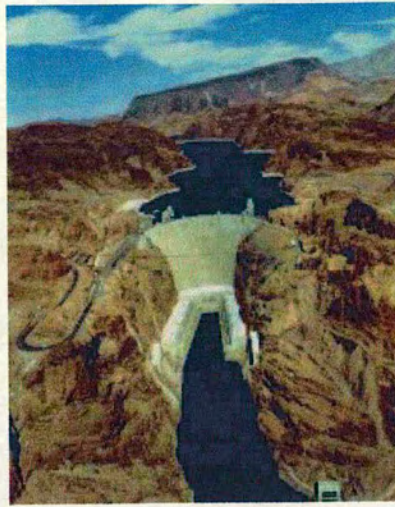
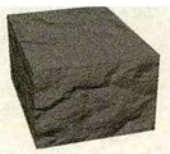
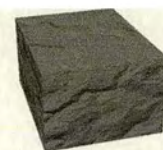


Figure 6 - Hoover Dam. 3,250,000 cubic yards of cement and aggregate.



2. Fluid Analysis Method

2.1 Experimental Method. – Ambient Pressure and Temperature

Batches of cement (see recipe below) were mixed in a laboratory blender for 35 seconds, before being transferred to a 1L polypropylene beaker. Samples (1.5mL – 5mL) were removed from the bulk, and the fluid extracted from these samples by vacuum filtration. This fluid was then transferred to a polypropylene sample vial and acidified with hydrochloric acid. Each vial was weighed empty, with the sample and with the sample plus the acid, with the volumes being calculated by difference.

Two types of cement were used in the trials. In the early stages, “Supamix” cement, an ordinary Portland cement with no additives, was used to refine the technique, and to monitor the repeatability. Later, two oil-well cements, one from Rugby, and one from Dykerhoff, were used to compare the ordinary Portland cement (OPC) results with those of genuine oil-well cements.

All trials were carried out under the conditions shown in the following table (1):

Table 1 - Recipe for cement used in fluid analysis trials.

Water to cement ratio (w/c) – 0.4	Temp – room temp.	Mixing – 30 secs, low speed in lab blender
Cement – 240g	Water – 600g	



2.2 Fluid Analysis

Fluid analysis was carried out on a Thermo-Jarrell Ash IRIS inductively coupled plasma atomic emission spectrometer (ICP-AES).

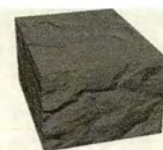
ICP-AES was chosen as the analysis method as it has many advantages over other techniques, most prominently Flame Atomic Absorption Spectroscopy (FAAS).

Both techniques distinguish elements by their differing internal electronic structures. Atoms and molecules can absorb energy by raising electrons from a ground state to a higher energy orbital. This excited state will exist for a certain lifetime after which it will decay back to a lower level, emitting a photon; the energy difference E between the levels is inversely proportional to the wavelength λ of the emitted photon:

$$E = hc/\lambda \quad (7)$$

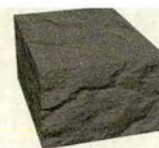
where h is Planck's constant and c is the speed of light. As the species in these techniques are either atoms or monatomic ions, there is no non-radiative decay pathway open to them, and therefore emission is always quantised, and photons are always emitted.

This is not the case for the absorption phase. There are two pathways available for exciting the molecule. First, there is the reverse of the emission process, where a photon is absorbed, raising an electron to an excited level. This is a quantised process, and only photons with energies that match orbital energy differences in the



target molecule will be absorbed. The other route is a non-quantised route where thermal energy is absorbed by the molecule in the form of collisions. This raises the energy of the atomic molecule to close to the ionisation energy in the very high Rydberg levels, or indeed over the ionisation threshold. For the molecules left in the high Rydberg states, these levels have short lifetimes ($\sim 10^{-10}$ seconds), and quickly emit high energy photons (even up to X-ray energies) to drop to lower, more stable excited levels. The differing stabilities of these levels are the basis for their differing populations. More stable, i.e. longer lived, species are more numerous and hence when these levels subsequently decay to lower or ground states, they produce a larger intensity of corresponding emitted photons than shorter lived, less stable species. This is why some emission lines are more intense than others in AES.

In FAAS, a beam of light is split into a reference beam that passes directly to a detector and another beam that passes through a flame containing the elements to be detected. In order that the beams contain photons of the correct energy to excite levels in the desired element, a hollow cathode lamp of that element is used as the source (i.e. a sodium lamp would be used in a sodium analysis). A monochromator is used to isolate the wavelength of interest after the beam has passed through the flame, and before it reaches the detector.



Like all absorbance techniques, the relative intensity of the analysing beam is proportional to the concentration as described by the Beer-Lambert law:

$$A = \epsilon bc \quad (8)$$

where A is the absorbance, ϵ is the molar absorptivity constant for the element in question, b is the beam's path length through the sample and c is the concentration of the sample. The absorbance, A , is calculated from the relative intensities of the reference and analysing beams:

$$T = I / I_0 \quad (9)$$

$$A = \log_{10} I / T \quad (10)$$

where T , the transmittance, is the ratio of the intensity of the analysing beam (I) to the reference beam (I_0) while the absorbance, A , is the logarithm, to the base 10, of the reciprocal of the transmittance.

In AES, however, the light emitted from the excited elements is collected and analysed by frequency using either a scannable monochromator and a detector, or a fixed monochromator and a detector array. An emission spectrum is the opposite of an absorption spectrum (See Figure 7).

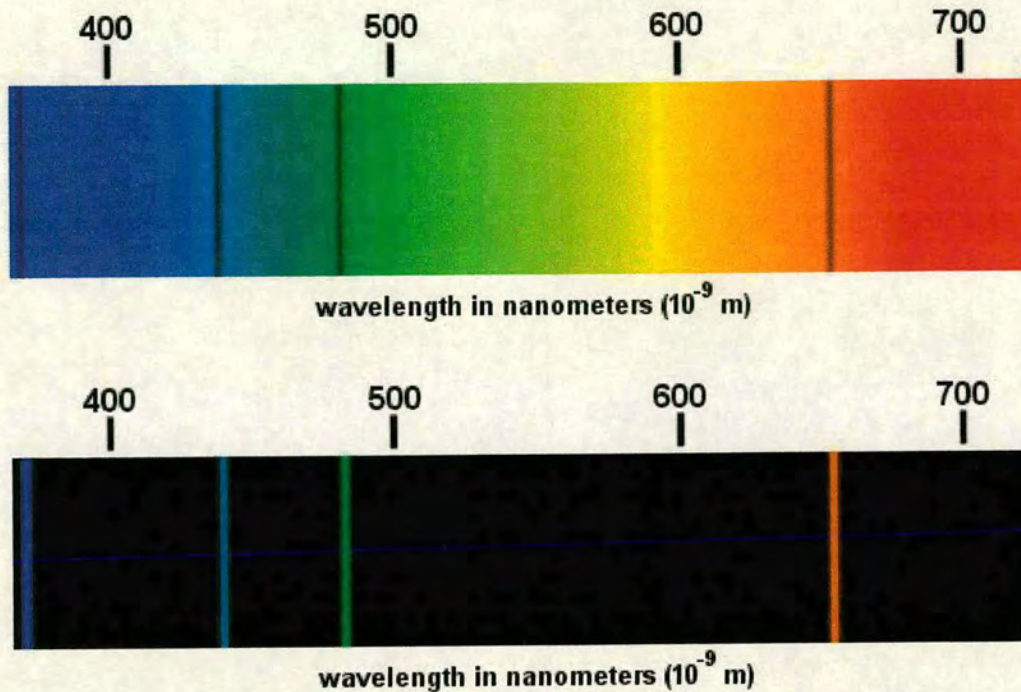


Figure 7 - Showing the difference between absorption (top) and an emission (bottom) spectra.

2.3 Emission vs. Absorption

The decision to detect absorbed or detected light from an atomised source (either a flame or a plasma) depends on the relative excited populations of elements, which are a function of the temperature of the source. At relatively low temperatures (e.g. in a flame, around 2000K) the ratio of excited to unexcited atoms is of the order of 1/10000, whereas in a plasma, at a temperature of 6000K, this would be around 1/10; 3 orders of magnitude larger.

In a flame, there are many unexcited atoms available, which could be excited by absorption of a photon, whereas there are relatively few excited atoms which could be



detected by emission. The opposite is true at the higher temperatures in a plasma; many excited atoms available to detect by emission, but only relatively few unexcited atoms available to detect by absorption. Therefore absorption spectroscopy is generally used for flame sources (flame emission spectroscopy does exist, but is unusual). Plasma sources produce so many excited atoms that emission spectroscopy is the only analysis technique used.

There is one other factor to be aware of - the “optical thickness” of the source. Flame emission spectrometry does exist, despite the lower number of excited atoms in the analysed region. However, flames are hotter in the centre than at the edge, which means that there are more excited (i.e. potentially emitting) atoms in the centre of the flame than in the outer regions, where there are more potentially absorbing atoms. This can lead to the complication of self-absorption where photons emitted in the centre of the flame are absorbed by unexcited atoms in the outer regions and are therefore not detected. This feature makes flames optically “thick” and induces curvature in calibration data.

The temperature gradient is reversed across plasmas, where the outer regions are the hottest, hindering self-absorption. (See Figure 8) Plasmas are therefore termed optically “thin”. This results in the calibration curves for plasmas being linear over several orders of magnitude which gives the technique a very large working range.

The signal to noise ratio of detected emission should be lower than that of detected absorption as the former relates to a small change in a small value whereas the latter



relates to a small change in a large value. Therefore, for low concentration samples, emission spectra will be more accurately quantifiable.

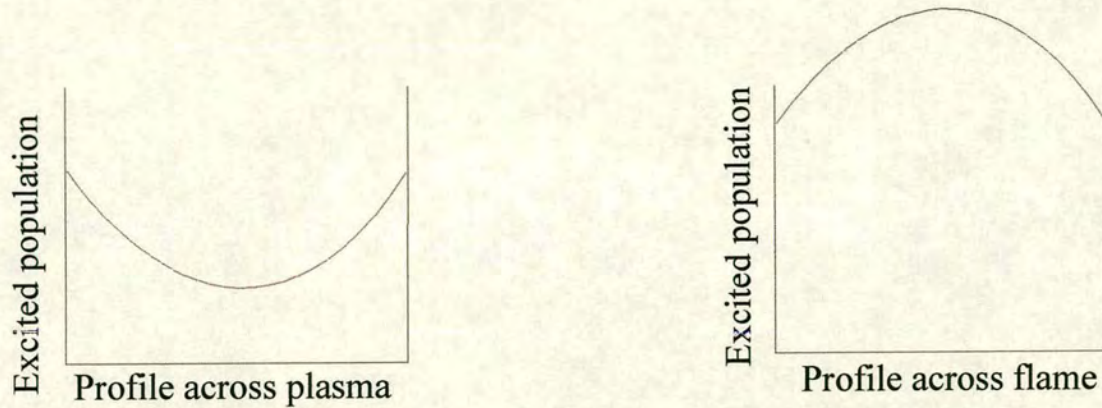


Figure 8 - Comparison of excited population across a flame and a plasma. Notice the higher excited population towards the edge of the plasma which limits auto-absorption.

Sample signals produced by inductively coupled plasmas are more stable than those from flames, reflecting the greater physical stability of the plasma under constant radio frequency induction conditions.

2.4 Use of the ICP-AES

Samples are supplied to the ICP torch via a sipper-probe, a peristaltic pump and a nebuliser (see Figure 9). Argon is used as the nebuliser carrier gas, the plasma gas and the coolant gas. Baffles set in the nebuliser barrel keep large droplets out of the analysed aerosol as these would distort the final result.



The torch is made from three co-axial tubes of special quartz, to withstand the high temperature of the 10,000K plasma. The central tube carries the sample aerosol; the second tube carries the plasma gas (argon) and the outer tube carries a helical flow of argon to keep the plasma away from the torch walls and the stabilise the “flame” (See Figure 10 and Figure 11).

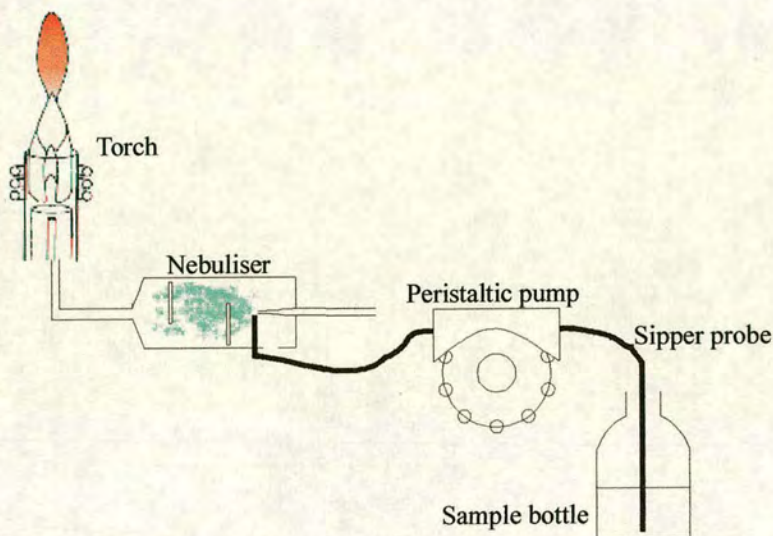


Figure 9 - Diagrammatic representation of the sample input apparatus on the Thermo-Jarrell Ash ICP-AES.

The plasma is initiated with a spark, and driven by a radio frequency field generated by a water cooled, three loop, coil around the top of the torch (See Figure 12, right.).

Thermal kinetic energy in the plasma is converted through the plasma gas to very high level electronic excitement in the sample molecules. These excited states have very short lifetimes ($\sim 10^{-10}$ seconds) and decay to lower excited states by emitting high energy, ultra violet, photons. The lower energy excited states subsequently decay again, emitting characteristic lower energy photons.

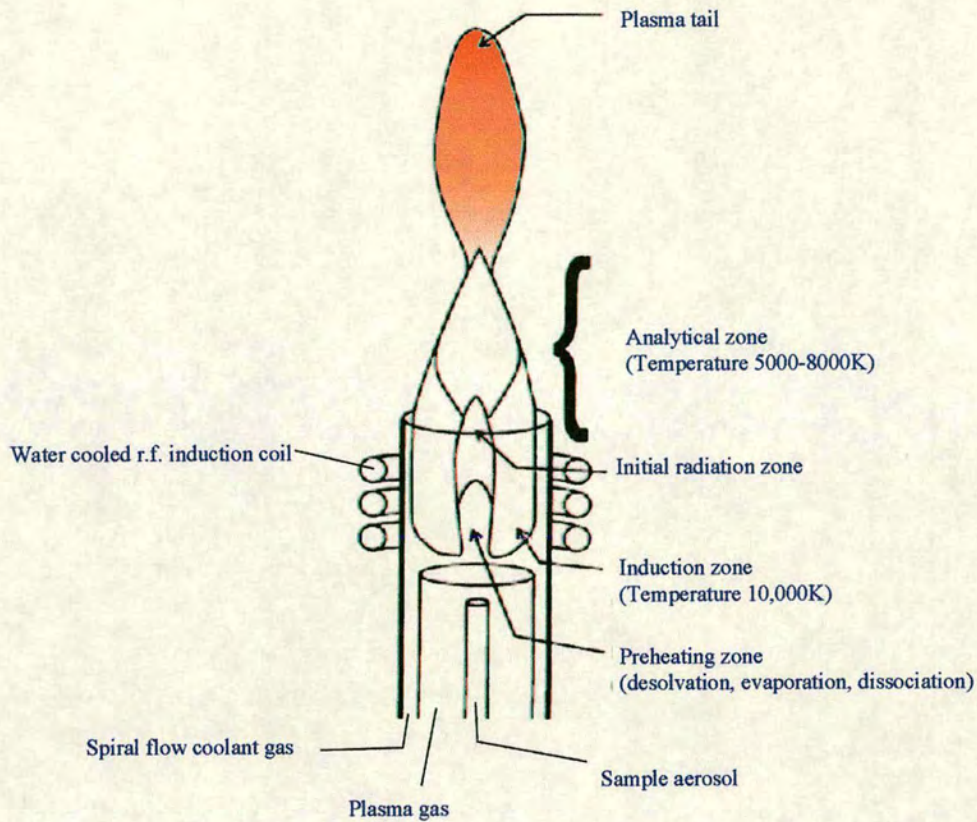
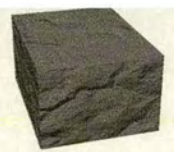


Figure 10 - Main features of an ICP torch.

Light emitted by elements in the plasma enters the optical analyser via a slit and a shutter. The different wavelengths are separated twice; first by a prism, and secondly by an Echelle grating. The subsequent spectrum is detected in a charge induced device (CID) array (512x512 pixels), where the wavelengths are identified by their position on the array. (See Figure 11 and Figure 12).

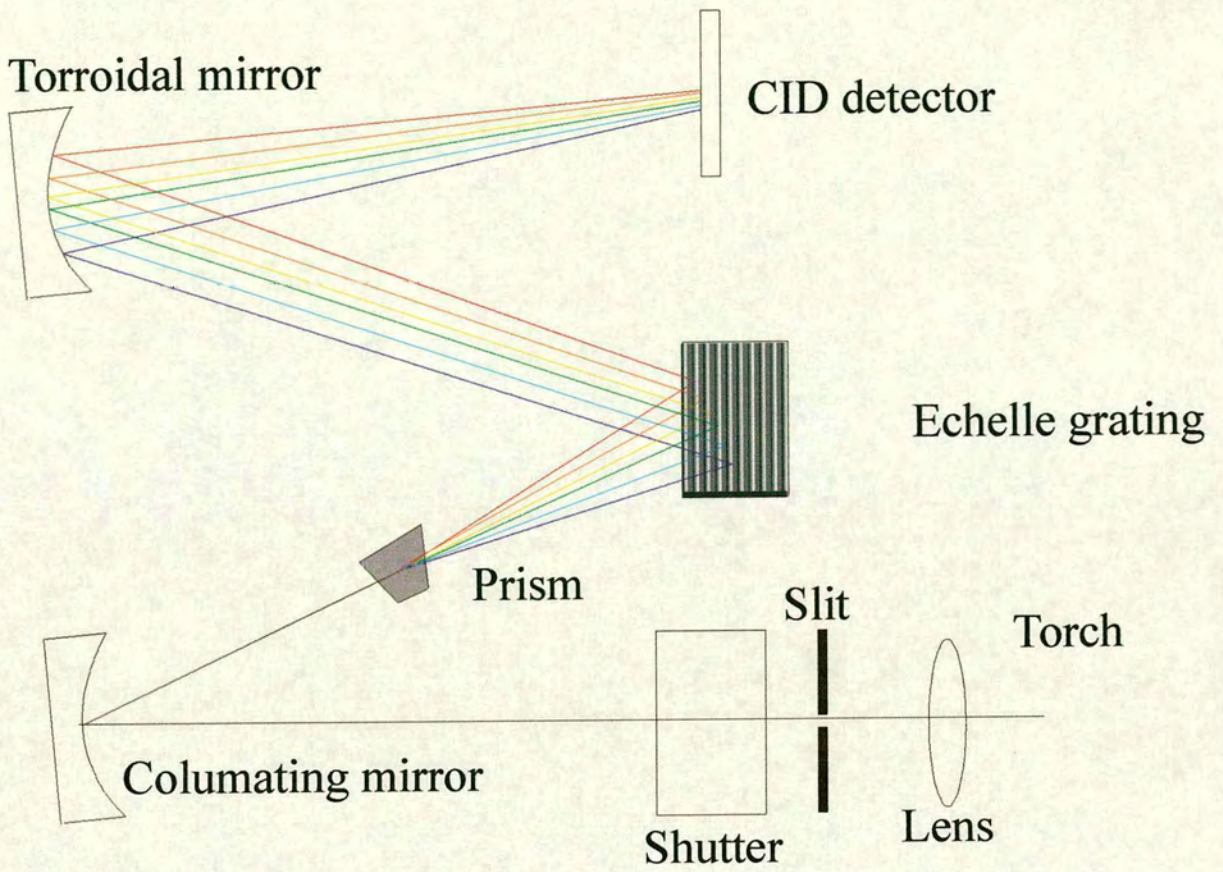


Figure 11 - Diagram displaying optical elements used to analyse emitted light in the Thermo-Jarrell Ash IRIS ICP-AES.

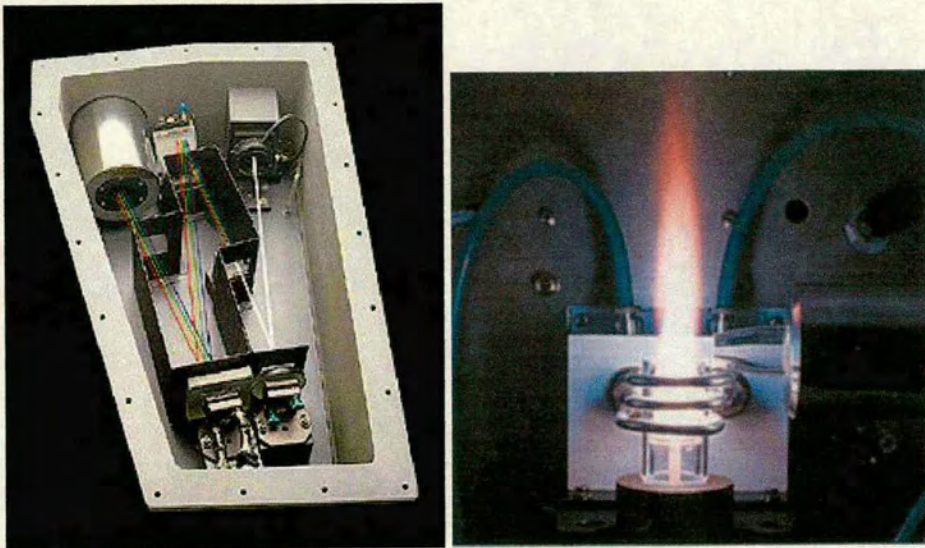
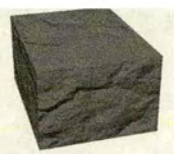


Figure 12 – Left - Photograph of optics within new model of Thermo-Jarrell Ash IRIS ICP-AES. Right – An example of an ICP plasma. The RF coil can be clearly seen around the top of the torch.

The intensities of the various element peaks are calibrated against 3 point calibration curves recorded at the beginning of the session. Four spectra are recorded, calibrated and averaged for each sample.



2.4 Analysis Procedure Standards

Seven elements were analysed: Ca, Na, K, Al, Si, Fe, S. The instrument was standardised for these elements with the following standard solutions:

Standard	Element Conc. (ppm)						
	Ca	Na	K	Al	Si	Fe	S
6 High	100	100	100	1.0	1.0	1.0	0
6 Med	50	50	50	0.5	0.5	0.5	0
6 Low	10	10	10	0.1	0.1	0.1	0
High SO4	0	215.100	0	0	0	0	150
Med SO4	0	143.399	0	0	0	0	100
Low SO4	0	71.6999	0	0	0	0	150

With the exception of the sodium sulphate standard solution, all solutions were made up from 1000ppm ICP specific, standard solutions, purchased from Fluka Chemika, a member of the Sigma-Aldrich group. No sulphur standard specifically designed for ICP-AES was available, so a sodium sulphate FAAS standard solution was used instead.

Element	Solution of	Conc.	Catalogue number
Ca	Ca(NO ₃) ₂	1000ppm	17062
Na	NaNO ₃	1000ppm	17038



Element	Solution of	Conc.	Catalogue number
K	KNO ₃	1000ppm	17072
Al	Al(NO ₃) ₃	1000ppm	17042
Si	Si, HNO ₃ (~1 M) and 2% HF	1000ppm	85351
Fe	Fe and HNO ₃	1000ppm	17066
S	Na ₂ SO ₄	0.5M	71968

Advantages:

- i) Multiple elements can be analysed simultaneously
- ii) Very large dynamic range - Four or more orders of magnitude quasi-linear
- iii) Sub ppm to ppb detection level of trace components

3. Results

The results, reported below, acquired during this study, are split into two groups:

- i) Supamix trials – experiments on Supamix ordinary portlandite cement.
- ii) Oilwell cement trials – experiments on oilwell cements.

The experimental conditions of the reported experiments are tabulated below:

**Table 2 - Table of experimental details for cement trials.**

Trial No	Cement	Type	W/C	Temp	Duration (Min)	No. of Samples
3	Supamix	OPC	0.4	Room	150	6
4	Supamix	OPC	0.4	Room	240	6
5	Supamix	OPC	0.4	Room	240	6
7	Supamix	OPC	0.4	Room	240	6
17	Supamix	OPC	12	Room	244	6
8	Dykerhoff	Oilwell	0.4	Room	360	6
14	Dykerhoff	Oilwell	0.4	Room	360	6
16	Rugby Class G	Oilwell	0.4	Room	360	6

Notes on Table 2:

- i) W/C is the water to cement ratio, by weight. 0.4 is a “normal” ratio.
- ii) In Trial 3, the first analysed trial, not all elements were successfully analysed.
- iii) Trial 17 was carried out at W/C 12 to test whether a significantly higher W/C ratio affected setting.
- iv) Dykerhoff cement, manufactured in Germany, is a genuine oilwell cement, used, and supplied to us, by Schlumberger.
- v) Rugby Class G is another oilwell cement, manufactured in the UK and used in the North Sea oilfield.

In addition to this project, there have been two similar studies carried out on this problem [12;13] , although neither of these projects had the same scope (either in the range of elements analysed for, or in the correlation of solution data with XRD



results). A comparison of the results this project to the previous projects is given in Appendix 1.

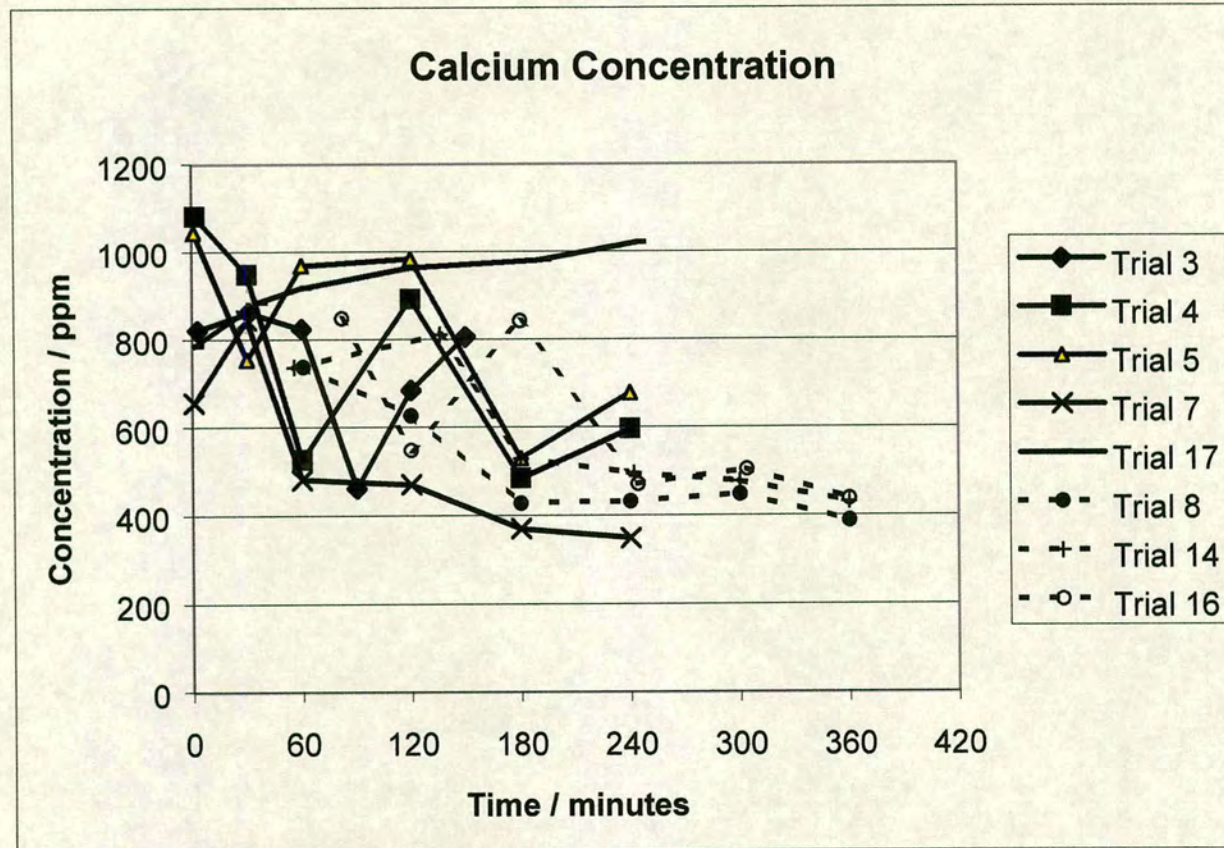


Figure 13 - Graph displaying the Calcium results from this study. Note the oscillation of the concentration on many of the lines. The reasons behind this are to be investigated.

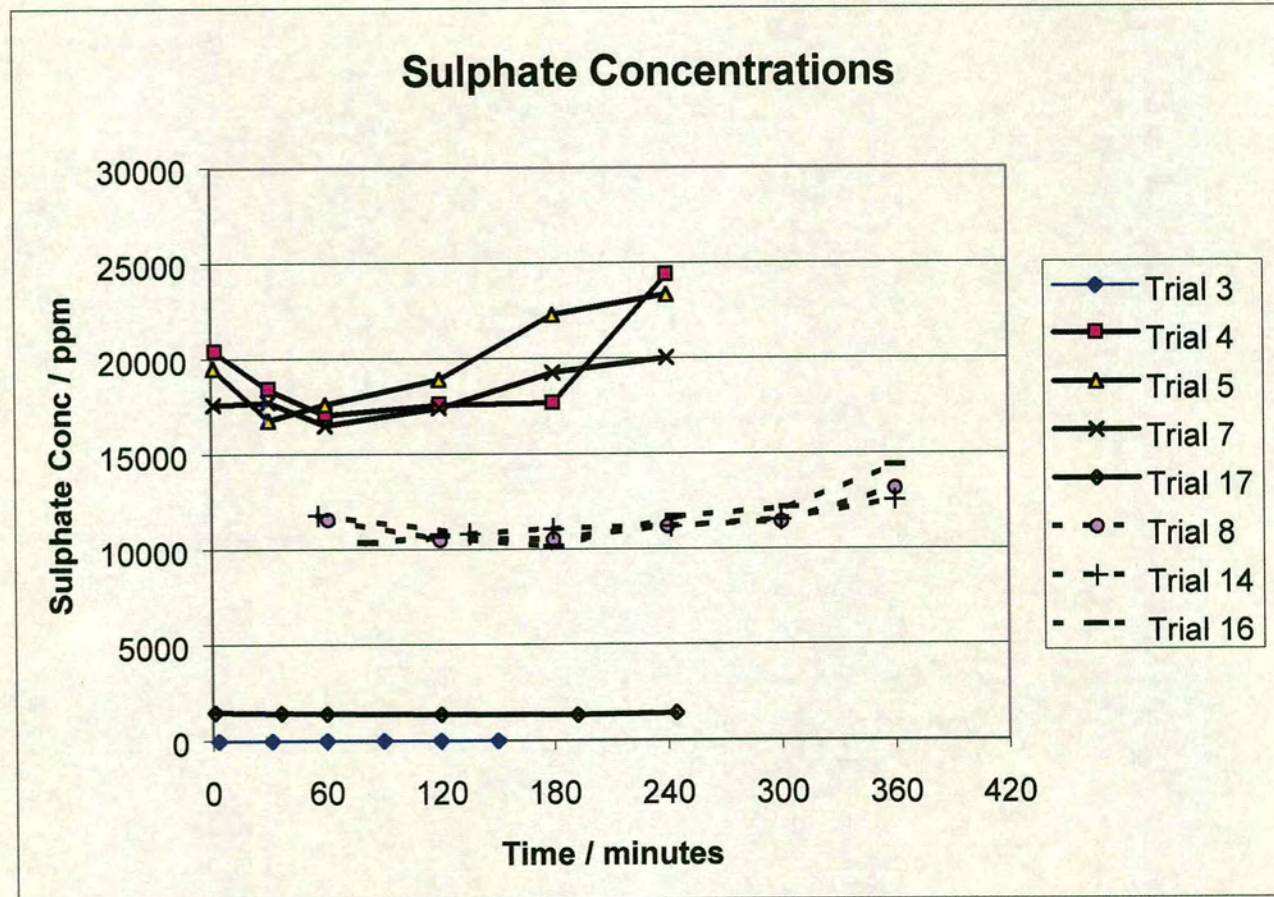
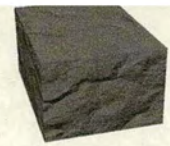


Figure 14 - Sulphate concentrations of trials. Trial 3 registers as zero as sulphate was not measured for this trial. Notice that the minima for the oilwell cements is shifted to later time, reflecting slowing of the setting reaction.

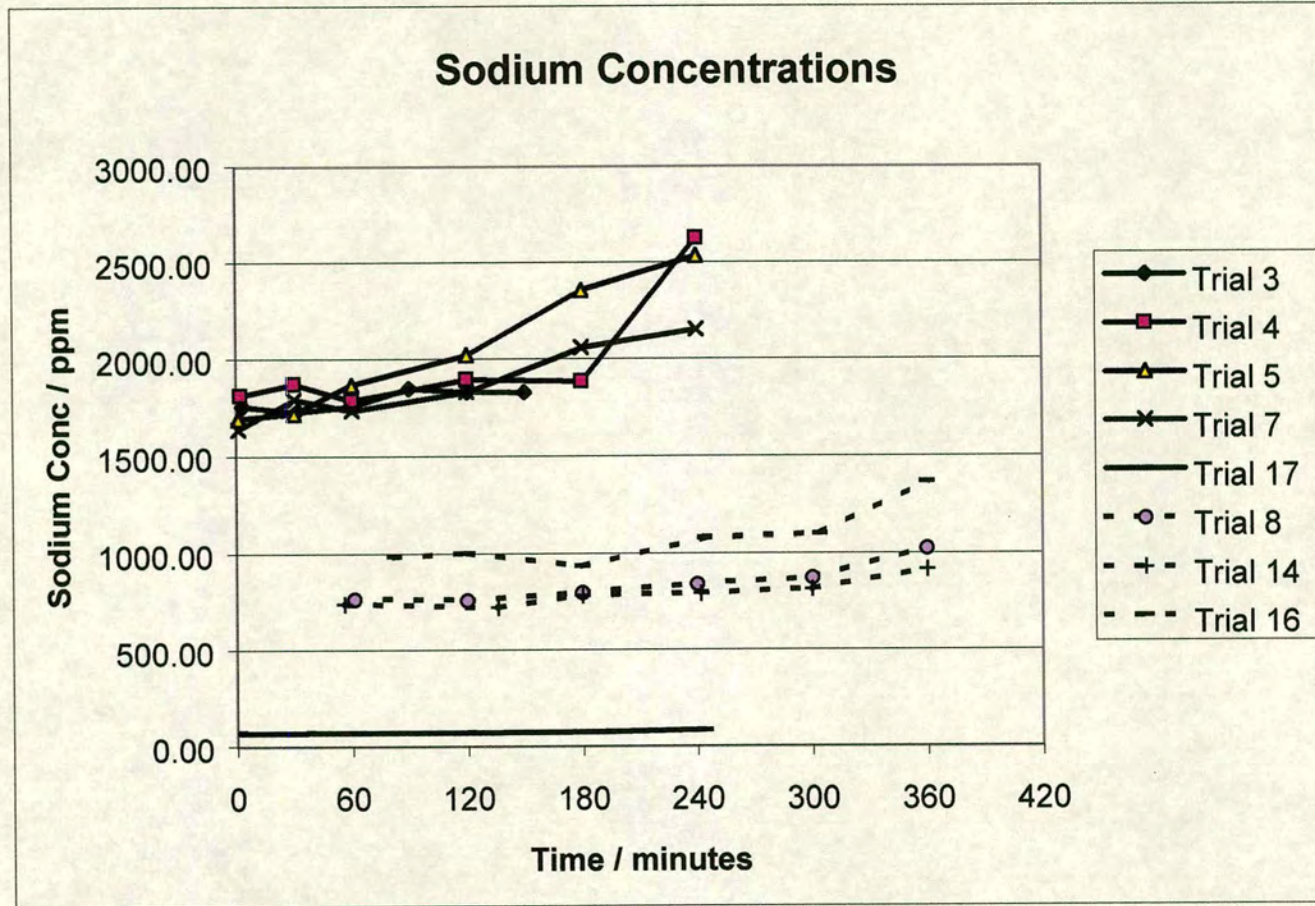
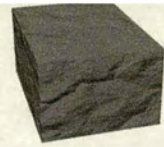


Figure 15 - Sodium concentrations vs. time. Notice the similarity between these and the potassium concentrations (next figure).

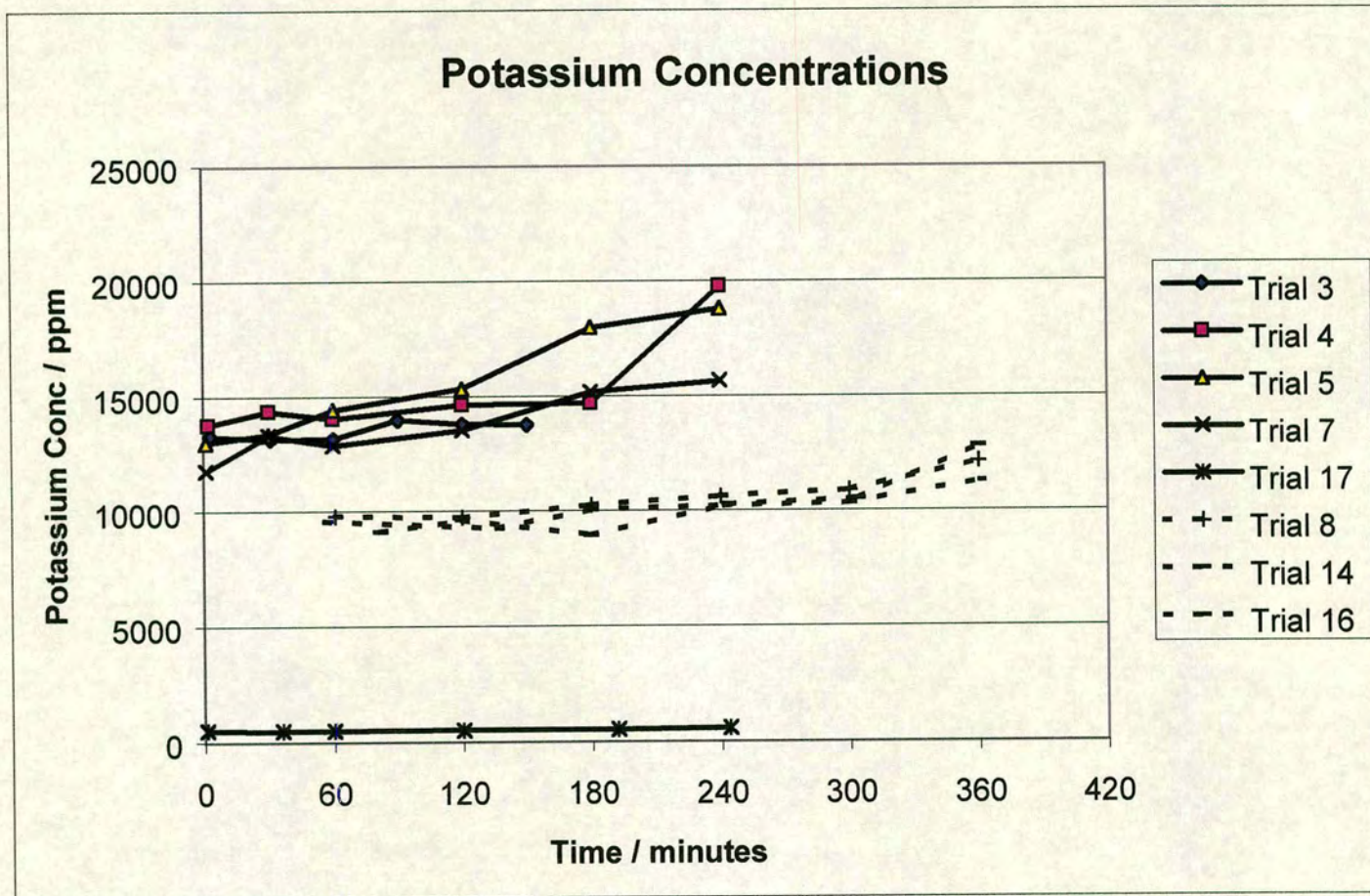
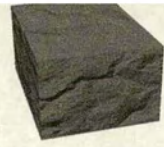


Figure 16 - Potassium concentrations vs. time. Notice the similarity between these and the sodium concentrations (prev. figure).

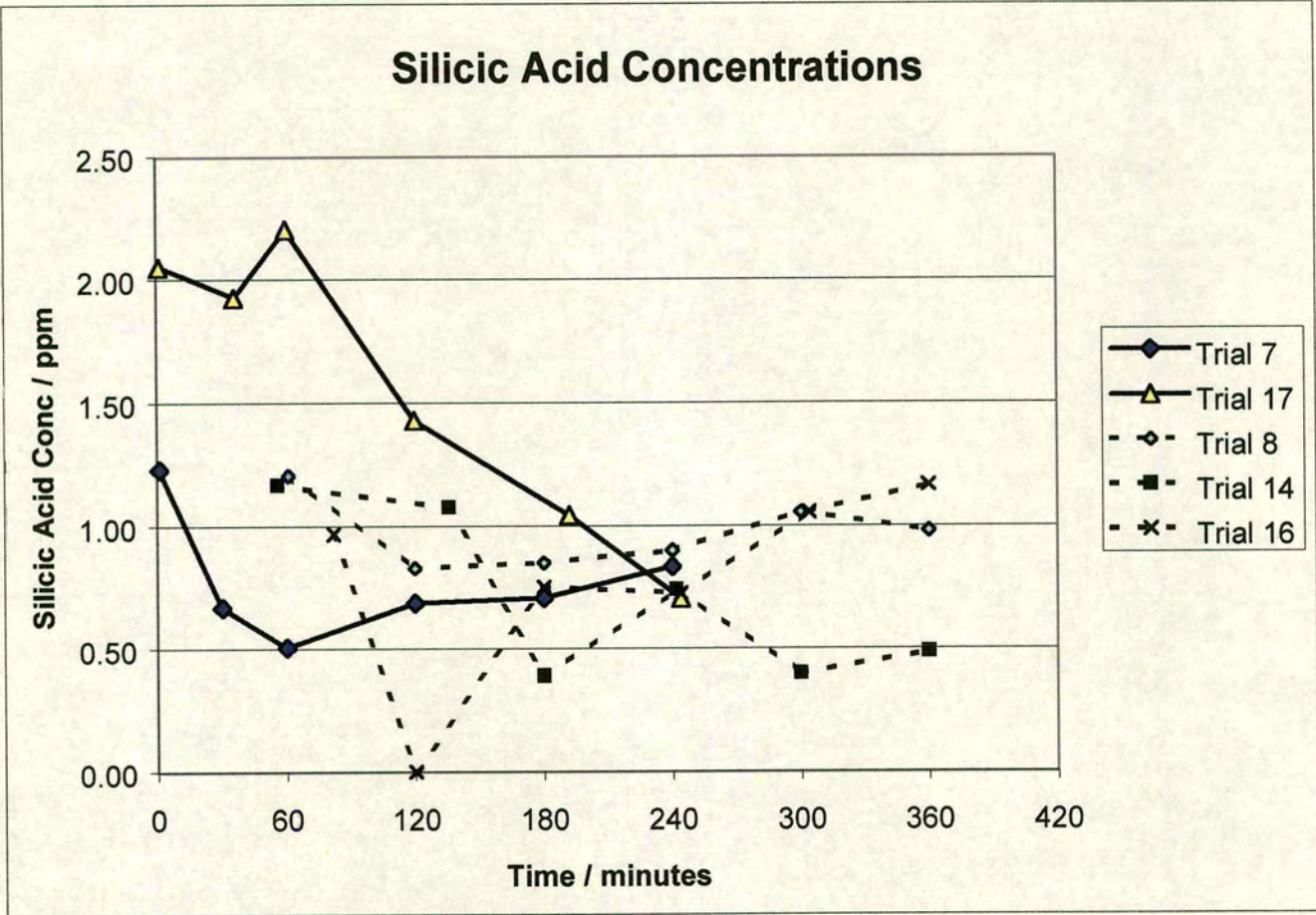
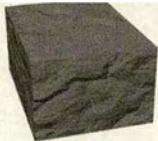


Figure 17 - Silicic acid concentrations vs. time. Trials 3, 4 and 5 are not plotted as the standardisation regime was being refined during these analyses.

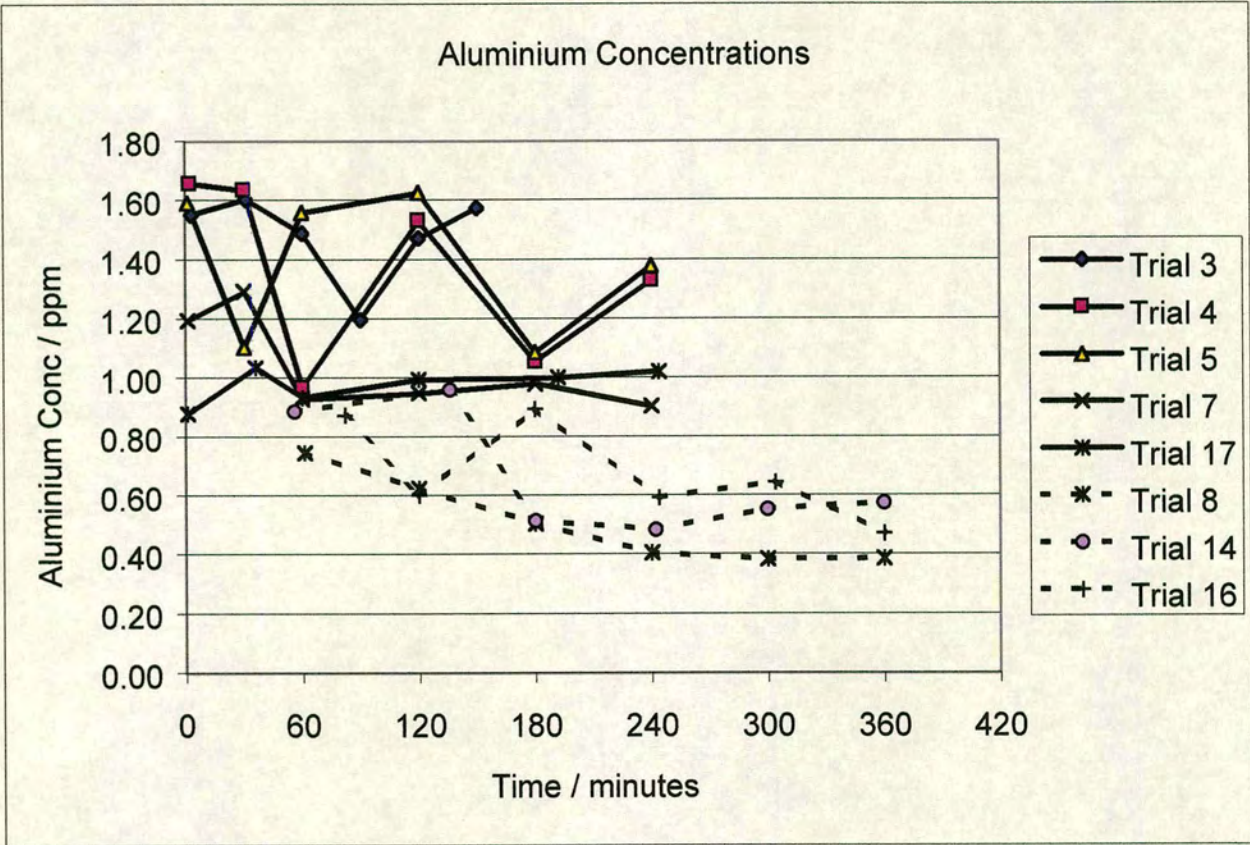
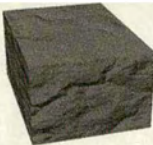


Figure 18 - Aluminium concentrations vs. time.



4. Discussion of Raw Concentration Results

Analysis of the raw element concentration data reveals some broad conclusions on concentration with time trends:

- i) With the exception of trial 17 (the high W/C trial) **calcium** concentration shows a broad negative trend with time. The oscillations in the calcium data are thought to be caused by stirring of mixing of the cement disturbing the ettringite gel that surrounds the cement grains. This would explain why it was irreproducible. It does appear to always lie within a consistent envelope.
- ii) **Sulphate** concentrations initially show a negative trend down to a minimum, followed by a positive trend that lasts until the end of the trials. The minimum occurs at around 60 minutes for the Supamix trials and around 160 minutes for the oilwell cements.
- iii) Sodium and potassium concentrations show a positive trend, and although the potassium concentrations are an order of magnitude higher, both trends are very similar.
- iv) Trends for silicic acid and aluminium are harder to identify. A slight negative trend for the aluminium concentrations may be apparent.

The results for Iron indicate that its concentration was below the detectable limit for this experiment. For this reason, the results have not been reported, but it was hypothesised that the iron concentration was below 0.5 ppm in all cases. The fact that Iron was not detected in the fluids concurs with previous work on cement [14].[15]



In addition, it can be seen that the results for this project, whilst not identical to those of previous projects, are nonetheless similar in both accuracy and precision [12;13].

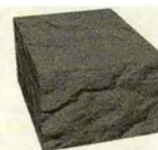
5. Thermodynamic Modelling of the Data

In order to interpret the results, and to investigate what effect the changing concentrations had on mineral stabilities, the raw element concentrations were input into the thermodynamic modelling program, “SCRAM 97”.

SCRAM 97 (The Schlumberger Cambridge Research Aquo-chemical Model) {Fletcher 1993 ID: 46} is a computer program that was written, in-house, for Schlumberger by Philip Fletcher to perform these types of calculations. It was written in Fortran 77 but, for commercial reasons, only the compiled version was available during this project. For this reason, only limited discussion of the internal workings of the program is possible.

SCRAM uses a number of thermodynamic expressions to predict the equilibrium composition, and related properties, of an assembly of reactive aqueous species by the equilibrium constant/mass balance method as described in Fletcher’s text book, “Chemical Thermodynamics for Earth Scientists”[16]. Owing to the fact that only the compiled version of the program was available during this project, it is difficult to speculate on the actual implementation of this method in the program code.

It is known that many of the expressions have been developed, following research by Schlumberger, including those for calculating activity coefficients and water activity.



In addition, the database of equilibrium constants contains much that is also a result of Schlumberger research.

When SCRAM is run, the program completes three stages in its calculations:

i) Stage 1 – Speciation.

SCRAM calculates the concentration of chemical species in solution, maintaining mass balance, by iteratively calculating the ionic strength, ion activities, water activity, pH and the distribution of species between the various phases[16;17]. In this context, there are three types of species:

- a) Primary species e.g. $\text{Na}^+_{(\text{aq})}$ and $\text{Cl}^-_{(\text{aq})}$.
- b) Secondary Species e.g. $\text{NaCl}(\text{s})$
- c) Complex species e.g. $\text{NaCl}^0_{(\text{aq})}$.

The Iteration is of a Newton-Raphson type, and follows the following scheme:

- 1) Estimate ionic strength, activity coefficients and water activity,
- 2) Calculate mass action quotients,
- 3) Select mineral assembly,
- 4) Solve equations to calculate molal concentrations of all free ions and the saturation products of all minerals,
- 5) Calculate molal concentrations of all complexes, and finally, improved estimates of ionic strength, activity coefficients and water activity,
- 6) Repeat steps 2 to 5 until difference between the calculated of ionic strengths, activity coefficients and water activities of one run and the previous, is below some threshold value chosen by the user.



ii) Stage 2 – Fluid Density.

The fluid density can only be calculated after the speciation stage is complete.

SCRAM was not written with a view towards user friendliness. It was designed to be run from a DOS prompt and uses a previously written text file for input and outputs to another text file. The formats of these input and output files are extremely complex. Examples of the input and output files can be found in Appendix 2.

It was found that creating the input files was complicated and extracting numbers from the output files was time consuming and non-trivial. For this reason, one of the first tasks in this project was to write a shell program to run SCRAM and to give it a more modern and easy to use graphic interface and a convenient method of extracting useful results from large data matrix generated. This program, the SCRAM 97 PC Interface is described in Appendix 1.

The SCRAM 97 PC Interface is capable of generating a very large data matrix – in excess of 2000 different output graphs for a small assembly! For this reason, only pertinent data will be presented in this thesis.



6. Modelled Data.

6.1 Average Supamix Trials

For the purposes of this section, the data set that has been modelled is the average of the data from the four repeat Supamix trials, 3, 4, 5 and 7.

Figures 22 and 23 illustrate some of the modelled data from SCRAM alongside the concentrations of sulphate, sodium and potassium. The modelled data set displayed is the calculated pH (calculated by charge balancing) and the saturation coefficients of gypsum and monosulphate. (The saturation coefficient is the quotient of the ion activity product and the solubility product).

More important than the actual values is the relative timing of various features of the graphs. These features are:

- i) The alkali metal concentration shows an early rise, followed by a hiatus, between 40 and 60 minutes, and finally an accelerating rise.
- ii) The pH rises until the same time as the alkali metal hiatus, and then flattens off.
- iii) The sulphate concentration begins high and then drops to a minimum at 60 minutes before rising again.
- iv) The saturation coefficients of monosulphate and gypsum cross somewhere between 40 and 60 minutes.

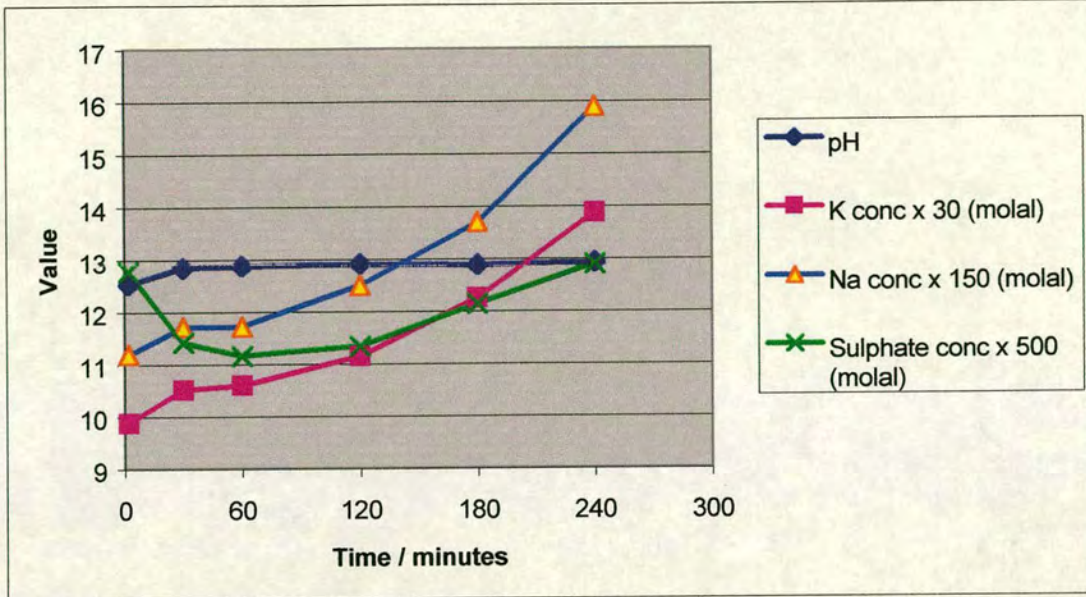


Figure 19 - Sample time, vs. value of calculated pH, ($[K^+] \times 30$), ($[Na^+] \times 150$) and ($[SO_4^{2-}] \times 500$) for the average Supamix trial.

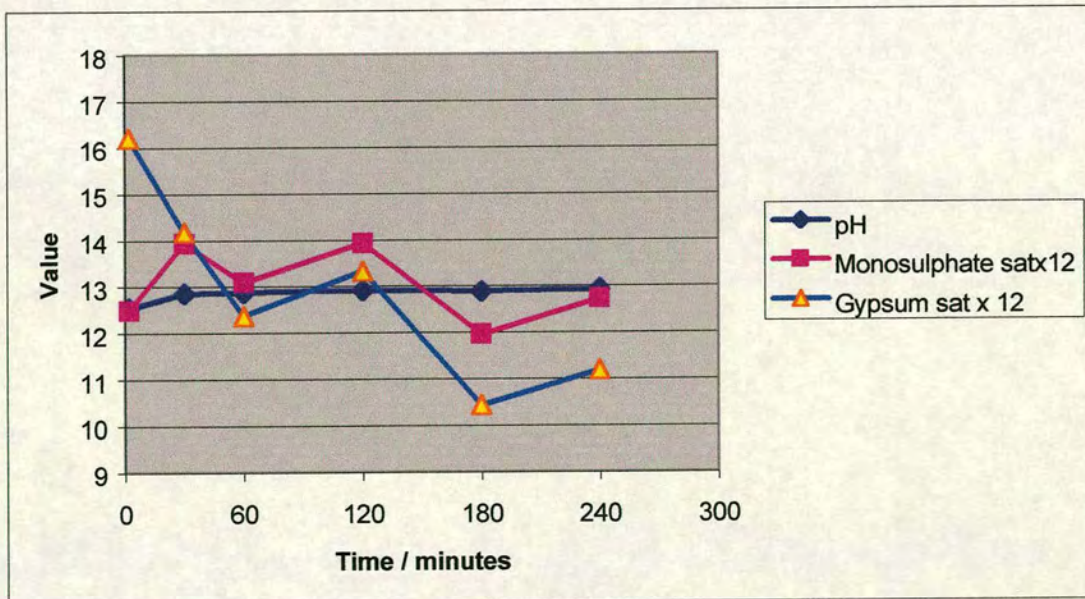


Figure 20 - Sample time, vs. value of calculated pH, (monosulphate saturation product x 12) and (gypsum saturation product x 12) for the Average Supamix Trial.

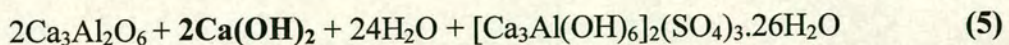


These features have been explained by this scheme.

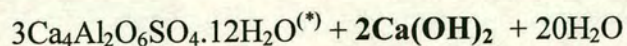
When first the cement is mixed with the water all grains begin to dissolve at their surface. Obviously, the larger the surface area and the faster the dissolution kinetics, the more prominent the dissolved components of a phase will be in the solution. This is seen in the rise of the calculated pH and the concentrations of the alkali metals (which exist in the clinker as accessory ions in the clinker phases, but do not precipitate out in any early forming minerals).

As C_3A reacts with gypsum to form the ettringite gel that covers the clinker grains, it takes sulphate out of solution and slows the dissolution of the clinker grains. This is seen in the decreasing sulphate concentration and the hiatus in the rise of the alkali metal concentrations.

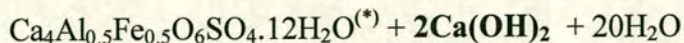
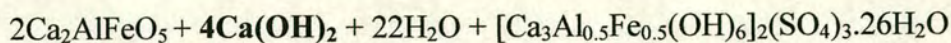
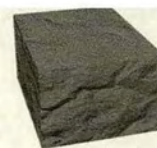
At the same time, the calculated pH flattens off. This is predicted by equations 5 and 6 where **portlandite** ($Ca(OH)_2$) is metabolised in the reaction of ettringite and gypsum to form monosulphate.



↓



and



(6)

(*) monosulphate series members

The abrupt switch from the production of ettringite to the metabolism of ettringite to form monosulphate is easily detected by X-ray diffraction (See Figure 21). This figure is intended solely to illustrate the abrupt monosulphate shift being co-temporal with the loss of gypsum. The figure shows a series of XRD traces, taken on samples of cement slurry as it set. (The first trace is the lowest, and the last trace is at the top.) This experiment was done under different experimental conditions from those reported here, but as it is only intended to help illustrate a point, one should assume that one trace was taken every 6 minutes.

It is readily apparent that the gypsum peak, highlighted in the figure ceases to exist after the 7th trace, and is indeed greatly reduced in that 7th trace, and that the monosulphate adsorption peaks appear for the first time in the 7th trace (albeit weakly), and grow from then on. Remember, that XRD detects crystalline ettringite while much ettringite produced during the setting of a cement is in an amorphous gel phase.

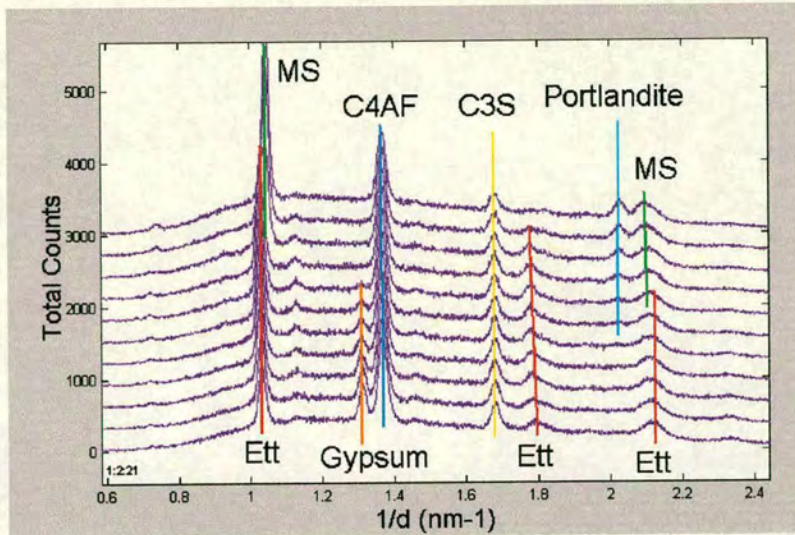
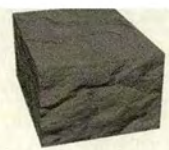
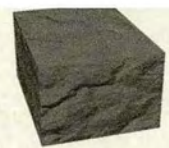


Figure 21 - XRD data. Displays 11 XRD traces of the same cement during setting, from early time at the bottom to later time at the top.

The reaction of ettringite, to form monosulphate, appears to allow dissolution of the clinker grains to restart, leading to the cement setting reaction accelerating again. This is reflected in the concentrations of the alkali metals rising again. It was noted that this point was approximately co-temporal with a pronounced change in the monosulphate saturation product.

6.2 Dykerhoff Trials

The same modelling techniques were also applied to the two experiments run using genuine oilwell cement manufactured by Dykerhoff, and were known as the Dykerhoff trials. Schlumberger uses this cement in oilwells. Unfortunately, sampling did not begin as early as in the trials involving Supamix, but despite this most of the



features identified in the “Average Supamix” trials can also be seen in the Dykerhoff modelled data except shifted to later time.

Features to note (See Figures 22 and 23 below):

- i) The early rise of the alkali metal concentrations occurs before the first data point, but the hiatus followed by the rise is apparent.
- ii) The minima in the sulphate concentration are visible.
- iii) The levelling off of the pH is also detected, although it is better viewed as the hydroxide concentration, $[\text{OH}^-]$.

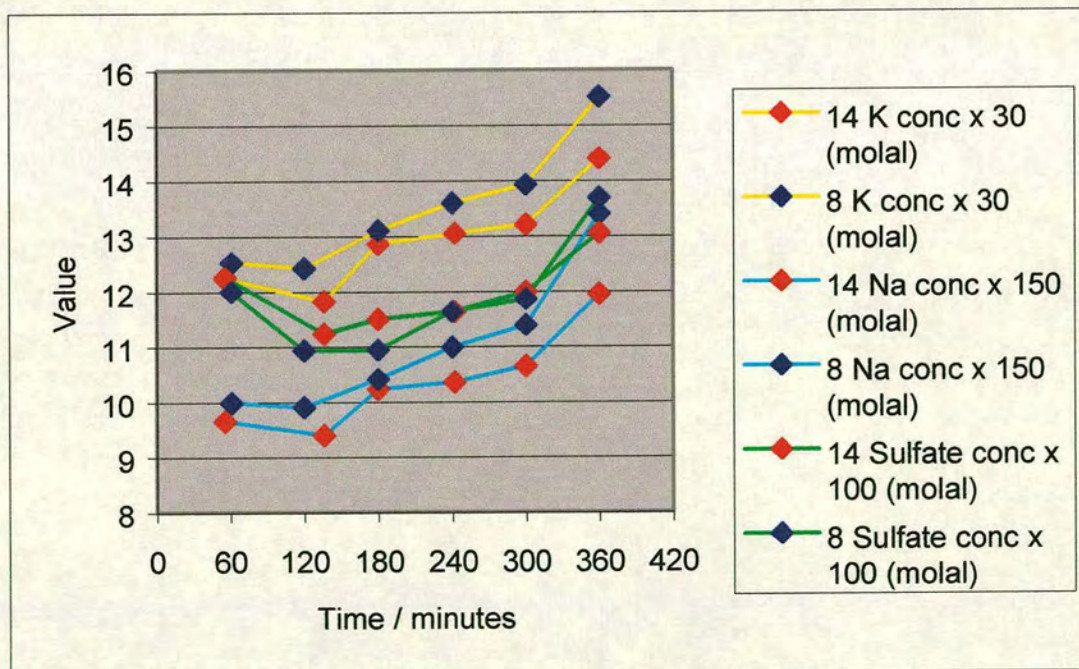


Figure 22 - Data from the Dykerhoff Trials. Time (minutes) vs. value.



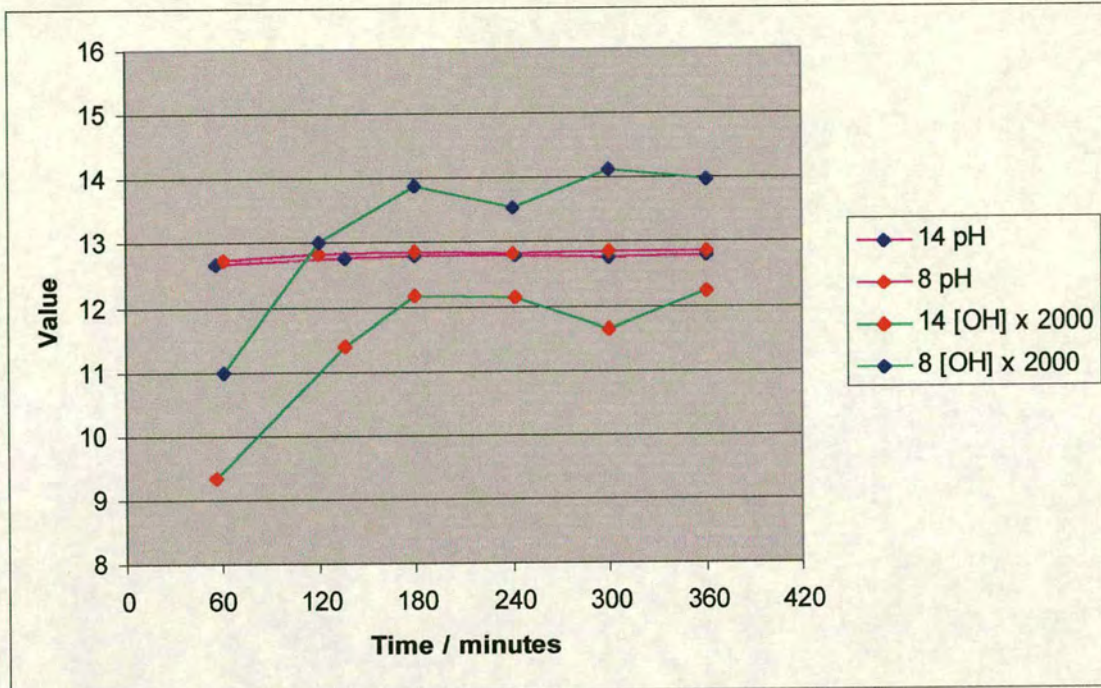


Figure 23 - Data from the Dykerhoff Trials. Time (minutes) vs. value.

7. Future Work

There will be three major routes of future work:

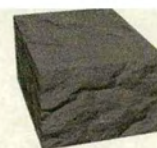
- 1) Increasing the time resolution. By decreasing the time between samples, greater resolution on the setting reaction would be achieved.
- 2) Extending the time window analysed. By extending the length of the experiments, the next stage of the reaction may be detected. It is envisaged that this would be the beginning of the massive portlandite precipitation phase.



Once the buffering effect of the ettringite to monosulphate reaction is lost, hydration of the major cement phases causes the pH of the system to rise until portlandite saturation is reached. At this point, massive portlandite crystals will begin to form, and the crystallisation of portlandite will buffer the solution at this new, higher level. It should be possible to detect the pH beginning to rise and the subsequent levelling off, which would signify this next stage of the setting reaction.

- 3) Simulating well conditions. The extreme depth of modern oil wells results in a high pressure and temperature regime at the bottom*. Many of the normal cement phases, including ettringite, are not stable in this environment. This experiment was the first in a series of experiments to be carried out at increasing temperatures and pressures until the whole range experienced by oil well cements has been investigated.

* Average geothermal gradient is 25°C/km depth. Approximate lithostatic pressure gradient is 27MPa/km.



8. Conclusions

Features, specifically the ettringite to monosulphate phase shift, have been detected in setting cements by a new, chemical method. This new technique should allow measurement of the setting kinetics of cements to be measured more economically in terms of both time and money, acting as an alternative to synchrotron X-ray diffraction.

Future work may detect the beginning of the massive portlandite phase, will result in an increase of the time resolution and will extend the research to cover deep well conditions.



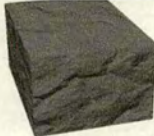
Appendix 1

In the graphs below, the results are labelled by the first named author. Kelzenberg results refer to those from reference (a) and Michaux to reference (b).

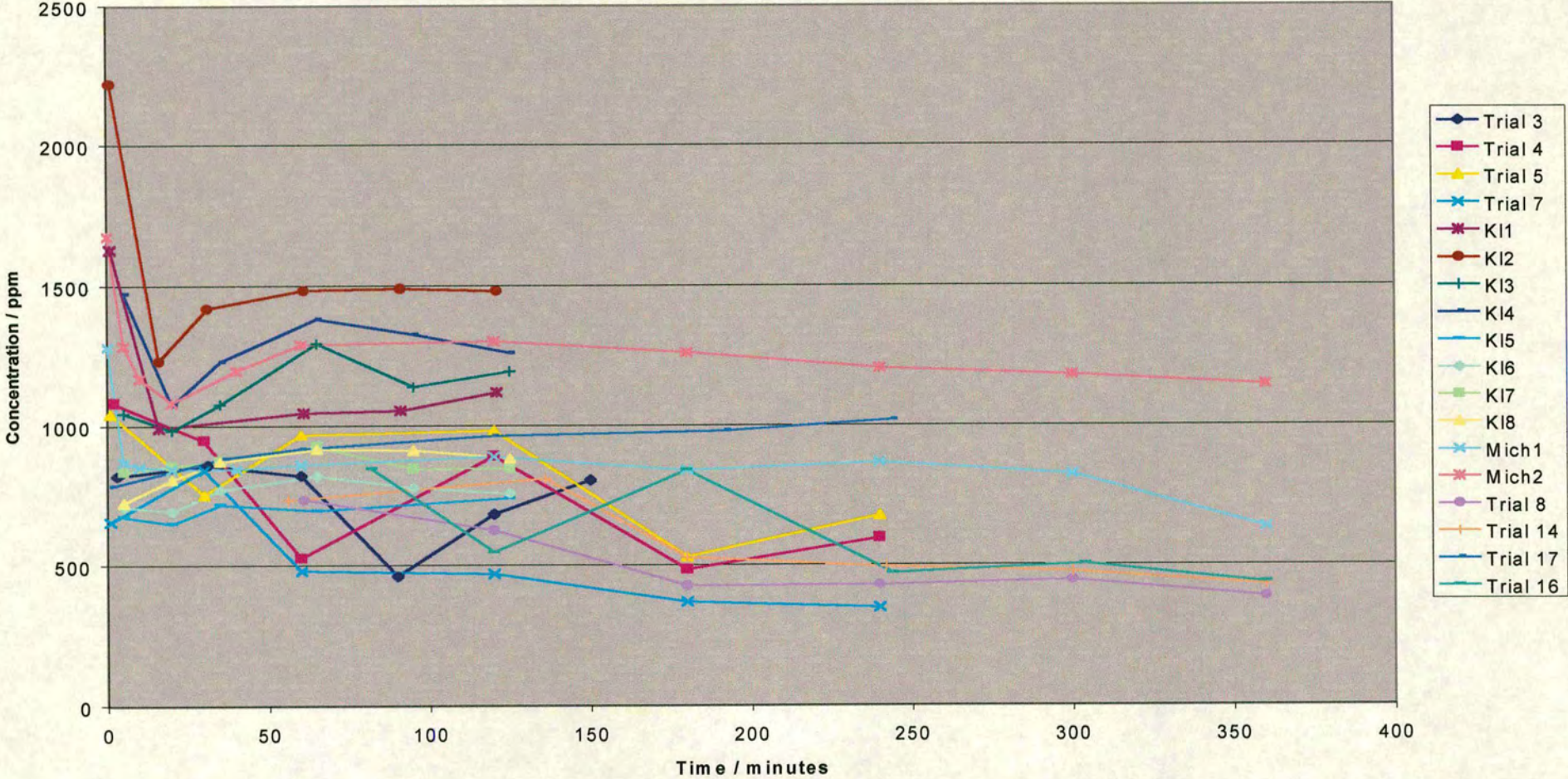
a) Chemistry of the Aqueous Phase of Ordinary Portland Cement Pastes at Early Reaction Times. Kelzenberg, A.L. et al. *J. Am. Ceram. Soc.*, Vol 81, No 9, pp2349-2359. 1998.

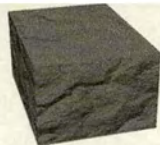
b) Evolution at early hydration times of the chemical composition of liquid phase of oil-well cement pastes with and without additives. Part 1. Additive free cement pastes. Michaux, M., Fletcher, P., Vidick, B. *Cement and Concrete Research*, Vol 19, pp 443-456. 1989.

In the following graphs, results from the Kelzenberg et al. reference have the prefix “KI” and those from the Michaux et al. reference, “Mich”.

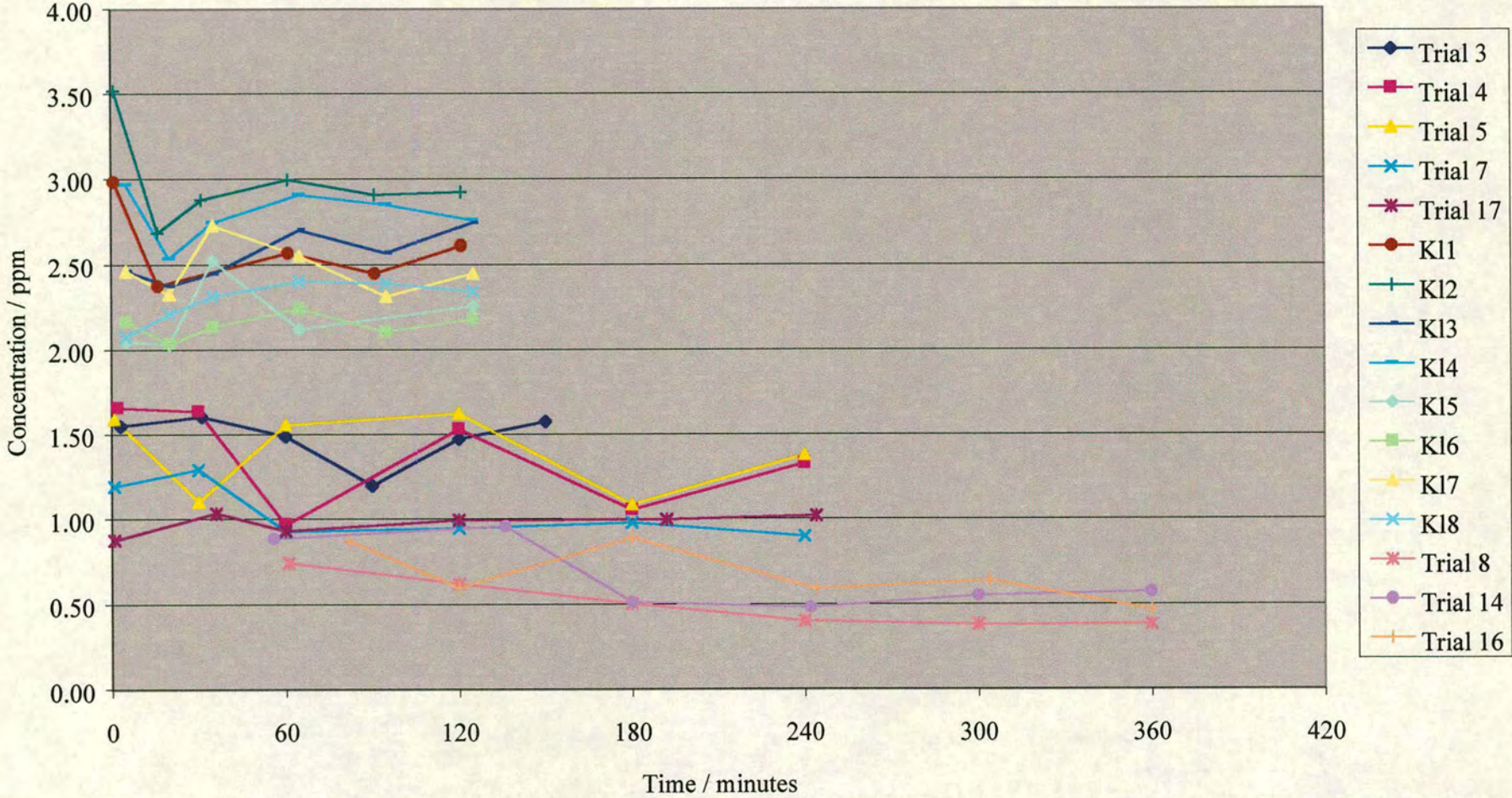


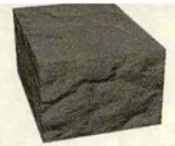
Calcium Data



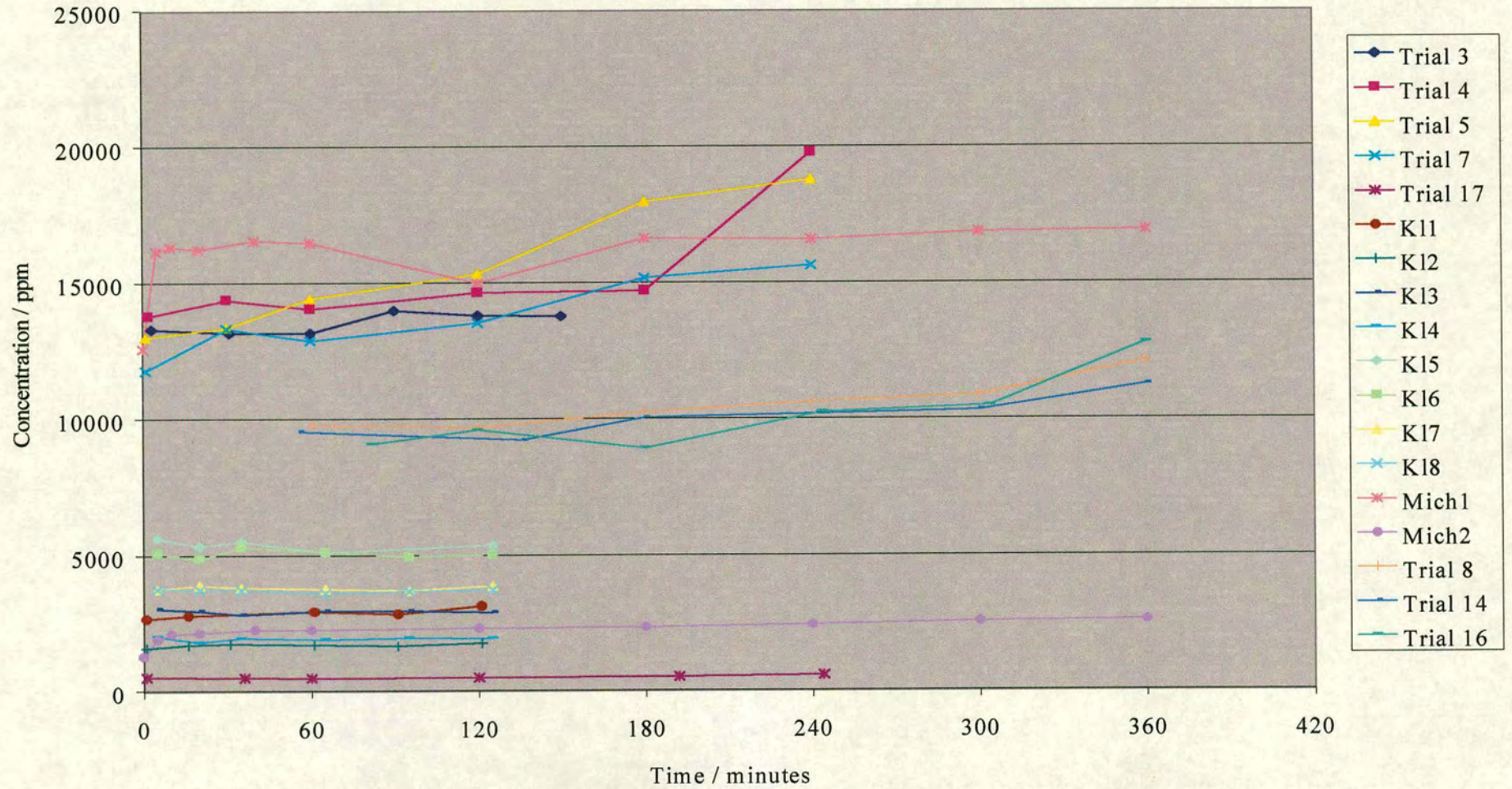


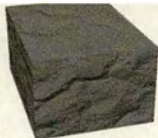
Aluminium Concentrations



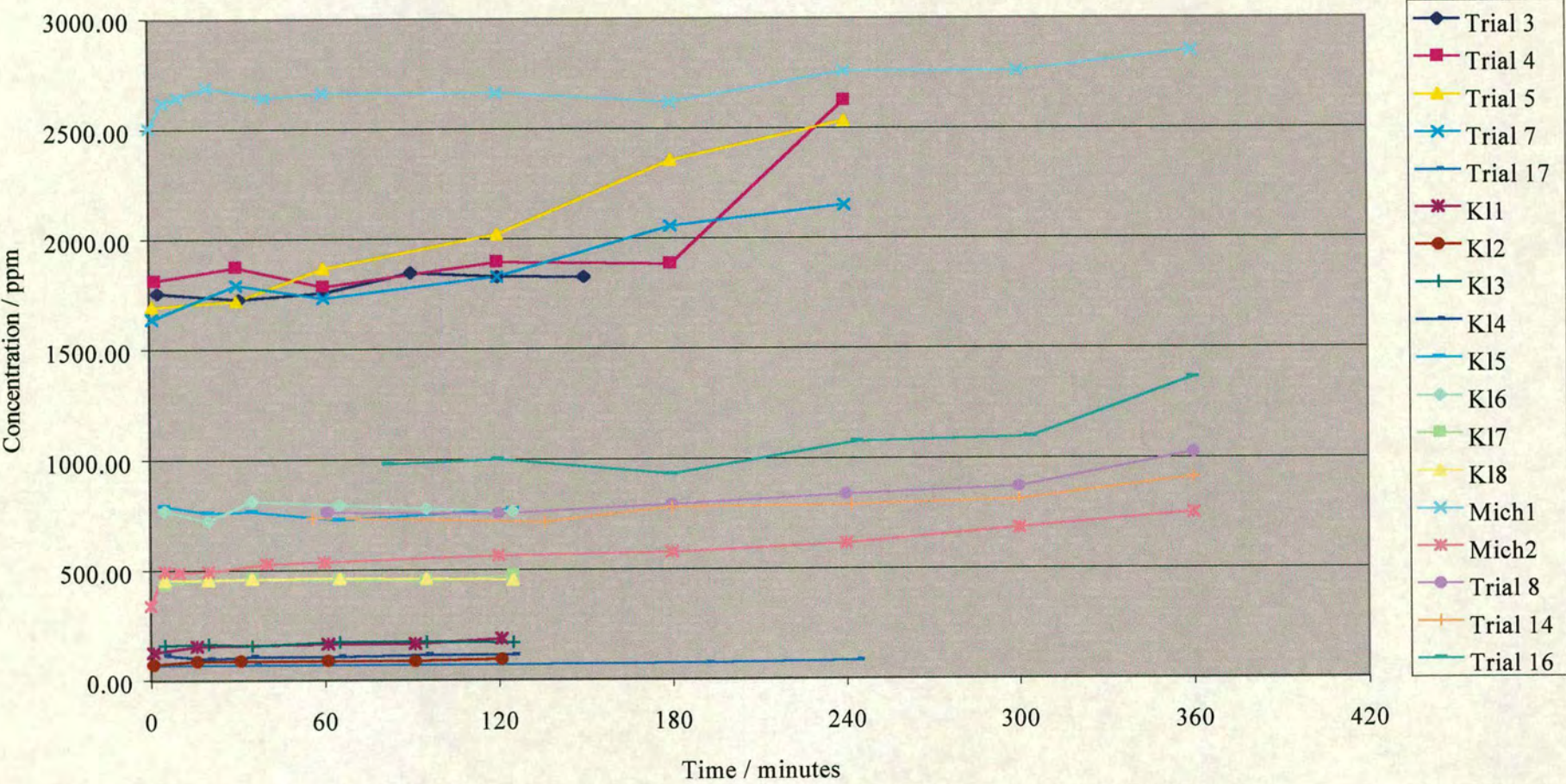


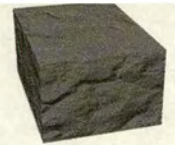
Potassium Concentrations



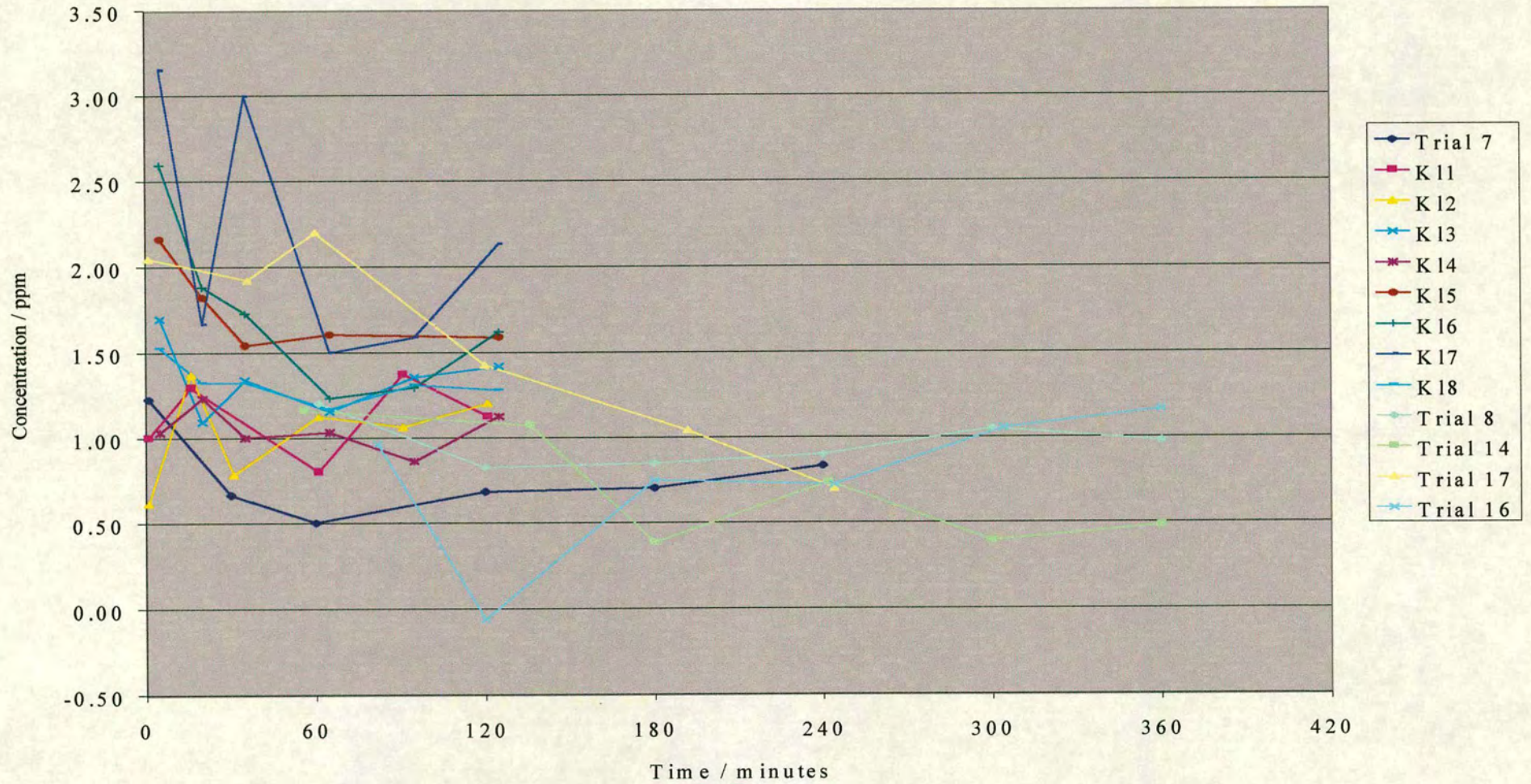


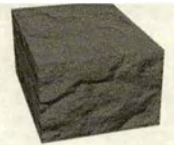
Sodium Concentrations



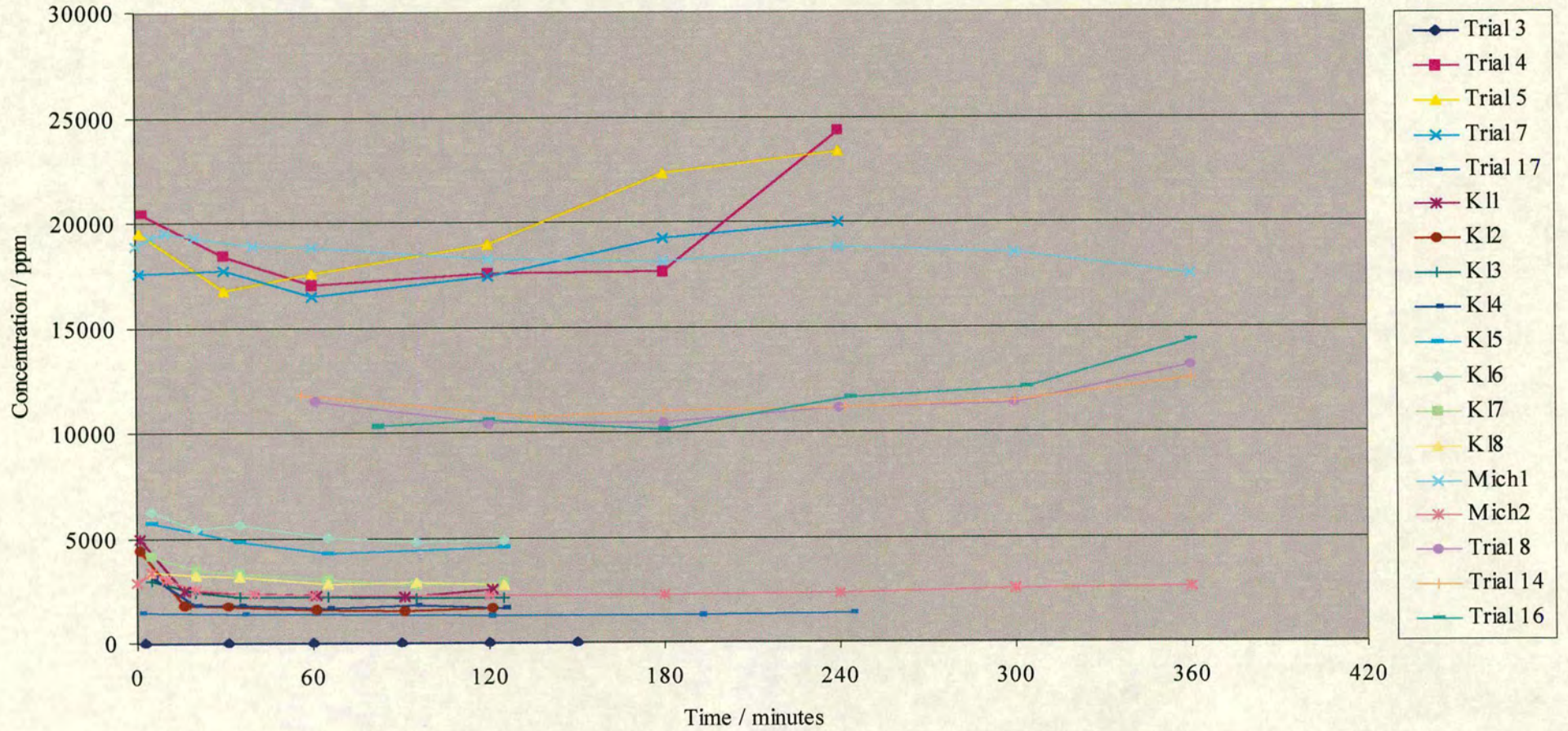


Silicic Acid Concentrations





Sulphate Concentrations

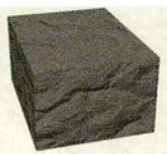




Appendix 2 – SCRAM97 PC Interface

The SCRAM97 PC Interface was written in National Instruments Corporation LabVIEW 6.0.

The following is a copy of the Documentation, written in HTML, which accompanied the SCRAM97 PC Interface.



Scram97 PC Interface

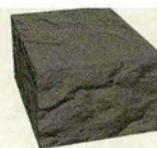
Documentation

Contents

- [Table of figures](#)
- [Introduction](#)
- [Main \(First\) Window](#)
- [Single Set, Define new](#)
- [Single Set, Reprocess](#)
- [Multi Sets, Define new](#)
- [Multi Sets, Reprocess](#)
- [Import Data Set](#)
- [Tutorial](#)

Table of figures

- [Figure 1 - Main Window](#)
- [Figure 2 - Fluid definition window](#)
- [Figure 3 - Output window.](#)
- [Figure 4 - dialog box.](#)
- [Figure 5 - Graph Output Window](#)



- [Figure 6 - Graph Output window, axes selection listbox.](#)
-

Introduction

SCRAM97, a Fortran77 program, written by Philip Fletcher, calculates the equilibrium composition and thermodynamic properties of an aqueous solution, or a series of solutions, defined by the physical conditions and concentrations of a suit of dissolved components. The original program used a complex .txt file to input this information and saved the output to another .txt file. The formatting and syntax for both of these files were complex, which made them difficult to use and to extract numbers from. The SCRAM97 PC Interface is designed to give the program a more user-friendly graphical interface, to make it easier to use and increase the speed of data processing.

The description of how SCRAM97 works can be found in "A Software Guide to SCRAM". This document describes how to use and understand the PC Interface.

[Back to top](#)



Main (First) Window

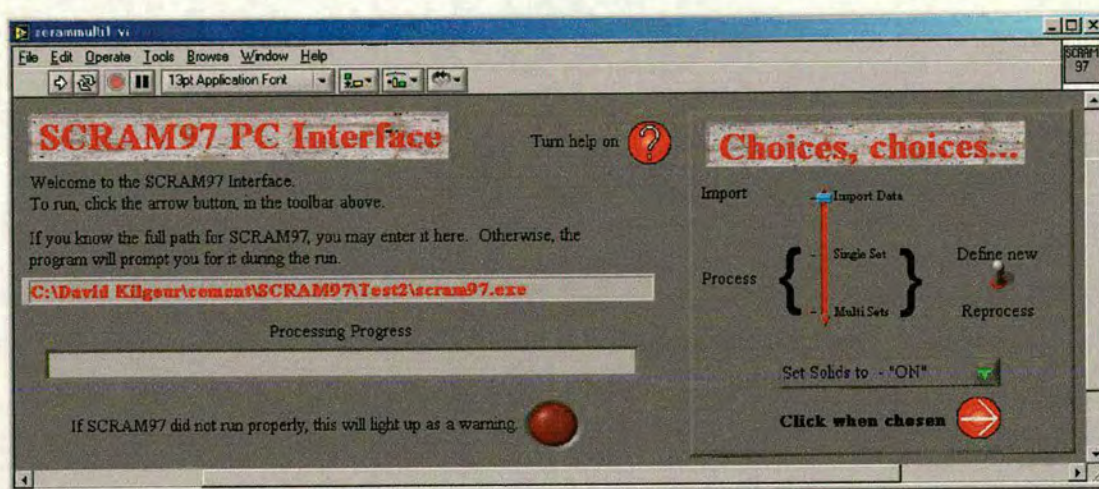


Figure 24 - SCRAM97 PC Interface main window.

This is the first part of the interface that a user will see. This screen asks the user for the specific information that SCRAM97 needs to run and to make choices that determine how the rest of the process will run. These choices are made in the "Choices, choices..." box at the right hand side of the screen.

The first choice concerns the number of fluids to be processed, and the source of the data for these fluids. The choices are import data from a tab delineated text file, process multiple fluids or process a single fluid. The import data function is used to convert a tab delineated text file into SCRAM readable files that can be processed using the mutiple fluids function. The format of the import file is described [later](#). Use the import function if you already have a spreadsheet file containing the data you wish to use. This function, however only allows access to a limited subset of the available ions (sodium, potassium, calcium, aluminium, silver, sulphate and silicic acid). To define a more complicated fluid series, or to input a series where the data does not



exist in a suitable format, or to reprocess previously input or imported fluids, use the multiple fluids (Multi Sets) option. To process a single fluid, use the Single Set option.

Choice 2 is between "Define new" and "Reprocess". Choosing "Define new" allows a new fluid, or a set of new fluids, to be defined before processing. These fluid definitions can also be saved for future "Reprocessing". "Reprocess" is used to reload and process these previously saved fluid definitions. Choices 1 and 2 work together. E.g. choose "Single Set" and "Define new" if you wish to define and process one fluid.

Choice 3. If "Multi Sets" and "Reprocess" have been chosen (i.e. you are reprocessing an old series) you can choose whether to have solid dissolution/precipitation allowed or prohibited using this menu control.

Choice 4 is the red "Turn Help On?" button in the top centre of the window and toggles whether to have the Interface display pop-up help during the run. For first-time users of any of the functions, this contextual help may prove useful. More experienced users are likely to prefer to turn help off, as this speeds up processing time.

Once these choices have been made, they are accepted by clicking the "Click when chosen" button, at the bottom of the box.

The following sections describe each of the five processing paths ("Single Set" with "Define new" or "Reprocess" and "Multi Sets" with both "Define new " and "Reprocess" and "Import Data Set") . You can use the linked contents table at the top to help navigate through these help files. In addition, there is a basic tutorial to help new users get started.

[Back to top](#)



Single Set, Define new

If Single Set and Define new have been selected, then the Fluid Definition Window will be displayed.

Do the concentrations require conversion from ppm to molal Values Entered?

Page 1 Page 2

Physical Information

Title 0.0000000
 Temperature (degC) 25.000000
 Pressure (kbar) 0.0010000
 Density (g/cc) 1.0400000
 Convergency Criterion? 0.0000010

Current file fluid2.dat

Chemical Information

Solids on?

The most common dissolved components are found on this page. Less common components can be found on page 2

As yet, it is not possible to use citrate, cmc-a, cmc-b, BF₄⁻, benzoate, diphosphate, mont or mont edge components. These will be added at a later stage

Component	Conc
proton	0.0000
hydroxide	0.0000
sodium	1733.0000
potassium	12894.0000
silver	0.0000
calcium	481.0000
iron(III)	0.0209
aluminium	0.9270
sulphate	16511.0000
silicic acid	1.7277
chloride	0.0000

Fixed pH pH 0.0000000

Figure 25 - SCRAM97 PC Interface Fluid Definition window.

The user should define the fluid physically and chemically here. The physical conditions should be entered in the Physical Information box. The concentrations of the dissolved components should be entered in the appropriate boxes in the four tables displaying all available components. One of these tables, containing the most common components, is on Page 1 while the remaining three are on Page 2. To change between pages, click on the tabs at the top left hand corner of the window. The concentrations may be inputted in ppm or molal units. As SCRAM97 requires molal units for its input, if ppm units are input here, then the interface must be instructed to convert



them to molal before processing. This is carried out automatically if the "Do the concentrations require conversion from ppm to molal" button has been activated. If this is omitted, SCRAM97.exe will almost certainly fail to complete. Checking this button should be one of your first checks should SCRAM fail to complete.

To allow solid dissolution and precipitation, activate the "Solids on?" button.

To set the pH, activate the "Fixed pH" button and enter the pH in the adjacent box.

Once the information has been entered, proceed by clicking the "Values Entered?" button at the top right corner of the screen.

There will now be the option to save this information in a "fluid definition" file that can be reloaded at a later date. Choose cancel if you do not wish to save the information. NOTE - these fluid definition files are different from the input file for SCRAM97.exe (for012.dat). They contain all the information that the SCRAM PC Interface requires to build a SCRAM97.exe input file, in a 2D array. The top row contains all the Boolean information (solids on/off, pH fixed/unfixed etc) and the physical information and the second row contains the concentration of the dissolved components in the same order as they appear in the fluid definition window.

Once this step is complete, the Interface will format the information into a valid SCRAM97 input file, save it, and invoke SCRAM97.exe. When SCRAM97.exe has completed, the Interface will read and deformat the output file that SCRAM97.exe has created and display the results in the Output window. This has a number of pages in the same style as the Fluid definition window which can be viewed by clicking on the tabs at the top of the screen. These display the various processed information separated into discrete tables. The output file, as created by SCRAM97.exe, is also displayed along with the input file.

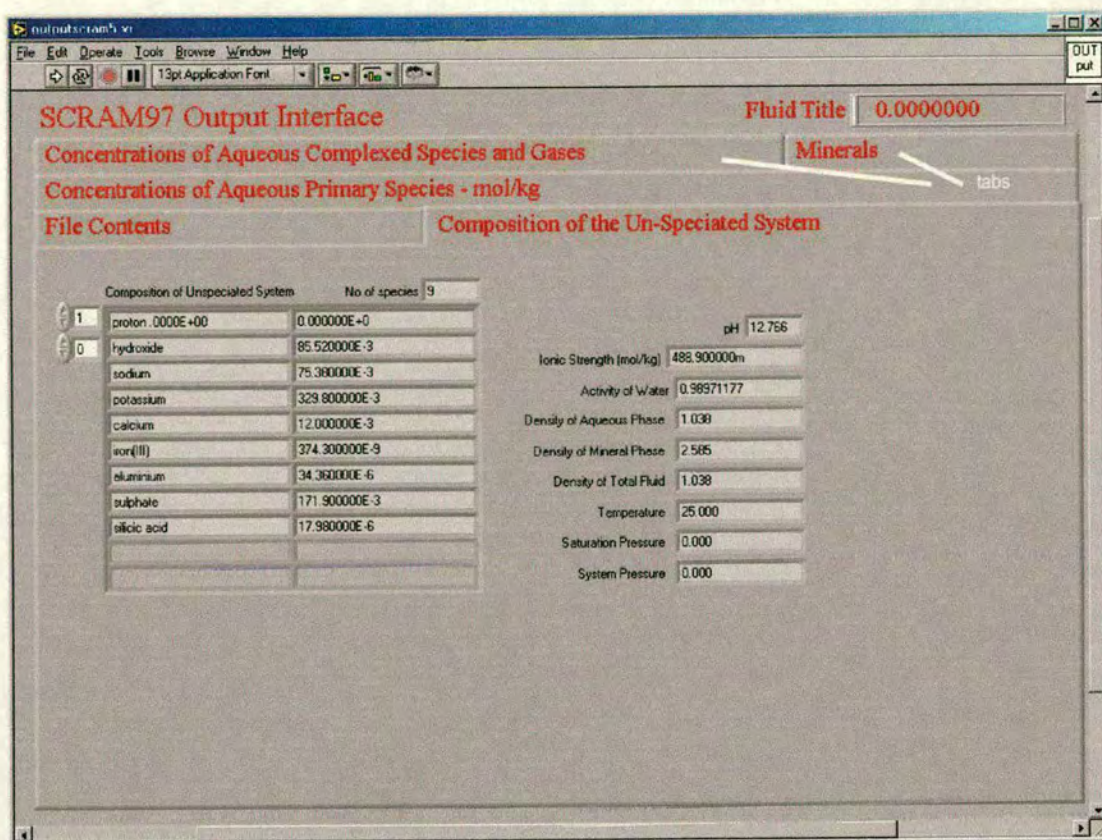
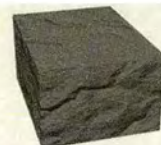


Figure 26 - SCRAM97 PC Interface Single Fluid Output window .

[Back to top](#)

Single Set, Reprocess

This selection follows much the same path as Single Set, Define new, except that a previously saved definition file will be uploaded, and its contents displayed. These may be altered before continuing. To continue, click the "Values Entered?" button, as before. The new definition may be saved, replacing the old file; or saved to a new one, or not saved.

The output is again displayed in the Output window.



Multi Sets, Define new

This function is used to input a series of fluids. The fluid definition files of this series must be saved in their own folder. When the "Click when chosen" button, in the Main Window, is clicked, the first box to appear will be a dialog box with three boxes. The first box is the name of the folder where the fluids definitions will be saved (this must be unique), the second box is the number of fluids in the series and the third is the base fluid name (this will be used to create the filenames of the fluid definition files (along with the number in the series)).

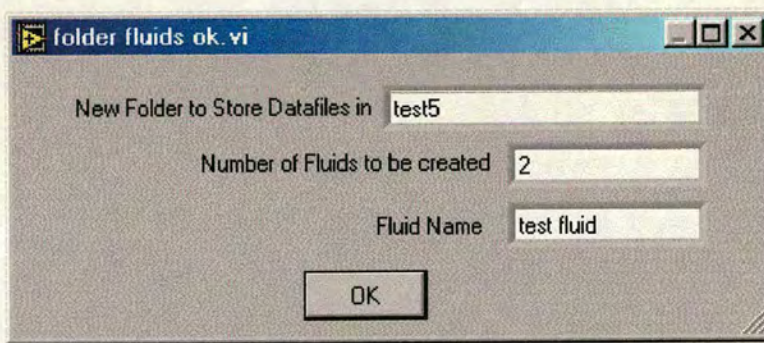


Figure 27 - SCRAM97 PC Interface dialog box.

A fluid definition window will pop-up for each fluid in turn. Define these as for a single fluid. Once all fluids have been defined, the Interface will run each one through SCRAM97.exe and collect the outputs from all of these.

This information is displayed in the Graph Output window. This is the most powerful section of the interface. It allows any of the output parameters of all files in the series to be plotted against any of the others, and any number of these output as spreadsheet files. The number of these graphs depends on the fluids concerned, but will almost certainly number in the thousands!

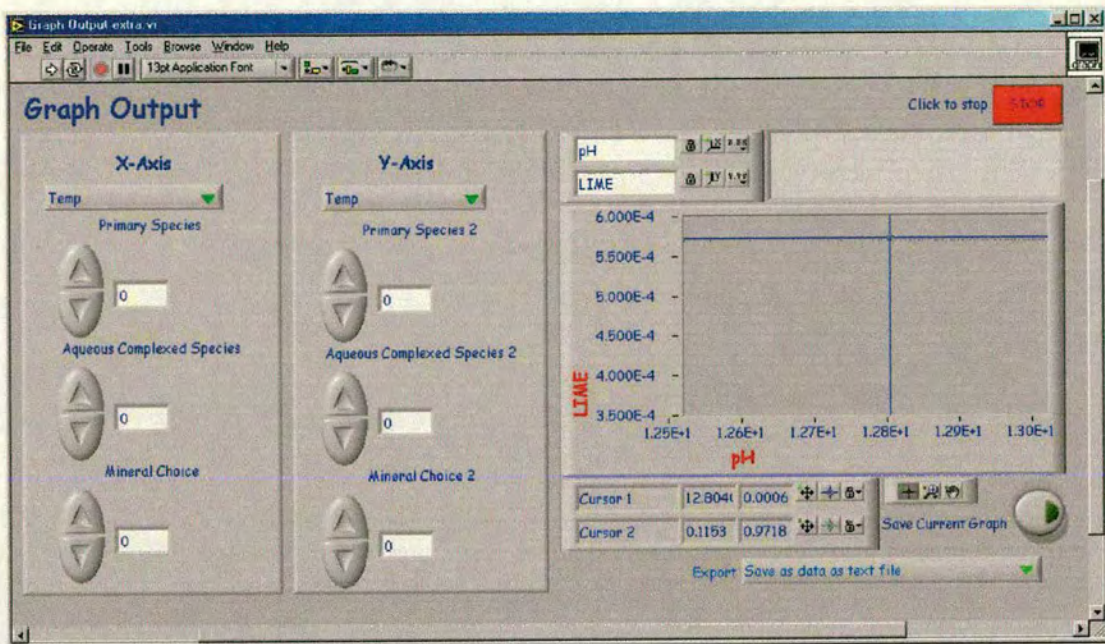


Figure 28 - SCRAM97 PC Interface Graph Output window.

The graphs are controlled by defining the parameters of the two axes. When first displayed, both axes will be displaying the Temperature. To change to another graph, click the X Axis list box (see Fig 6).

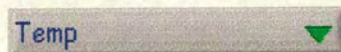


Figure 29 - SCRAM97 PC Interface Graph Output window, axes selection listbox.

Choose from the menu of possible parameters. Some of these are complete (in that they are a unique parameter) e.g. Temp, Fluid Number, pH etc. Most options, however, are not complete, e.g. IAP/SP (Mineral) or mol/kg (Complex). These refer to a column in one of the output tables, from which various components may be



chosen by selecting different rows. For example, IAP/SP, the saturation product, refers to the dissolved minerals table, whereas mol/kg (Complex), refers to the Concentrations of Aqueous Complexed Species and Gases table. To choose which component of these table to display, use the up and down controls beneath the listbox. Use the one which refers to the correct table in the output file. The correct one will flash to help identify it. This sounds more complex than it will prove to be in practice. Select a different Y Axis, in the same way, to complete a new graph.

There are 3 export options available:

- i) Save as .txt file. This saves the current graph data as a tab delineated text file. This data format is readable by most spreadsheet packages.
- ii) Print current graph. This prints the current graph to your default printer. It uses Excel97 to do this. Therefore, if you do not have Excel97 on your system, do not use this function.
- iii) Export to Excel (draw graph and save). Self explanatory. However, the same caveat applies as above.

Click the "Click to save" button to execute the exportation.

When finished, click the "Stop" button at the top right corner.

Multi Sets, Reprocess

With this selected, simply select any one of the fluid definition files in the Multi Set to be processed in the file dialog that pops up. The Interface will detect how many fluids there are in the series. Confirm the selection. The system then jumps directly to the processing stage, and thence to Graph Output. Use the menu box front panel to turn solids "ON" or "OFF". Because of the large number of other possible changes that could be made to a fluid series, there are no more automated facilities for this



available. If changes are to be made to fluid series files, then load and change them individually, using the Single Set and Reprocess options.

[Back to top](#)

Import Data Set

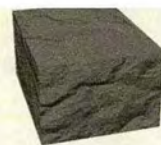
[Top](#) This function was added to speed the processing of fluid series, analysed using the ICP-AES. It allows the user to import specially formatted tab-delimited text files, created by excel or any spreadsheet program. The correct format style is saved as Template.xls in the SCRAM helpfiles directory, and looks like Figure 30:

	A	B	C	D	E	F	G	H	I	J
1	proton	hydroxide	sodium	potassium	silver	calcium	iron(III)	aluminium	sulphate	silicic acid
2										
3										
4										
5										
6										
7										
8										
9										
10										
11										
12										
13										
14										
15										
16										

Figure 30 - SCRAM97 PC Interface Import Spreadsheet Template.

[Top](#)

In each column, enter the concentration of the appropriate ion, in ppm, for each fluid, downwards (fluid 1 in row 2, fluid 2 in row 3 etc...). Save the finished file as a tab delimited text file.



To Import these fluids into SCRAM, first choose the import "Import Data" option on the Main Window. In the first dialog box which will open, find this file. Another window will open, displaying the imported fluid data:

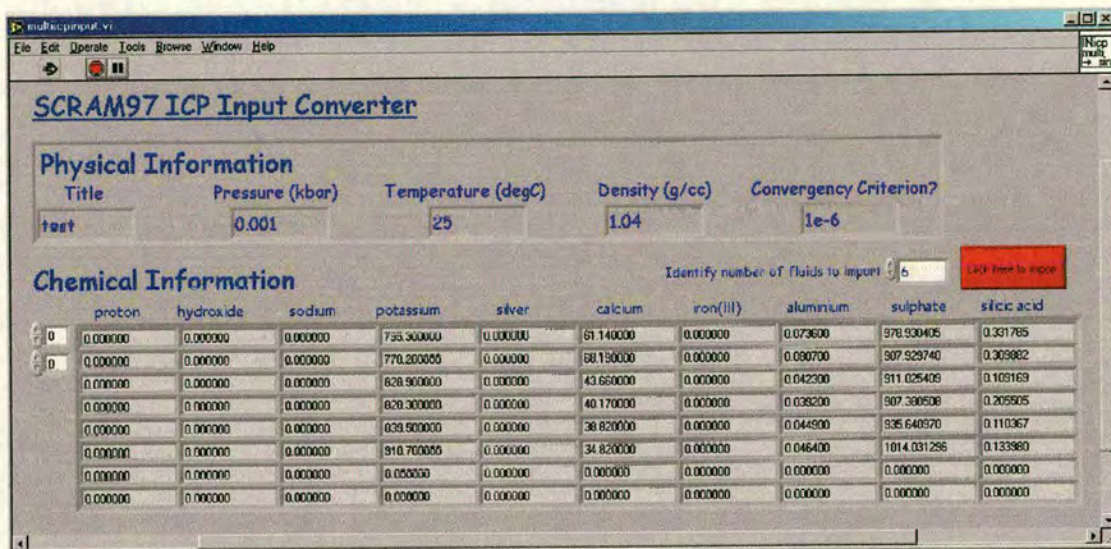


Figure 31 - SCRAM97 PC Interface Import window.

[Top](#) The system should identify the number of fluids in the series, but it is possible to correct this estimate in the "Identify number of fluids to import" box.

Enter the Physical conditions of the fluid in the Physical Information boxes (these must be the same for each fluid in the series).

Click the "Click here to import" button to continue with the import.

The system now creates the same style of fluid definition files as would be created by the normal Multi-set and Define route, for this new series. These are saved in a new folder, with the same name as the original .txt file, in the same directory as SCRAM97.exe. To process these fluids, use the normal [Multi Sets, Reprocess](#) option.

[Back to top](#)



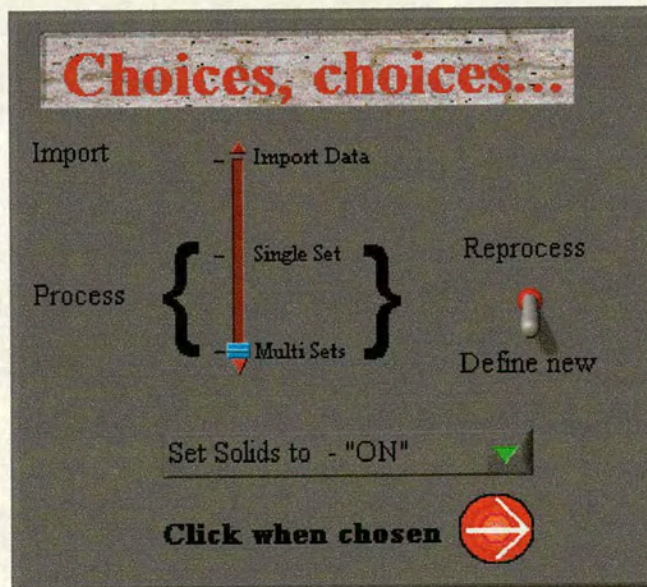
Tutorial

Use this simple tutorial to get started with the main aspects of the SCRAM PC Interface.

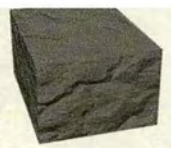
1. [Part 1](#) - Setup on Main Window.
2. [Part 2](#) - Fluid definition.
3. [Part 3](#) - Processing.
4. [Part 4](#) - Graph Output and printing a graph.

Part1

On the main window, select "Multi Sets", "Define new" and set help to off (red button background - on is green). The Choices choices....section should look like this:



Then click "Click when chosen" button. If this is the first time the interface has been run since being loaded, in this instance a file dialog will pop up, prompting you to "Please find SCRAM97.exe". SCRAM97.exe is used to calculate the results, and must be stored on your computer somewhere. Find it and click the save button (save is the default name for this button). If you have previously and correctly identified



SCRAM97.exe on your system, in this instance this stage will be omitted. Next, another dialog box will appear. There are three items of information to be inputted in this box:

(i)First, choose a name for the folder that will hold the fluid definition files. This will be a subdirectory in the same directory that holds SCRAM97.exe. It must be different from any other directories there. For this example, enter "Tutorial" in the box.

(ii)Secondly, you must tell the interface how many fluids there will be in the series. In this case, enter "4".

(iii)Lastly, choose a fluid name which will be used as a base for the fluid definition files. Enter "fluid" here.

(iv)Click <OK> to continue.

[Back to top of Tutorial](#)

Part 2

The Fluid Definition window will appear. This is where each fluid will be defined.

The box in the top right hand corner of the window displays the fluid number to help keep track of where you are in the series.

The following concentrations are in ppm units, so activate the "Convert to molal from ppm" button (the arrow will light up). Leave the "fixed pH" button unactivated. Turn solids off.



Enter the following information in the concentration column:

Component	Concentration
Na	1638
K	11786
Ca	656.2
Fe	0.04684
Al	1.194
SO4	17607
H4SiO4	4.211

In the physical information section, set the temperature to 25 deg C, pressure to atmospheric (0.001 kb), density to 1.04 and the convergency criterion to 0.000001.

The window should look like this:

multinput v1

File Edit Operate Tools Browse Window Help

SCRAM97 Input Interface

Fluid Number 1

Convert from to molal from ppm? Values Entered?

Page 1 Page 2

Physical Information

Title test

Temperature (degC) 25

Pressure (kbar) 0.001

Density (g/cc) 1.04

Convergence Criterion? 1e-6

Chemical Information

Solids on?

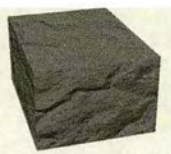
The most common dissolved components are found on this page. Less common components can be found on page 2.

As yet, it is not possible to use citrate, cmc-a, cmc-b, BF4-, benzoate, diphosphate, mont or mont edge components. These will be added at a later stage.

Fixed pH pH

Dissolved component Conc in ppm

proton	0
hydroxide	0
sodium	1638
potassium	11786
silver	0
calcium	656.2
iron(III)	0.04684
aluminium	1.194
sulphate	17607
silicic acid	4.211
chloride	0



Leave all the concentrations on page 2 set to 0 for this example.

Click "Values Entered?" to continue. This will save the definition of fluid one and open up the fluid definition for fluid 2.

The fluid 2 definition window should carry over the setting from fluid one. Fill in the following concentrations for fluids 2, 3 and 4, clicking "Values Entered?" to save each one in turn.

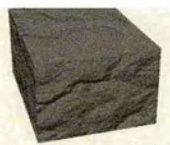
Component	Fluid 2	Fluid 3	Fluid 4
Na	1792	1733	1829
K	13329	12894	13549
Ca	843.0	481.0	470.0
Fe	0.0401	0.0209	0.0186
Al	1.291	0.927	0.947
SO4	17732	16511	17435
H4SiO4	2.286	1.728	2.349

[Back to top of Tutorial](#)

Part 3

Once the last fluid has been entered, and the "Values Entered?" button clicked, the fluid definition window will disappear, and the main window will be displayed. The Progress bar will show the processing progress as the interface:

- loads each fluid definition file in turn
- converts it to a SCRAM97.exe input file
- runs SCRAM97.exe



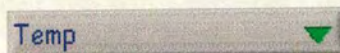
- loads the output file
- parses the output file to extract the data
- loads the next fluid definition file and so on.

[Back to top of Tutorial](#)

Part 4

When processing is complete, the Graph Output window will appear.

Click on the list box in the X Axis box. Choose Fluid Number (the last option - use the scroll bar).



The list box

Click on the listbox in the Y Axis box. Choose IAP/SP (Mineral). The bottom one of the three up and down controls in the list box should now be flashing. Click the up button to cycle through the available minerals until Ettringite is the displayed mineral. You may check which mineral is being displayed in the Y axis title of the graph, or in the Graph Title box at the top of the window.

Click the Export listbox (bottom right of the window) and select Print data.

Click the Save Current Graph button. This will export the data to Excel97, draw it as a new chart, and send it to your default printer.

Close excel (don't bother to save this time).

Back on the Graph Output window, click STOP to end the run.

[Back to top of Tutorial](#)



Example of Input file –

1

6 # no of tabulation options

'calcium' 'tconc'

'calcium' 'conc'

'calcium' 'act'

'calcium' 'pX'

'GYPSUM' 'conc'

'temp C' 'tconc'

'0.0000000000E+0'

2.5000000000E+1

1.0000000000E-3

'mol/kg' 1.0400000000E+0

1.0000000000E-6

5

'sodium' 1.187920E-1

'potassium' 5.187182E-1

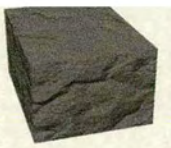
'calcium' 1.825191E-2

'aluminium' 1.553284E-4

'sulphate' 2.621597E-1

'solids off' "

'unfixed pH'



'redox off'

'closed'



Example of Output File -

(Formatting set by SCRAMPC.)

SCRAMPC - A COMPUTER PROGRAM TO CALCULATE
CHEMICAL SPECIATION AND MINERAL SOLUBILITY
IN AQUEOUS ELECTROLYTES

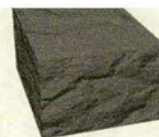
Version 4.0 (PC Version)

Author: Phil Fletcher - Schlumberger Cambridge Research

Input Database: Assigned to Channel 10 Input Datafile: Assigned to Channel

12

Output Data: Channels 007 and 025



This program and the data generated therein are the properties of Schlumberger. They must not be copied or used, in whole or in part, without prior authorisation.

1 Schlumberger Cambridge Research Aquochemical Model

0.0000000000E+0

Temperature 25.00 C

Saturation Pressure 1.000 bar

System Pressure 1.000 bar

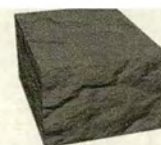
Composition of the Un-Speciated System

	Primary Component	Concentration - mol/kg
1	proton	.0000E+00
2	hydroxide	.1502E+00
3	sodium	.1188E+00
4	potassium	.5187E+00
5	calcium	.1825E-01
6	aluminium	.1553E-03
7	sulphate	.2622E+00

Concentrations of Aqueous Primary Species - mol/kg

	Total Aqueous	Single Ion	Activity	gamma i	-log a
1 proton	.3409E-12	.1287E-12	.9971E-13	.77450	13.0013

Schlumberger Cement Project



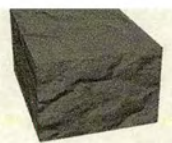
2 hydroxide	.1502E+00	.1454E+00	.9854E-01	.67766	1.0064
3 sodium	.1188E+00	.1004E+00	.6362E-01	.63338	1.1964
4 potassium	.5187E+00	.4453E+00	.2762E+00	.62023	.5588
5 calcium	.1825E-01	.9039E-02	.1110E-02	.12281	2.9546
6 aluminium	.1553E-03	.8049E-31	.1792E-32	.02227	32.7466
7 sulphate	.2622E+00	.1653E+00	.2677E-01	.16200	1.5723

Concentrations of Aqueous Complexed Species and Gases

	mol/kg	log10 Keq	Activity	gamma c	-log a
1 Al(OH)++	.1324E-23	.9254E+01	.3170E-24	.23946	24.4989
2 Al(OH)2 +	.2466E-15	.1899E+02	.1701E-15	.68984	15.7693
3 Al(OH)4-	.1553E-03	.3280E+02	.1072E-03	.68984	3.9700
4 AlSO4+	.7876E-31	.3054E+01	.5434E-31	.68984	31.2649
5 Al(SO4)2-	.1422E-30	.4883E+01	.9807E-31	.68984	31.0085
6 KSO4-	.7346E-01	.8360E+00	.5068E-01	.68984	1.2952
7 NaSO4-	.1835E-01	.9182E+00	.1411E-01	.76877	1.8506
8 Ca(OH)+	.4121E-02	.1415E+01	.2843E-02	.68984	2.5463
9 CaSO4	.5092E-02	.2308E+01	.6041E-02	1.18637	2.2189
10 HSO4-	.2122E-12	-.1201E+02	.2635E-12	1.24208	12.5792

Solid Precipitation/Dissolution Prohibited

pH 13.001



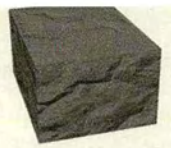
Ionic strength .74220E+00 mol/kg

The activity of water .98337928

SOLUTION SATURATION CONDITION

Number of Possible Minerals is 18

Mineral	IAP/SP	log(IAP)	Condition
K2SO4	.494E+00	-.269E+01	Undersaturated
ETTRINGITE	.235E+01	-.100E+03	Moderate Oversaturation
MONOSULPHOALUMI	.131E+01	-.910E+02	Slight Oversaturation
C4AH13	.121E+01	-.914E+02	Slight Oversaturation
C2AH8	.567E+00	-.815E+02	Undersaturated
C3AH6	.321E+00	-.864E+02	Undersaturated
SYNGENITE	.111E+01	-.722E+01	Slight Oversaturation
BASSANITE	.362E+00	-.906E+01	Undersaturated
CORUNDUM	.784E-01	-.715E+02	Undersaturated
ANHYDRITE	.896E+00	-.453E+01	Undersaturated
GYPNUM	.106E+01	-.454E+01	Possible Equilibrium
LIME	.755E-03	-.496E+01	Undersaturated



POTASSIUM OXIDE	.159E-14	-.312E+01	Undersaturated
BOHEMITE	.144E+00	-.358E+02	Undersaturated
DIASPORE	.236E+00	-.358E+02	Undersaturated
GIBBSITE	.398E+00	-.358E+02	Undersaturated
PORTLANDITE	.132E+01	-.497E+01	Slight Oversaturation
ALUNITE	.951E-02	-.108E+03	Undersaturated

Predictions of Density

Density of Aqueous Phase 1.053 g/cc

Iterations 5 3 3 3 2 2 2 2 1 1 0 0 0

Primary charge balance is 1.501606052000000E-001 mol per kg

Final mass balance is 1.110223024625157E-016 mol per kg

Solution Charge Balance is 7.500950617904384E-017 mol per kg



Reference List

1. Prinz B: Mesolithic Adaptations on the Lower Danube. Oxford: 1987;
2. Petrovic, S. Lepenski Vir : Arhitektura.
<http://www.yuope.com/people/nena/Vir/arhitekt.html> . 1999.
3. Bensted, J. Cements: Past Present and Future. 1997. Woolwich, Greenwich University Press.
4. Lea FM: The chemistry of cement and concrete. London: Edward Arnold, 1970;
5. Michaelis W: Die hydraulische mortel. Publisher unknown., 1867;
6. Le Chatelier H: Recherches experimentales et theoriques sur les equilibres chimique. Annales des Mine 1888; 13: 157-378.
7. Le Chatelier H: Sur un ennonce general de lois des equilibres chimique. Comptes Rendus 1884; 99: 786-789.
8. Tornebohm AE: Title not known. Possibly untitled. Tonind Zeitung 1897; 21: 1148
9. Double DD: New developments in understanding the chemistry of cement hydration. Philosophical Transactions of the Royal Society of London. Series A 1983; 310: 53-66.
10. The Virtual Visit Project, Blue Circle.
<http://omni.bus.ed.ac.uk/ehja36/transient/main/nose.htm>. 1996.
11. Xi Y: Fe₂O₃ Solid solution of ettringite. 9th International Conference on the Chemistry of Cement 1992; 3: 377-383.
12. Kelzenberg AL, Tracy SL, Christiansen BJ, et al: Chemistry of the aqueous phase of ordinary Portland cement pastes at early reaction times. Journal Of The American Ceramic Society 1998; 81: 2349-2359.
13. Michaux M, Fletcher P, Vidick B: Evolution at early hydration times of the chemical composition of liquid phase of oil-well cement pastes with and without additives. 1. Additive free cement pastes. Cement And Concrete Research 1989; 19: 443-456.
14. Clark BA, Brown PW: Phases formed from the hydration of tetracalcium aluminoferrite and magnesium sulfate. Advances In Cement Research 1999; 11: 133-137.
15. Goldschmidt A: About the hydration theory and the composition of the liquid phase of cement. Cement And Concrete Research 1982; 12: 743-746.



16. Fletcher P: Chemical thermodynamics for earth scientists. Harlow: Longman Scientific and Technical, 1993;
17. Fletcher P: A software guide to SCAM - Schlumberger internal document. 1993;



Section 2:

Determining the Origin of Cannabis Resin.



Table of Contents

Table of Contents90

Table of Figures92

1. Introduction94

 1.1 *Why Choose Cannabis?*94

 1.2 *Drugs Gangs in the UK*.....95

 1.3 *Drugs, Internationally*97

 1.3.1 *Case 1 – Hizbollah and Ciudad del Este, Paraguay*.....99

 1.3.2 *Case 2 – The Taliban and Afghanistan.*103

2. *The Drug Trafficking Industry*104

3. *Gleaning Intelligence from Drug Seizure Information*.....106

4. *Cannabis*.....108

 4.1 *Marijuana*.....111

 4.2 *Hashish*.....112

 4.3 *Hash Oil*114

5. *Cannabis Samples Used in This Study*116

6. *Analytical Protocols*117

7. *Previous Work : Chemical Fingerprinting*.....117

8 *Stable Isotope Ratio Analyses*.....120

 8.1 *Introduction to Stable Isotope Ratios*.....120

 8.2 *Isotope Fractionation*.....122

 8.3 *Equilibrium Fractionation*130

 8.4 *Ab initio Calculation of Partial Equilibria*132

 8.5 *Examples of Natural Isotopic Fractionations*135

 8.6 *Metabolic Effects*140

 8.7 *Using Stable Isotope Ratios for Drug Source Region Identification*.....142

 8.8 *Experimental Method*.....146

 8.9 *Results*148

 8.10 *Discussion*.....150

9 *Advanced Biosynthesis Monitoring*154

 9.1 *Introduction*154

 9.2 *Previous Work*.....155

 9.3 *Experimental Method: Gas Chromatography-Mass Spectrometry*158

 9.4 *Results*160

 9.4.1 *Detected Compounds*161

 9.4.2 *Quantification of Results*169



<i>9.4.3 Degradation Rate Estimation</i>	175
<i>9.4.4 Identifying Differences in Biosynthesis</i>	178
<i>9.4.5 Conclusions</i>	182
Future Work	182
10 Project Conclusions	185
Appendix A - Stable Isotope Ratio Measurement Mass Spectrometers.....	186
Appendix B – Proposed Identification of Components in Hashish GC-MS Analysis.	191
Appendix C – Mass Spectra of all Quantified Components of GC-MS analysis of Cannabis.....	192
Appendix D – Dataminer Program.....	203
Reference List	204



Table of Figures

Figure 1 - World major Cannabis production areas. [4].....98

Figure 2 - World major Coca and Opium roduction areas. [4].....98

Figure 3 - Left; Picture of the Bekaa Valley. Right; Map of Lebanon showing Bekaa Valley in the north east. [5].....99

Figure 4 - Map of Paraguay. Note position of Ciudad de Este, on the triple border of Paraguay with Brazil and Argentina, in the south east of Paraguay. [5].....100

Figure 5 - Images of the aftermath of the attack on the AMIA Headquarters in Buenos Aires.....101

Figure 6 - News, of the arrest of Abdul Bari Mirha in connection to the September 11 2001 attack on the World Trade Centre, NY. [13].....102

Figure 7 - Afghan poppy field in March 1999. [16].....103

Figure 8 - Left: Herbal cannabis. Right: Cannabis resin.106

Figure 9 - Left: Hops in flower. Right: *Cannabis sativa* plants.....108

Figure 10 - Examples of cannabinoids. Clockwise from top left; Tetrahydrocannabinol (THC), cannabidiol and cannabinol.....109

Figure 11 - Biosynthesis of THC from geranyl pyrophosphate and olivetolic acid. Adapted from [21] and [22]110

Figure 12 - Marijuana (in this case, dried flowering tops).....111

Figure 13 - Photomontage showing the collection of cannabis resin in Central Asia. [26]112

Figure 14 - Cannabis brick with diamond design stamped onto it. [27]113

Figure 15 - Picture of Hash Oil [29].114

Figure 16 - Pulverised cannabis resin with 1 pence coin for scale.116

Figure 17 - THC oxidises to cannabinol.....118

Figure 18 - Photograph of the enormous K-25 Gas Diffusion Plant at Oak Ridge. As an aid to scale, the building is four stories high!.....125

Figure 19 - Diffusive isotopic fractionation through a single orifice into a closed environment.126

Figure 20 - Schematic representation of the potential energy well experience by bound molecules.....128

Figure 21 - Volumes of water involved in various stages of the water cycle per year. [34]135

Figure 22 - Global pattern of annual evaporation in cm. [35].....136

Figure 23 - World-wide distribution of the annual mean of $\delta^{18}\text{O}$ in precipitation, based on the GNIP data set [36].138

Figure 24 - Meteoric Water Line. Displays relationship between δD and $\delta^{18}\text{O}$ in meteoric water and the latitude at which it is found. [37]139

Figure 25 - C_3 CO_2 fixation. Ribulose biphosphate reacts with CO_2 and H_2O enzymatically catalysed by ribulose biphosphate carboxylase/oxygenase.140

Figure 26 - Initial C_4 CO_2 fixation step (notice 4 carbons in diacid, hence “ C_4 ”). The carboxylation of phosphoenolpyruvate.....141

Figure 27 - Carbon Isotope Ratios of natural, terrestrial, carbon sources. [37]142

Figure 28 - Denton results143

Figure 29 - Carbon and nitrogen Isotope ratios of heroin (black circles) and associated morphine samples (green circles) originating from the main growing regions (1)



Mexico, (2) Southwest Asia, (3) Southeast Asia and (4) South America. After (Ehleringer et al 1999, For Sci Int).....145

Figure 30 - Key for all - **Old Bar**, **New Bar**, **K Bars**. Error bars show standard deviation. Top - $\delta^2\text{H}$ vs. $\delta^{15}\text{N}$. Second Top - $\delta^2\text{H}$ vs. $\delta^{13}\text{C}$. Second Bottom - $\delta^{13}\text{C}$ vs. $\delta^{15}\text{N}$. Bottom - 3D projection of all series.149

Figure 31 - Graph showing data from this project (grouped in red outline) compared with data from the Denton project.....150

Figure 32 - Map showing approximate sources of the Denton samples.151

Figure 33 - Map of Morocco showing relative spread of sites samples in Queensland (to same scale).....152

Figure 34 - Graph of Total Truxilline (w/w%) vs. Trimethoxycocaine (w/w%) for Ehleringer cocaine samples. (After [45]).....156

Figure 35 - Identification of geographic regions in South America where cocaine is commonly grown. Left - regions from which samples were taken. Right - plot of results of stable isotope and chemical analyses, grouped by sampling region. X-axis - $\delta^{13}\text{C}$ - ($10 \times [\text{trimethoxycocaine}]$). Y-axis - $\delta^{15}\text{N} + (0.1 \times [\text{truxilline}])$. (After [45]).....157

Figure 36 - Example Chromatogram showing results of a GC-MS analysis of hashish. Peaks corresponding to cannabinoid components are numbered. Two chromatograms are shown as not all components were expressed in all chromatograms.160

Figure 37 - Example chromatogram showing peaks A and B as used in the explanation of Peak Normalisation.169

Figure 38 - Dataminer's user interface showing No Isotopes output window.....171

Figure 39 - Dataminer showing Isotopes output window.173

Figure 40 - Dataminer showing Scale and Components output window.....174

Figure 41 - Graph showing amounts of cannabinoids in resin after different time periods.....176

Figure 42 - Biosynthesis of THC showing relationship to cannabigerol and cannabidiol. (Copy of Figure 11).178

Figure 43 - Both graphs show total original THC content (THC+CBN) normalised against CBG vs. CBD normalised against CBG. Bottom graph is a magnification of the upper graph to show detail.180

Figure 44 - Graph of cannabidiol vs total THC showing two parallel groups.181

Figure 45 - Schematic of the main components of an isotope ratio mass spectrometer.186

Figure 46 - Diagram of detector array and circuitry in a conventional SIRMS instrument.189



1. Introduction

The aim of this project was to develop analytical techniques for the determination of the source regions and distribution networks of the illegal cannabis trade. This information could then be used to probe national and international organised crime and terrorism, acting as an alternative to current intelligence techniques.

1.1 Why Choose Cannabis?

Cannabis is largely ignored by intelligence services (both national security and criminal intelligence) compared with the attention paid to other illegal drugs. This may be, in the UK at least, a symptom of the system whereby the scope of the attention of intelligence services is set by government [1], and therefore heavily influenced by broad public opinion. As cannabis is viewed as a low priority, low impact drug by the public, the government instructs the security services to concentrate on more high profile “hard” drugs such as cocaine and heroin, at the expense of cannabis.

There can be little doubt that the primary effects, behaviour of users under the influence, addiction etc., of cannabis have a considerably lower social impact than “harder” drugs. However, the secondary effects, other crimes and activities associated with the drugs industry, which are often ignored, are of major importance.



1.2 Drugs Gangs in the UK

Data from Her Majesty's Customs and Excise and the National Criminal Intelligence (NCIS) Service [2] confirm the importance of cannabis in the UK drugs trade:

- In 1997, the last year for which data are publicly available, 75% of all drug seizures in the UK were of cannabis.
- 150 tons of cannabis were seized (30 times the amount of cocaine and heroin combined).
- 56% of all organised criminal gangs deal in drugs, usually multiple drugs.
- The vast majority of drugs gangs are also involved in other criminal activities.

Table 1 shows a breakdown of the other crimes committed by drugs gangs, as published by NCIS (2000 UK Threat Assessment) [2].



Table 1 - Table showing crimes associated with organised drugs gangs.[2]

Crime	% of Drugs Gangs Involved	Crime	% of Drugs Gangs Involved
Money Laundering	79	Counterfeiting/Forgery	26
Inland Revenue Fraud	23	Excise Fraud	21
Vehicle Theft	21	VAT Fraud	21
Other Theft	19	Arms Trading	18
Social Security Fraud	17	Robbery	16
Extortion	13	Other Serious Fraud	12
Kidnapping	11	Illegal Immigration	9
Art and Antiques Theft	7	Prostitution	6
Illegal Gambling	5	Child Pornography	1
		Other Illegal Activities	10

The public perceives that certain drugs are more damaging than others, irrespective of the actual national magnitude of the damage done by particular drugs, and therefore these drugs receive more attention from the media, the government and other agencies. It is a matter of interest that the crimes listed in Table 1 are also commonly viewed through the distorted eyes of public perception, and opinion of their importance is often a result of sensational media coverage and politically motivated “spin”. For example, child pornography and illegal immigration are heavily covered in the media and receive much governmental discussion. These are of course serious



crimes for those individuals concerned, but they probably affect a far smaller number of people than crimes such as Social Security Fraud and Counterfeiting, where the criminals are, sadly, sometimes perceived as being mere rogues.

Cannabis is the most widely used illegal drug in the UK (in fact three times as common as the next most common drug, ecstasy*)[2]. As most criminal gangs deal in multiple drugs and other serious criminal activities [2], cannabis offers a very large target for intelligence gathering on these multi-arm criminal gangs and their connections. For this reason, we decided to concentrate on cannabis analysis.

1.3 Drugs, Internationally

On the global scale, a larger picture can be seen. It is apparent, from Figures 1 and 2, that many of the areas of global drug production are the same as areas associated with terrorism and international organised crime, e.g. Colombia and Afghanistan. What is not clear from the map are the covert connections of certain terrorist groups to production areas [3]. Two examples of these connections are found in Paraguay and Afghanistan.

* 3, 4-Methylenedioxyamphetamine (MDMA)

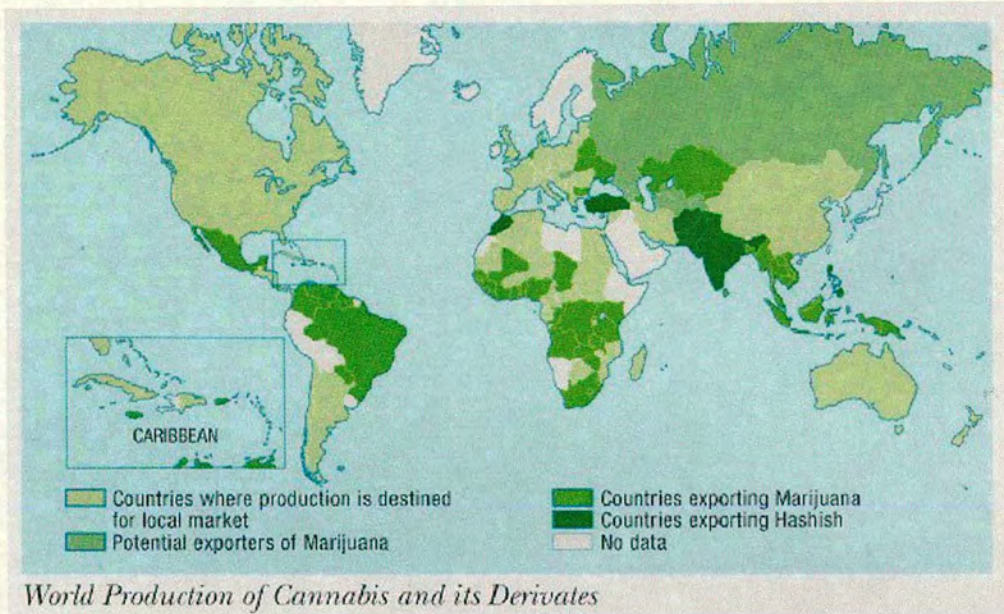


Figure 1 - World major Cannabis production areas. [4]

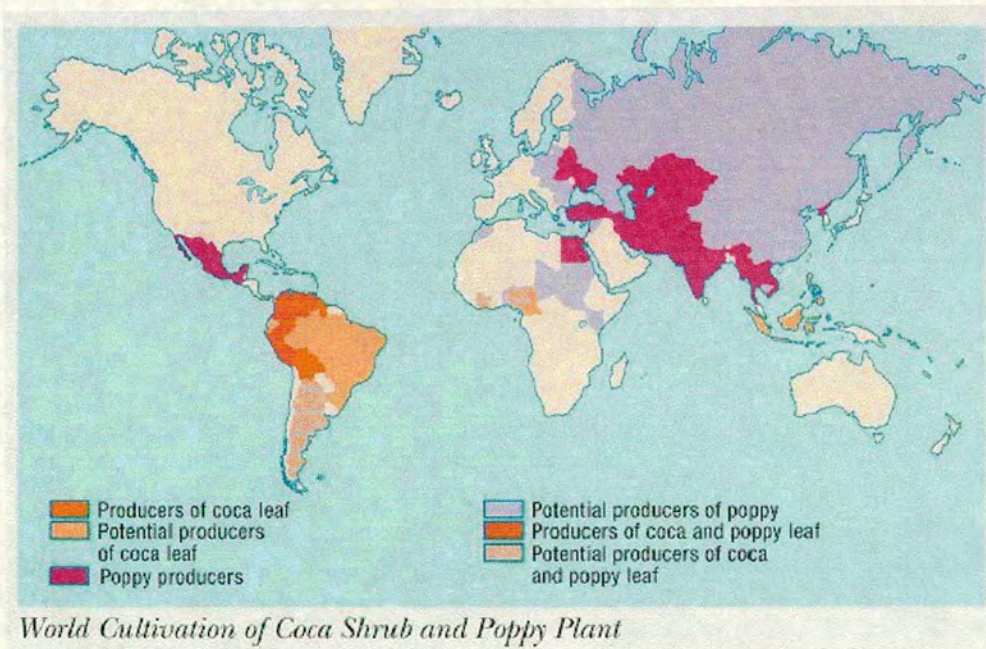


Figure 2 - World major Coca and Opium roduction areas. [4]



1.3.1 Case 1 – Hizbollah and Ciudad del Este, Paraguay

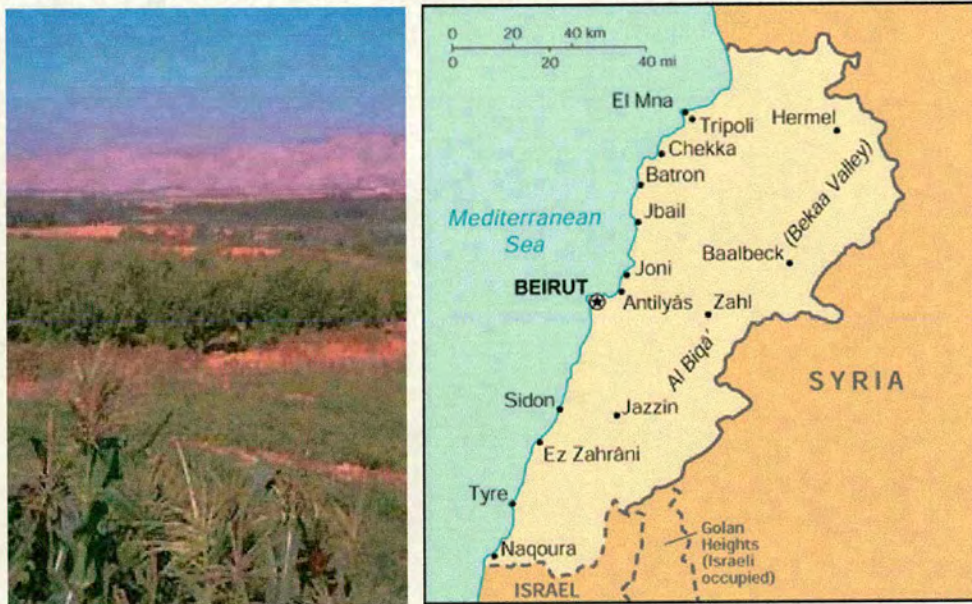


Figure 3 - Left; Picture of the Bekaa Valley. Right; Map of Lebanon showing Bekaa Valley in the north east. [5]

Up until the end of the Lebanese Civil War, in 1991, the Bekaa Valley in the Lebanon (See Figure 3) was a major global production area for cannabis and opium. The proceeds of this crop were an important funding source for the Islamic terrorist group, Hizbollah, amongst others [6]. Since the end of the civil war, the Lebanese Authorities, with Syrian backing, have clamped down on the drug growing areas and production has decreased dramatically [5]. However, this has apparently had little effect on the finances of Hizbollah, as it has relocated much of its drugs operations to South America.

Determining the Origin of Cannabis Resin



The frontier town of Ciudad del Este sits on the banks of the Rio Parana in the so-called “tri-border” region where Paraguay, Brazil and Argentina meet. Thanks to the endemic corruption and mismanagement that pervade Paraguayan national affairs, the remoteness of the area and its proximity to two populous, relatively rich countries, Ciudad del Este has become one of the most important criminal border crossings in South America, if not the world. It is particularly infamous as a centre for smuggling counterfeit goods [7], stolen vehicles and drugs, notably cocaine [8] and cannabis [6]. The main source regions for the drugs that pass through Ciudad del Este are Colombia, Bolivia and Paraguay itself. It has been estimated that 3 tons of cocaine pass through Ciudad del Este per month. [6]



Figure 4 - Map of Paraguay. Note position of Ciudad de Este, on the triple border of Paraguay with Brazil and Argentina, in the south east of Paraguay. [5]

Ciudad del Este is fairly small; reliable population information is sparse (a reflection of the lawless nature of the city), but it is estimated to have a population of



somewhere between 90,000 and 250,000. Of these, approximately 30,000 are of Arabic origin [6]. The Arab speaking proportion of the population is so large that Ciudad del Este is the home of South America's only Arabic language TV station. Argentinean authorities estimate that 60% of the billion dollar economy of Ciudad del Este is controlled by the Arab minority. [9]

The Brazilian, Paraguayan and Argentinean authorities are investigating a number of Islamic Fundamentalist groups in Ciudad del Este. They have uncovered links to both Hizbollah and Islamic Jihad. Even before the September 11 2001 attacks on the World Trade Centre, the local authorities were investigating terrorist attacks on the Israeli Embassy and the Jewish AMIA Headquarters, both in Buenos Aires, in 1992 and 1994, respectively, which resulted in 114 deaths. [10] (See Figure 5).



Figure 5 - Images of the aftermath of the attack on the AMIA Headquarters in Buenos Aires.

In 2000, Ahmad Behbahani, an ex-Iranian spy living in exile in Turkey, blamed the Popular Front for the Liberation of Palestine for the attack on the Asociación Mutual Israelita Argentina (Argentine Israelite Mutual Aid Association or AMIA) Headquarters and implicated the Iranian secret service [11]. Indeed investigations have shown that some Iranian agents did enter Argentina through Ciudad del Este.



However, the Argentinean Authorities are following up a different of a Hizbollah agent also with connections to Ciudad del Este [12]. In either case the connection with the Ciudad del Este drug trade is considered firm [10].

Since the September 11 2001 attack on the World Trade Center there have been seventeen connected arrests, in and around Ciudad del Este. Figure 6 shows the arrest of one of these, Abdul Bari Mirha [13]. The national banks of Brazil and Argentina are tracing the finances of a number of Arab families associated with Islamic fundamentalist groups and the Ciudad del Este drug industry.



Figure 6 - News, of the arrest of Abdul Bari Mirha in connection to the September 11 2001 attack on the World Trade Centre, NY. [13]



1.3.2 Case 2 – The Taliban and Afghanistan.

On the other side of the world, despite their supposed anti-drugs stance, the Taliban authorities in Afghanistan profited hugely from the sale of heroin after they imposed a tax on poppy sales [14]. In 1986, the Afghan opium crop was estimated at 350 tons and in 1992/1993, the opium crop was cultivated on 20,000 hectares (US State Department figures). By the 1999/2000 season, the area had increased to 91,000 hectares and the total mass of dry opium produced rose to 3656 tons [15]. This despite the fact that the Taliban had supposedly banned poppy cultivation in 1997 and had promised to cut production down by a third in 1999. United Nations Drug Control Program Inspectors saw no downturn in production either year. The 2000 figure represents 72% of the global total illicit opium produced that year. (See Figure 7).



Figure 7 – Afghan poppy field in March 1999. [16]



The Taliban's grand panjandrum, Amir-ul-Momineen, Mullah Omar, officially imposed a new ban on poppy cultivation in July 2000. While most sources agree that probably 90% of opium production in Afghanistan had been stopped, following brutal enforcement of the ban by Taliban militia, more cynical observers have pointed out that just before the ban was imposed, the price of opium had begun to drop dramatically due to over supply. After the ban, the price of raw opium increased dramatically [17], so that the remaining stockpiles held by the Taliban were now worth substantially more than before, and the Taliban had (temporarily) improved their international public relations by enforcing the ban.

After the beginning of American bombing of Afghanistan, the Taliban began to sell their stockpiles of opium at the new, inflated prices.

These two examples should reinforce the erroneous nature of the claim that as cannabis is considered a low impact drug, there is little value in studying its movements. In reality, drug trafficking organisations deal in multiple drugs alongside cannabis, and are intimately associated with other serious crimes both on a local and international scale.

2. The Drug Trafficking Industry

The United Nation Drug Control Program, based in Vienna, estimates that the global drugs trade is worth around \$400 billion per annum[18]. This was almost double the annual defence budget of the USA in 2001[19]. Controlling any industry of this



magnitude requires a high degree of sophistication and organisation [8], and as an additional complication, the illegal drugs industry must carry out its business in secret.

The illegal drugs industry is very bottom heavy: there are a relatively small number of big dealers and importers feeding a very large number of street level dealers. The groups controlling the growth areas are not necessarily the same as those who deal in the long distance transportation or the final selling. Each time a shipment passes from the hands of one group to another is a security risk. For this reason, such handovers must be kept to a minimum and only involve groups between which there is a mutual trust. This probably results in a fairly static chain of supply between harvesters and small scale dealers where each link of the chain trusts their own suppliers and clients, but probably knows little about the rest of the chain. In this respect these set-ups resemble traditional spy rings.

Evidence supporting this view is in the public domain. For example, cannabis supplied to Cambridge mainly comes in herbal form, whereas in Edinburgh, resin predominates. The difference in the product, herbal versus resin (See Figure 8), supplied to each area is a reflection of their different sources, and the fact that the products are not mixed *en route*, supports the theory that the chains remain unconnected. That this state of affairs has existed over a period of time, supports the theory that these supply chains remain reasonably constant over long periods of time.



Figure 8 - Left: Herbal cannabis. Right: Cannabis resin.

3. Gleaning Intelligence from Drug Seizure Information

The inherent secrecy of drugs gangs is often backed up by the real threat of extreme violence. This makes it dangerous, as well as difficult for a criminal intelligence agency to infiltrate a drug supply chain at a significant level, and therefore another technique is required in order to gather information on the trafficking gangs.

Imagine if drugs bore some chemical signature from where they were grown.

At the most basic level, it would then be possible for the police in one area to analyse seizures of drugs from street level, small scale dealers and trace them back into larger batches from which they originally came. They would then be able to group together all the small dealers depending on what batches they were selling. All the dealers in one group must be connected by a single supplier somewhere up the chain.



If drugs seized in many places around the country bore the same signature, then a very large traffic must be involved, and at some stage, all these seizures probably came through a common point.

In fact, whatever point on the supply chain a seizure was made, the authorities would be able to tie it into a bigger picture. This information would allow police and criminal intelligence agencies to target their investigations towards the largest and most important traffickers.

In addition, if drugs were collected from known growth areas and analysed, and this information stored as a global database, the original source of drug seizures could be quickly ascertained. This information could give vital evidence of the effect of anti-drug measures taken in growth areas or could provide clues to new growth areas etc.



4. *Cannabis*

Cannabis is a member of the Hemp family, *Cannabaceae*, which also includes hops.

(See Figure 9)



Figure 9 – Left: Hops in flower. Right: *Cannabis sativa* plants

There are believed to be up to three species of *Cannabis*; *C. sativa*, *C. indica* and *C. ruderalis* [20]. All three produce psychoactive chemicals in varying levels. These psychoactive chemicals are members of the cannabinoid group of prenylated polyketides (See Figure 10).

Cannabis is thought to have originated in central Asia, but as it has been cultivated since prehistoric times, it is difficult to be precise about its origins.

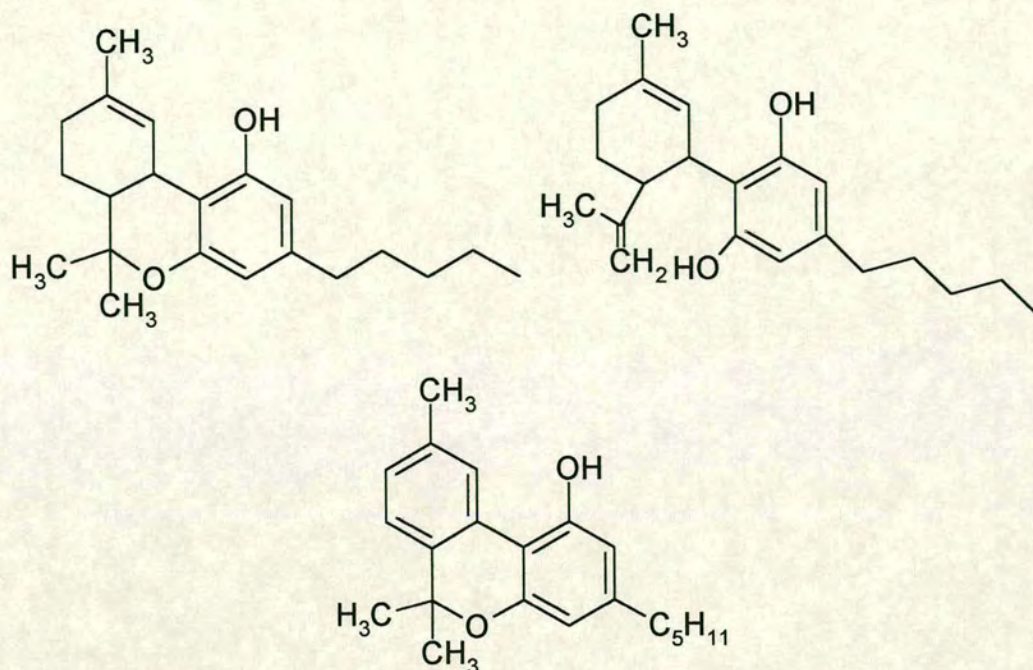


Figure 10 - Examples of cannabinoids. Clockwise from top left; Tetrahydrocannabinol (THC), cannabidiol and cannabinol.

The biosynthesis route of the most abundant psychoactive cannabinoid, THC, is not completely understood, but it is thought to be biosynthesised from geranyl pyrophosphate and olivetolic acid [21] and [22] (See Figure 11).

Determining the Origin of Cannabis Resin

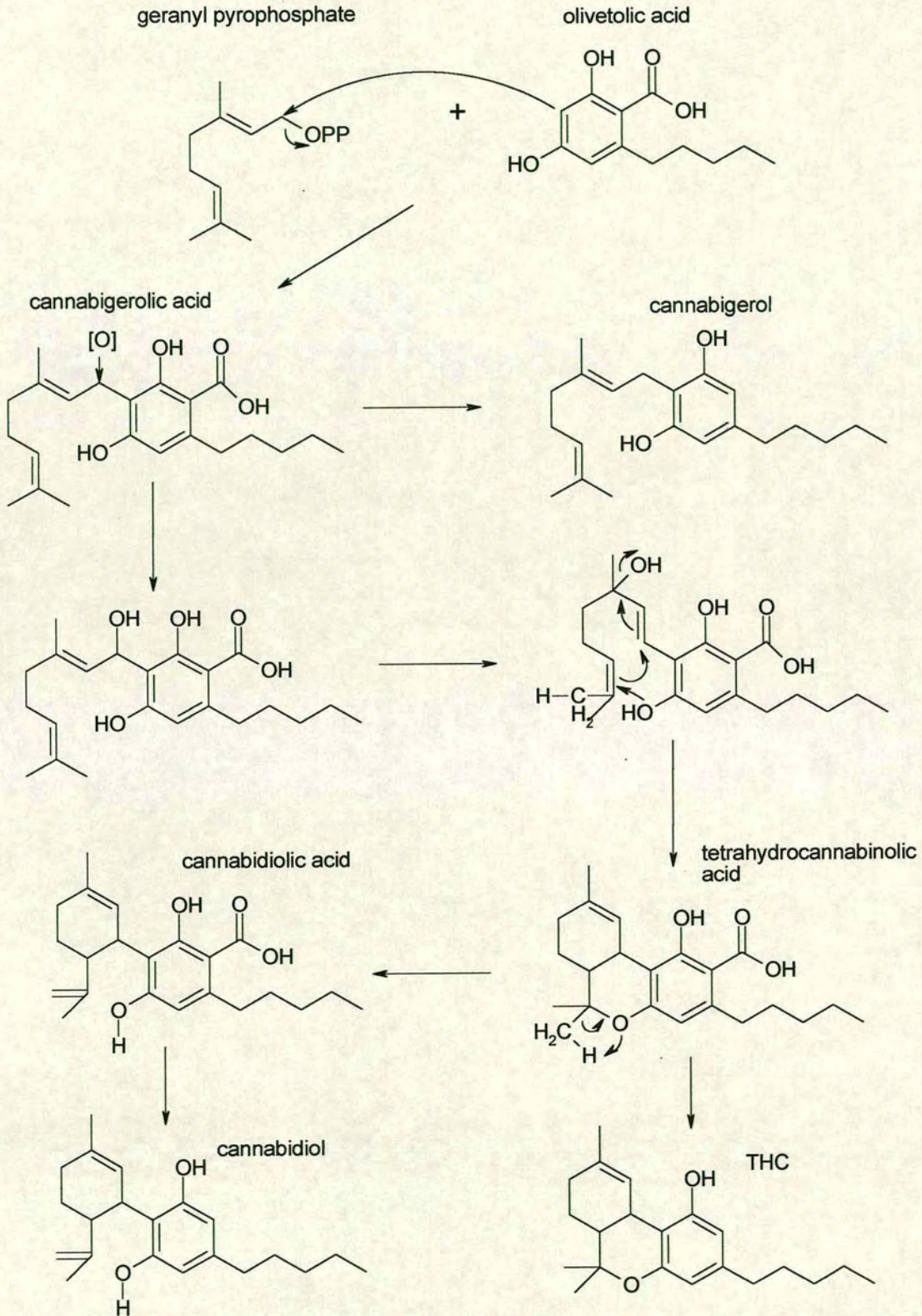


Figure 11 - Biosynthesis of THC from geranyl pyrophosphate and olivetolic acid. Adapted from [21] and [22]



The drug producing capacity of cannabis has been artificially enhanced in some varieties by selective cultivation. For example, US Government figures show that the THC content of marijuana seized in the USA, increased from <1.5% in 1980 to 4.2% in 1997 as a result of selective cultivation [23].

Cannabis, in drug form occurs as marijuana (herbal form), hashish (resin form) or as an oily extract (hash oil).

4.1 Marijuana

The herbal form of cannabis, usually known as marijuana, is the leaves and flowering tops of the cannabis plant (See Figure 12).

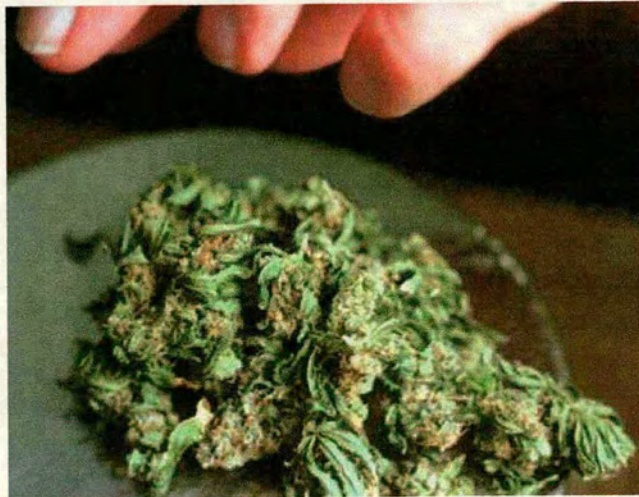


Figure 12 - Marijuana (in this case, dried flowering tops).

It is usually taken by smoking (either by itself or with tobacco) or by ingestion.



4.2 Hashish

Cannabis plants exude a resinous material from the flowering tops as they grow. This material is rich in cannabinoids and is collected and sold as “hashish”. The method of collection differs by region, but in Central Asia, it is generally collected by hand and rolled into small balls (See Figure 13).

In other areas, it is collected by the seemingly improbable method of donning a leather apron and running through the field. The resin is rubbed from the plant during the run onto the apron and is collected from the apron between runs [24] [25].

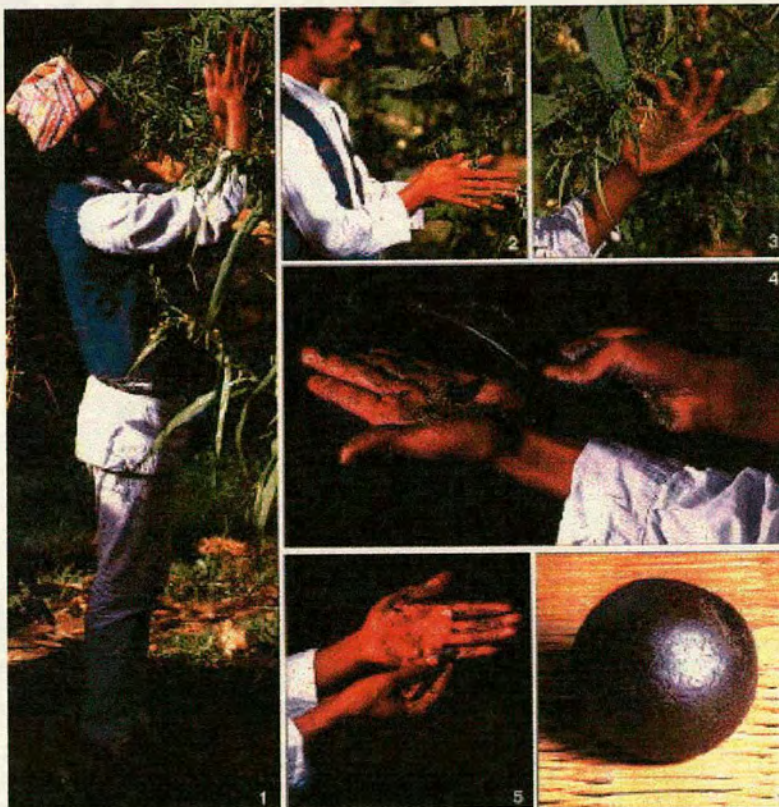


Figure 13 - Photomontage showing the collection of cannabis resin in Central Asia. [26]



Once collected, in whatever manner, the resin is compressed into larger bricks for export and stamped with an identifying mark (See Figure 14). The morphology of the bricks and the identifying designs stamped onto them are not, however, good indicators of origin. As certain regions are reputed to produce resin of high potency, resin from these regions carries a higher price. Therefore, suppliers from other regions disguise their product to resemble the more valuable product by copying the morphology of the bricks and the identifying stamps on them.



Figure 14 - Cannabis brick with diamond design stamped onto it. [27]



4.3 Hash Oil

“Hash Oil” is produced by boiling off the excess solvent from an organic extract of either of the other forms of cannabis. Various recipes are available in books [28] or on the internet, but most are some elaboration of:

1. Finely grind or chop the raw material.
2. Add an organic solvent (e.g. petrol, alcohol, etc.)
3. Leave for a period of time.
4. Filter off solids.
5. Repeat 2-4 with the solids and new solvent.
6. Combine the two extracts.
7. Boil off most of the solvent leaving a dark brown, dark green or honey coloured oil.



Figure 15 - Picture of Hash Oil [29].

As if boiling off large volumes of flammable solvent was not bad enough, the chosen method of using Hash Oil is to, using an eye dropper, place two or three drops in the



centre of a tin-foil “spoon” (specially crafted for the purpose). Then, holding an empty BIC pen tube, or something similar, over the top, heat the underside with a cigarette lighter, and inhale the vapour.



5. Cannabis Samples Used in This Study

By far the most common type of cannabis encountered in Edinburgh is hashish. Therefore, it was decided to concentrate the research on this substance.

22 samples of cannabis resin were obtained from the Lothian and Borders Police Forensic Laboratories. These were split into three groups:

- 1) Large “Old Bar” - 2 samples of a 20 year old large cannabis resin bar.
- 2) Large “New Bar” - 9 samples of a 4 year old seized large cannabis resin bar. Samples were taken from different points on the bar to highlight any heterogeneity. Additionally, 1 sample of a mixture of all points across the bar.
- 3) 10 “K” samples - samples of 10 smaller seized cannabis resin finds.

All samples were ground to a fine powder (See Figure 14).



Figure 16 - Pulverised cannabis resin with 1 pence coin for scale.



6. Analytical Protocols

This section describes the three stages in the search for an analytical protocol capable of distinguishing different cannabis batches.

7. Previous Work : Chemical Fingerprinting

Chemical Fingerprinting is a technique whereby samples are analysed for their component chemicals, and the amounts of these chemicals, that they contain. These patterns are matched between related samples. This technique is used to confirm the source of oil spills.

An early study of this type was carried out by The Home Office Central Research Establishment (H.O. CRA) in 1973[30]; analysing for the relative amounts of the three principal cannabinoids (Tetrahydrocannabinol (THC), Cannabinol and Cannabidiol) in marijuana and hashish samples by gas chromatography*. While this experiment was successful to a certain extent, some of the conclusions drawn must be re-examined. The principal error was the discussion of an increase in THC, relative to cannabinol, in samples from Pakistan. In the paper, Jenkins and Patterson initially hypothesise that the difference may be due to seasonal climactic or harvesting differences. The possibility of the, now well recognised, oxidation of THC to cannabinol is only given a secondary mention, although we now know that this

* 1/2inch OD, 6ft column packed with 60-80 mesh Chemsorb. Temp 120 degrees Centigrade.



process is in fact the principal cause of the relative decrease in the amount of THC compared with cannabinol (See Figure 17).

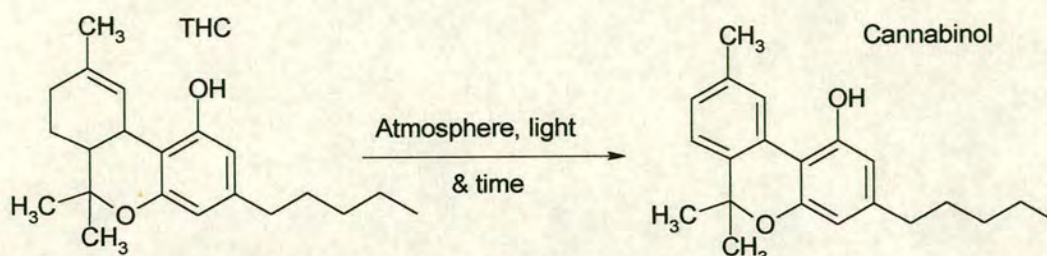


Figure 17 - THC oxidises to cannabinol.

The conclusions of the H.O. CRA report were that although it was possible to prove that the samples from one country could be grouped by analysis of their principal cannabinoids, many countries' sample groups showed significant overlap with those of other countries. They therefore concluded that the method might be used to indicate changes in the source region supplying an area, but that it would not be possible to define what the source area was by chemical analysis alone.

The results of the H.O. CRA work probably showed that, in 1973, there was a small number of cultivar strains of *Cannabis Sativa* being grown by drug producers around the world. Wild type cannabis contains very low levels of psychoactive components. Selective cultivation is responsible for the production of plants with significant quantities of the active cannabinoids in them. As the world's drug producers have become more technologically advanced, and as the drug trade has matured, more emphasis has been put on potency of the final product. This, in turn has led to increased selective cultivation, so that there are now a larger number of cultivar



strains in existence. The different histories of these strains may be reflected in their composition.

Following on from the H.O. CRA work, The Lothian and Borders Police Forensic Laboratory completed their own study into the potential of chemical fingerprinting applied to cannabis analysis in September 1998 [31;32].

They took a number of samples from two seized cannabis resin bars (The “Old” and “New” bars used in this study) and, again, analysed the relative amounts of the principal cannabinoids by GC-MS.

The variation in the absolute cannabinoid content of samples was significant, even between samples from the same bar. Therefore, they concluded that analysis of the principal cannabinoids was not a good technique to use for grouping batches of cannabis.

In retrospect, this result is not surprising. When cannabis resin is harvested, it is not mixed, but is merely pressed into shape. (See Figure 13) The lack of a homogenising step, such as mixing, combined with the known degradation of primary cannabinoids after harvesting leads to these significant variations in composition over short distances (~5mm) in seized resin bars. This error has been repeated over many studies (including [33]), and is discussed further in “Advanced Biosynthesis Monitoring” below.



8 Stable Isotope Ratio Analyses

Having studied the Police research, it was decided that the goal of grouping cannabis seizures back into their original batches or determining the source region of the drugs should be attained by a different method. The method chosen was Stable Isotope Ratio Analysis.

8.1 Introduction to Stable Isotope Ratios

Isotopes are nuclides of the same element that have different atomic weights. They are written with their approximate mass as a superscript prefix to the chemical symbol. E.g. carbon 12, the most common isotope of carbon, is written as ^{12}C . Isomers of the same molecule where the only difference is the presence of different isotopes are known as isotopomers. e.g. $^1\text{H}^1\text{H}^{16}\text{O}$ and $^2\text{H}^1\text{H}^{16}\text{O}$ are two of the isotopomers of water.

For most elements, one isotope is predominant. The predominant isotope is known as the major isotope and the other(s) as the minor isotopes. (See Table 2)



Table 2 - Table showing elemental isotopic composition and relative abundance.

Element	Isotope	Protons	Neutrons	Average Abundance (%)
Hydrogen	¹ H	1	0	99.985
	² H	1	1	0.015
Carbon	¹² C	6	6	98.90
	¹³ C	6	7	1.10
Nitrogen	¹⁴ N	7	7	99.63
	¹⁵ N	7	8	0.37

The extent of isotopic fractionation is expressed as a “delta value” in parts per thousand.

$$\delta_x = 1000 [(R_x/R_{std})-1]$$

where δ_x is the delta value of the isotope, R_x is the ratio of that isotope to the major isotope within the sample and R_{std} is the ratio of that isotope to the major isotope in the standard for that element. These isotope standards are kept by the International Atomic Energy Authority. (See Table 3)



Table 3 - Table of isotopic ratio standards and their relative isotopic abundances.

Element	Standard	Minor Isotope Abundance (%)
Hydrogen	Standard Mean Ocean Water (SMOW)	0.01557
Carbon	Peedee belemnite (PDB)	1.12372
Nitrogen	Atmospheric Nitrogen	0.36765
Sulphur	Canyon Diabolo troilite (CDT)	4.50045

As an example, the isotopic fractionation of the ^{13}C isotope would be calculated:

$$\delta^{13}\text{C} = 1000 \left[\left(\frac{^{13}\text{C}/^{12}\text{C}}{^{13}\text{C}/^{12}\text{C}} \right)_{\text{sample}} / \left(\frac{^{13}\text{C}/^{12}\text{C}}{^{13}\text{C}/^{12}\text{C}} \right)_{\text{PDB}} - 1 \right]$$

Absolute measurements of isotopic abundance are not taken as these are very small and are prone to relatively large errors. Measuring against a standard removes many of these errors and increases the sensitivity and resolution of the technique.

8.2 Isotope Fractionation

If isotopic ratios were constant the world over, their study would elicit scant interest. Fortunately, this is not the case. The isotopic abundances given in Table 2 are global averages. There are a number of processes that cause these to vary, one way or the other, over the surface of the earth (and even within it). This is known as isotopic fractionation. Isotopic fractionation can occur in systems under both non-equilibrium



and equilibrium conditions. Examples of non-equilibrium processes that lead to fractionation are diffusion, evaporation/condensation, metabolic processes and the kinetic isotope effect.

All of the fractionation processes, however, are manifestations of two fundamental differences between isotopomers:

i) The Kinetic Energy Difference.

The kinetic energy of molecules is proportional to their temperature.

$$kT \propto E_K = \frac{1}{2}.mv^2$$

where E_K is the kinetic energy, k is the Boltzmann constant, T is the temperature, m is the mass of the molecule and v is the velocity.

By this relationship, heavier isotopomers have lower translational velocities.

Therefore, lighter isotopomers have a longer path length per unit time and are more likely to hit a target during that time.

Hence:

- a) Lighter isotopomers are more likely to collide with other molecules, and react, and**
- b) Lighter isotopomers diffuse faster.**



Example – Diffusive Fractionation

(It should be noted that in the following discussion, diffusion and effusion are collectively described as diffusion alone, as is the convention.)

Imagine a container of a gas, say CO_2 , at a certain temperature.

The Kinetic Energy Difference Effect states that, as the mass of the molecule increases, the velocity must decrease. Therefore, in our CO_2 bottle, those molecules containing $^{12}\text{C}^{16}\text{O}^{16}\text{O}$ will move faster than those molecules containing $^{13}\text{C}^{18}\text{O}^{18}\text{O}$. The other isotopomers will have velocities somewhere between these two end members.

Now, if there was small hole in the side of the bottle, then the faster molecules, i.e. those containing the lightest isotopes, would have a statistically higher chance of encountering the hole and escaping during any given time period than the slower, heavier, molecules. Therefore, the gas left inside the bottle will become richer in the heavier isotopes while the escaped gas will be isotopically lighter.

This process was used during the Manhattan Project (the WWII project to develop the atomic bomb) to separate the ^{235}U , used in the bombs from the more abundant ^{238}U . The uranium was converted to volatile UF_6 , which was allowed to diffuse through filters to fractionate it. As the relative difference in mass between ^{235}U and ^{238}U is not large and therefore the velocity difference is low, the diffusion process had to be



carried out on a large scale in very long diffusion columns with multiple diffusion stages. The process was carried out at the Oak Ridge Facility in Tennessee in the K-25 plant (See Figure 18).

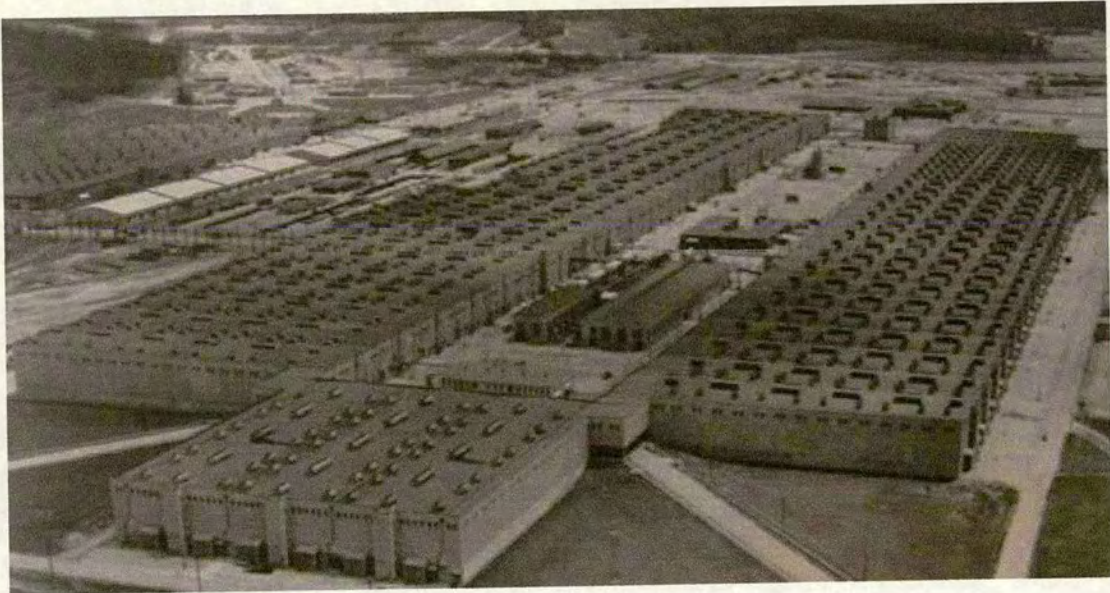


Figure 18 - Photograph of the enormous K-25 Gas Diffusion Plant at Oak Ridge. As an aid to scale, the building is four stories high!

To return to our CO₂ bottle with the hole, if the system was enclosed, so that there was no loss of any of the components, the system would approach equilibrium where the components were completely mixed. The more evenly mixed the system, the lower the fractionation. So, as the system approaches equilibrium, the isotopic fractionation would return to zero. (See Figure 19)

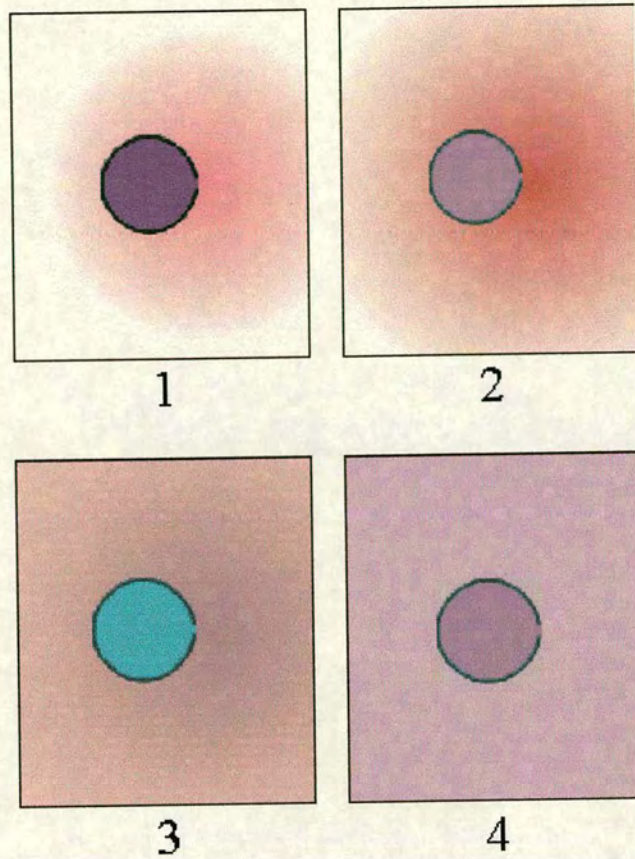


Figure 19 - Diffusive isotopic fractionation through a single orifice into a closed environment.

Figure 19 shows this diffusion effect. Starting with (1), there is a gas bottle containing a mixture of a red and a blue gas; hence it appears purple. It is enclosed in a box containing a colourless gas. There is a small hole in the right hand side of the bottle through which the gasses are diffusing. The cloud of gas that has escaped through the hole has a red tinge because it contains relatively more of the more of red gas. This is because the red gas is lighter than the blue gas, and so it has diffused faster.

A short time later, in (2), more of the gas from inside the bottle has diffused through the hole. The gas cloud outside the bottle is still mainly red gas, but by this time some



blue gas has also escaped, so the escaped cloud is a bit bluer in the middle than the fringes (which escaped earlier). Because more red gas than blue gas has escaped, the gas left in the bottle is a bit bluer.

Similarly, by the time we reach (3) red gas is still escaping faster than blue gas, so the bottle is more blue, but the relative amount of blue gas escaping is also increasing, so the escaped cloud is also a bit bluer.

By the time we reach (4), the two gas clouds have completely mixed. This is the equilibrium condition (entropy is maximised). Notice how the gas concentrations are equal through the entire box. By the time a closed diffusing system has reached equilibrium; however, the fractionation that was created at the beginning of the diffusion process has been reversed, and the overall fractionation is zero.

Notice that the greatest fractionations of the red gas occurred in (1) outside the bottle and the greatest fractionation of the blue gas occurred in (3) and inside the bottle.

ii) The Binding Energy Difference

Between any two atoms or molecules, connected by a chemical or physical bond, there are two competing forces: attraction and repulsion. The attractive force varies between two end members of a series, from being approximately proportional to r^{-2} in ionic solids to r^{-7} , between uncharged molecules. The repulsive force is approximately proportional to r^{-13} . (“ r ” is the distance between the two molecules.) If one of the molecules is placed at the origin, the other will reside in the potential



energy well created by the combination of the opposing forces (attraction - repulsion)

(See Figure 20).

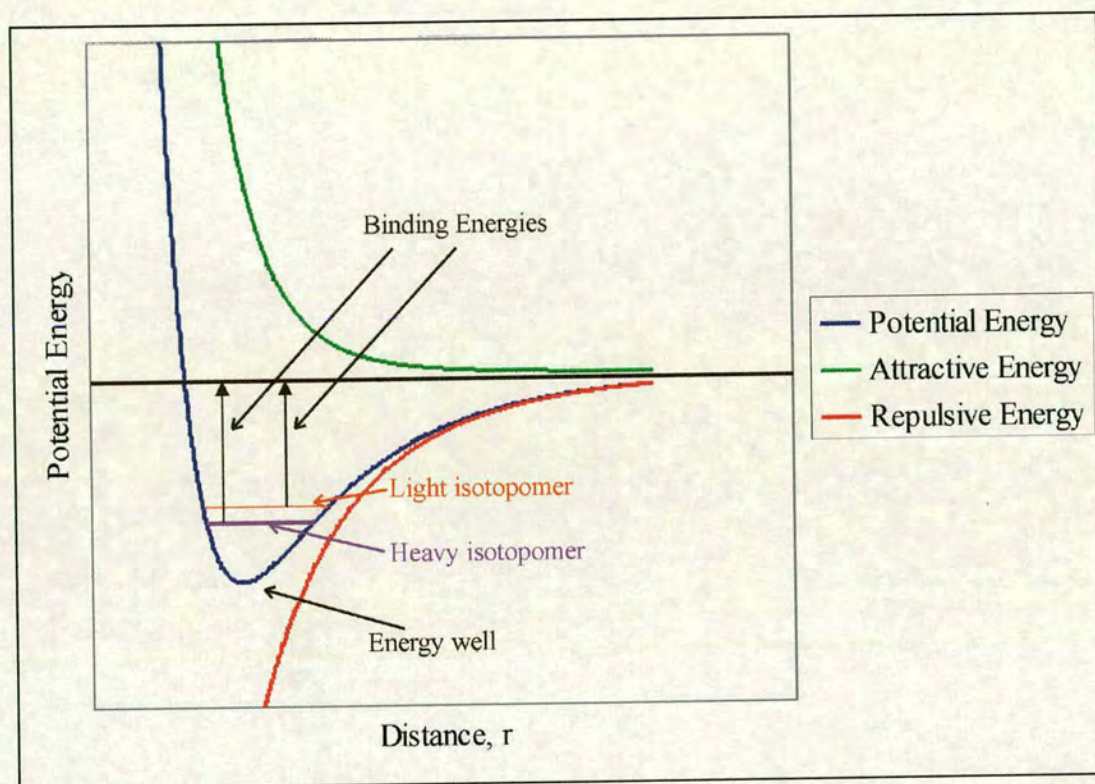


Figure 20 – Schematic representation of the potential energy well experience by bound molecules.

Molecules never rest at the bottom of the well even at zero kelvin. Their height above the bottom of the well is the sum of their translational, rotational and vibrational energies. With the molecule at the origin at rest, the other molecule will vibrate between the maximum and minimum distances (“r” values) available to it. Raising the temperature of the system will raise the molecule further up the energy well which will increase the amplitude of these vibrations. The distance below zero potential energy, i.e. the energy at which the molecule would escape from the well, is known as the “Binding Energy”. An example of this is heat of evaporation.



The frequency of vibration is given by the formula:

$$\omega = \frac{\sqrt{k/\mu}}{2\pi}$$

where ω is the frequency in Hz, k is the force constant of the bond, μ is the reduced mass and c is the speed of light.

As

$$E = h \cdot \omega$$

where E is energy and h is Planck's constant, we can also write:

$$E = (h \cdot \sqrt{(k/\mu)})/2\pi$$

i.e. as the mass increases, the energy decreases (See Figure 20).

Therefore, **bonds containing heavier isotopes are deeper in the potential well, have greater binding energies and are therefore more stable.**



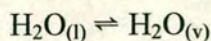
Example - The Kinetic Isotope Effect

It has been shown above that the replacement of an atom at one end of a covalent bond, for a heavier isotope decreases the bond vibration frequency, and that this decrease in vibration frequency strengthens the bond. Consider then a bond, the breaking of which is the rate-determining step of a reaction. If the atoms at the ends of this bond are isotopically light, then the bond vibration frequency will be higher, and the bond weaker than the same bond where heavy isotopes are involved. Therefore, the isotopically light versions are more likely to react in an incomplete reaction, and therefore, under these circumstances, the products of incomplete reactions are likely to be more isotopically light than the unreacted reactants. If the reaction was allowed to progress to completion, the fractionation would be zero.

8.3 Equilibrium Fractionation

Both the kinetic energy difference and the binding energy difference also affect reactions at equilibrium. The larger the relative mass difference between isotopes, the larger the isotopic fractionation. i.e. there is a bigger energy difference between isotopomers of water containing H or D than there will be between those with ^{16}O and ^{18}O .

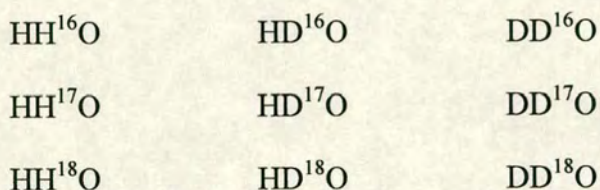
Because of the combination of these energy differences, the equilibrium of liquid water with water vapour is not a single reaction:



Hydrogen will be either ^1H (H) or ^2H (D).

Oxygen will be either ^{16}O , ^{17}O or ^{18}O .

Hence, in an imaginary bucket of water sealed in a chamber with a pure water vapour atmosphere, there are nine different types of water:



Each one of these will have its own equilibrium constant. These will all be independent on the relative quantities of the other components as the position of equilibrium will be affected by the partial pressure of the vapour phases.

The overall position of equilibrium will be determined by the combination of the 9 partial equilibria.

Statistical mechanical calculations these equilibrium values are extremely complex (see below) and only possible for ideal mono-atomic and diatomic gases, so they are not usually calculated. Instead, the actual isotopic compositions are determined empirically.



8.4 *Ab initio* Calculation of Partial Equilibria

Because of the quantum nature of energy, the translational, rotational and vibrational energies of a molecule are restricted to certain specific levels. The probability of any particle being at a certain energy level ϵ_r is:

$$p_r = \frac{e^{-\epsilon_r/kT}}{q}$$

where k is the Boltzmann constant, T is the temperature and q is the *partition function*.

The probability that the particle exists in any energy level is 1:

$$\sum_{r=0}^{\infty} p_r = 1$$

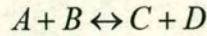
Therefore:

$$q = \sum_{r=0}^{\infty} e^{-\epsilon_r/kT}$$

The equilibrium constant can be calculated from the partition functions of the reactants and products of a reaction:



for the reaction:



the equilibrium constant K is:

$$K = \frac{q_C q_D}{q_A q_B}$$

The translational, rotational and vibrational energies are independent. The total partition function of a molecule, q , is the product of the three fundamental modes.

$$q = q_{trans} q_{rot} q_{vib}$$

For a diatomic gas molecule that does not collide with other molecules, the three fundamental q 's can be calculated as:

$$q_{trans} = \left[\frac{2\pi mkT}{h^2} \right]^{3/2} V$$

$$q_{rot} = \frac{8\pi^2 \mu r_0^2 kT}{sh^2}$$

and

$$q_{vib} = \frac{1}{1 - e^{-hv/2kT}}$$

where

$$\left(\nu = \frac{1}{2\pi c} \sqrt{\frac{k'}{\mu}} \right)$$



and

V = The volume that the molecules have to move in.

m = The mass of the molecule.

h = Planck's constant.

μ = Reduced mass of the bond.

k = Boltzmann's constant.

s = Symmetry term.

ν = Frequency.

k' = Force constant.

The formulae work well for isolated ideal gas molecules, but quickly become impossible to calculate in real world situations. Here, chaotic perturbations caused by intermolecular collisions, multiple degrees of freedom of rotation and extra harmonics in bond frequencies caused by adjacent bond vibrations alter the bond frequency on a molecule to molecule scale changing the simple, single values calculated above, to ranges.

Usually, non-equilibrium processes produce greater isotopic fractionations than equilibrium processes.



8.5 Examples of Natural Isotopic Fractionations

8.5.1 Geographic Fractionation of Water Isotopomers

Non-equilibrium and no-equilibrium processes combine to fractionate hydrogen and oxygen isomers in the hydrosphere. In this context, the degree of fractionation of both elements is measured against Standard Mean Ocean Water (SMOW).

All meteoric waters (water evaporated into the air, rainwater and all other waters derived from rainwater) are depleted in ^2H and ^{18}O relative to SMOW and hence $\delta^2\text{H}$ and $\delta^{18}\text{O}$ are negative numbers.

The following two figures illustrate the main transport paths in the hydrological cycle and the volumes of water passing through them annually (Figure 21) and the distribution of evaporation over the earth's surface (Figure 22).

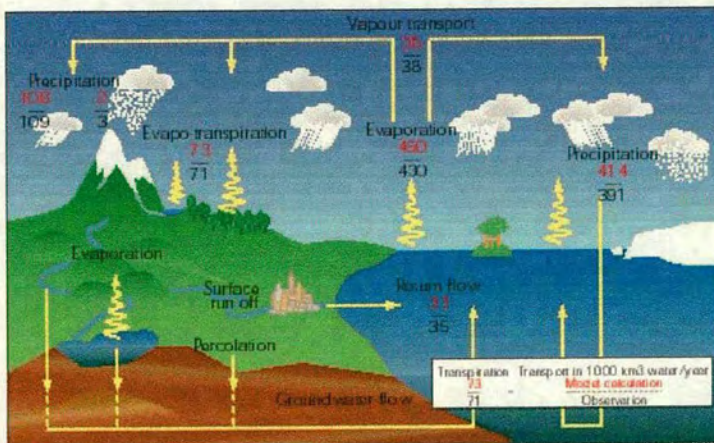


Figure 21 – Volumes of water involved in various stages of the water cycle per year. [34]

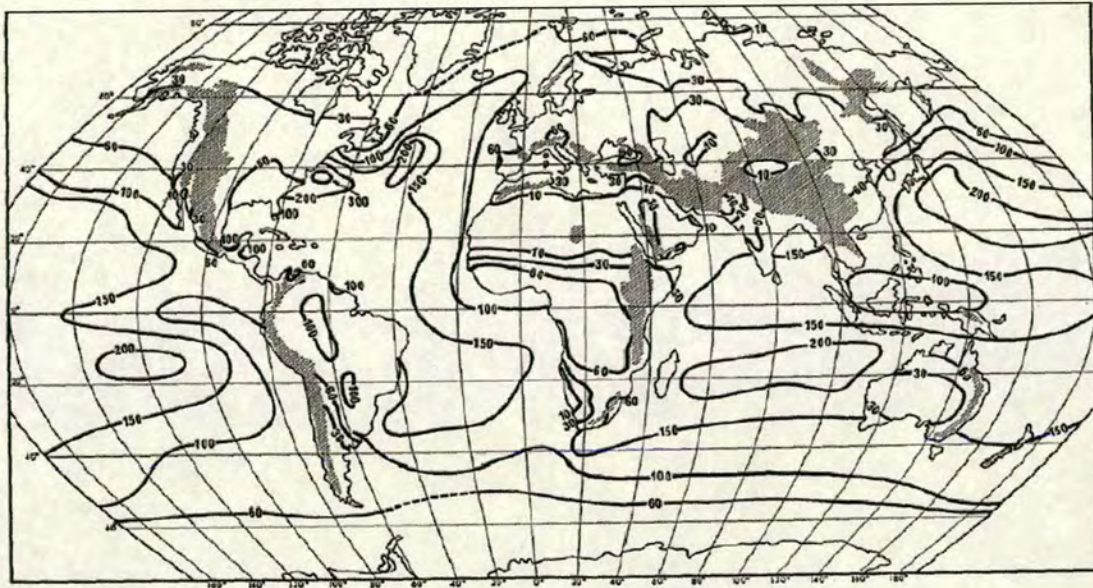


Figure 22 - Global pattern of annual evaporation in cm. [35]

It can be clearly seen in Figure 22 that most evaporation occurs over the ocean in the tropics. Most of this water precipitates out again in the tropics, but there is a slight excess which travels away from the equator to higher, colder latitudes precipitating out gradually on the way. By the time that this air reaches very high, polar, latitudes, the vapour content is very low as most of the water has rained out on the way.

This view of increased latitude leading to decreased temperature is, of course, simplistic. It would be true if temperature was solely controlled by incident sunlight. However, the ocean is a dynamic heat engine, and moves heat around the earth in oceanic currents. The effect of this can be seen in Figure 22. Notice the large northern bulge in increased evaporation in a north-easterly direction over the North Atlantic, corresponding to the path of the warm Gulf Stream and North Atlantic Drift



currents. Conversely, the cold Peru Current flowing from the Southern Ocean up the western coast of South America depresses evaporation rates in that area.

Mountain ranges also strongly influence the amount of rainfall, and therefore the water content of the atmosphere affected by them.

The actual fractionation of the isotopomers in the hydrological cycle is caused by the Rayleigh rainout effect which views the process as having separate evaporation and condensation/precipitation stages. The evaporation stage is considered as being non-equilibrium whereas the condensation/precipitation stage is thought to be at equilibrium.

- i) Evaporation – The rate-determining step in this stage is the diffusion of water vapour away from the liquid surface into the atmosphere. This stage fractionates in favour of lighter isotopomers because of the Kinetic Energy Difference, and therefore the vapour produced is deficient in heavy isotopes and has negative $\delta^1\text{H}$ and $\delta^{18}\text{O}$ values.

- ii) Condensation – As the air moves away from the areas of evaporation, towards colder areas (caused by either latitude or altitude) the water vapour begins to condense. The initial water droplets are small enough to remain suspended in the atmosphere and this gives them time to equilibrate with the surrounding water vapour.



The equilibrium vapour pressure of heavier isotopomers of water is lower than that for lighter isotopomers. (For example, $^1\text{H}^1\text{HO}$ has a vapour pressure of 23.756 Torr and $^2\text{H}^2\text{HO}$ has a vapour pressure of 20.544 Torr.) For this reason, in any evaporation or condensation process at equilibrium, the liquid becomes richer in the heavier isotopomers and the gas richer in the lighter isotopomers. The less energy available for this stage, i.e. the lower the temperature, the stronger the fractionation will be. (At very high temperatures, all the liquid would evaporate, and therefore there would be no fractionation. At low temperature, the energy difference between the evaporation stages between the heavier and light isotopomers becomes more pronounced.)

The result of these fractionating processes is reflected in the global distribution of $\delta^{18}\text{O}$ in precipitation (See Figure 23). Notice, again the bulges corresponding to the North Atlantic Drift and the Peru currents.

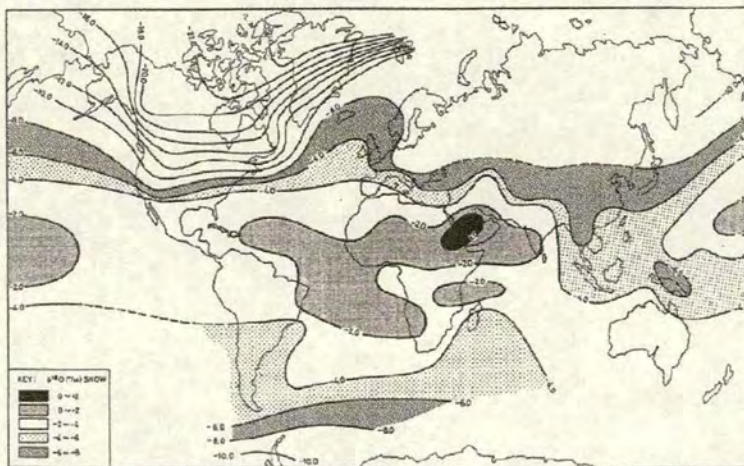


Figure 23 - World-wide distribution of the annual mean of $\delta^{18}\text{O}$ in precipitation, based on the GNIP data set [36].



The effect on oxygen isotope is also seen in the deuterium fractionation data. When the $\delta^{18}\text{O}$ and $\delta^2\text{H}$ data from collected rainwater from all over the world is plotted on a graph, the data gives a straight line known as the “Meteoric Water Line” or MWL (See Figure 25).

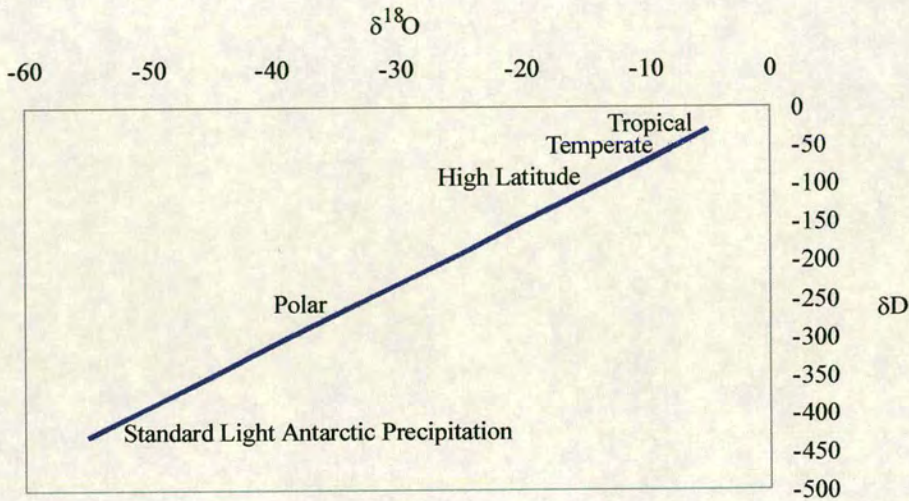


Figure 24 - Meteoric Water Line. Displays relationship between δD and $\delta^{18}\text{O}$ in meteoric water and the latitude at which it is found. [37]

Samples from the Tropics plot near the origin and polar samples at high negative values. Other sources plot in between. Notice how the fractionation of deuterium is much higher than the corresponding $\delta^{18}\text{O}$ value.



8.6 Metabolic Effects

Combinations of the Fractionation Processes outlined above result in important isotopic fractionations within the biosphere. These are usually grouped under the heading Metabolic Effects.

Two of the most important Metabolic Effects are the carbon isotope fractionation caused by the processes that first fix carbon dioxide in C₃ and C₄ plants.

8.6.1 C₃ CO₂ Fixation:

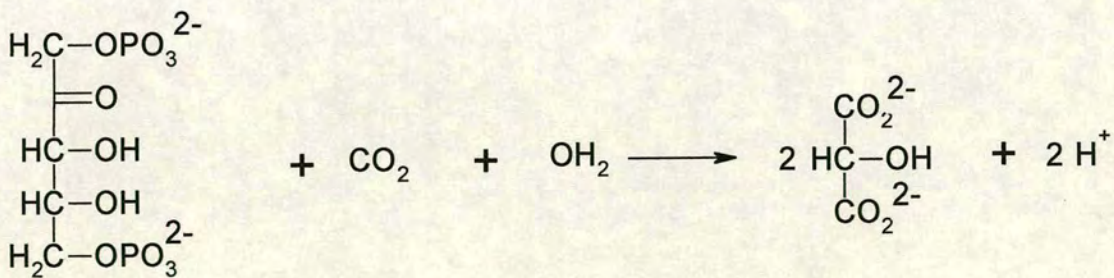


Figure 25 - C₃ CO₂ fixation. Ribulose bisphosphate reacts with CO₂ and H₂O enzymatically catalysed by ribulose bisphosphate carboxylase/oxygenase.

The carbon isotope fractionation associated with C₃ photosynthesis is the result of the combination of three fractionating processes:

- i) CO₂ diffusing into the leaf, through stoma, during respiration.



- ii) The internal CO₂ concentration in the leaf.
- iii) The fractionation involved in the enzymatic reaction of ribulose biphosphate with CO₂ and water, catalysed by the enzyme ribulose biphosphate carboxylase/oxygenase (See Figure 25).

The fractionation associated with the fixing reaction in C₃ plants is 29 ‰. [38]. However, the total δ¹³C remains negative because the diffusion step is strongly negative. The average δ¹³C range for C₃ plants is between -20 and -30 ‰. [37]

8.6.2 C₄ CO₂ Fixation:

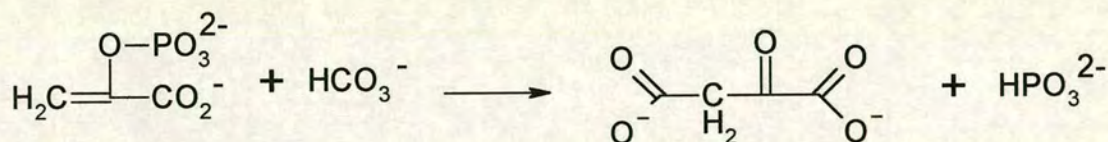


Figure 26 – Initial C₄ CO₂ fixation step (notice 4 carbons in diacid, hence “C₄”). The carboxylation of phosphoenolpyruvate.

C₄ plants also use the CO₂ fixing step described in the C₃ section above. However, the initial CO₂ fixation stage, before they transport the CO₂ to special organs in the middle of the leaves, uses the fixation reaction shown in Figure 26. The overall fractionation of this step (going from CO₂ gas, and not bicarbonate as shown in the figure) is -5.7 ‰.

Figure 27 shows the ranges of carbon isotopes as found in many naturally occurring carbon sources.

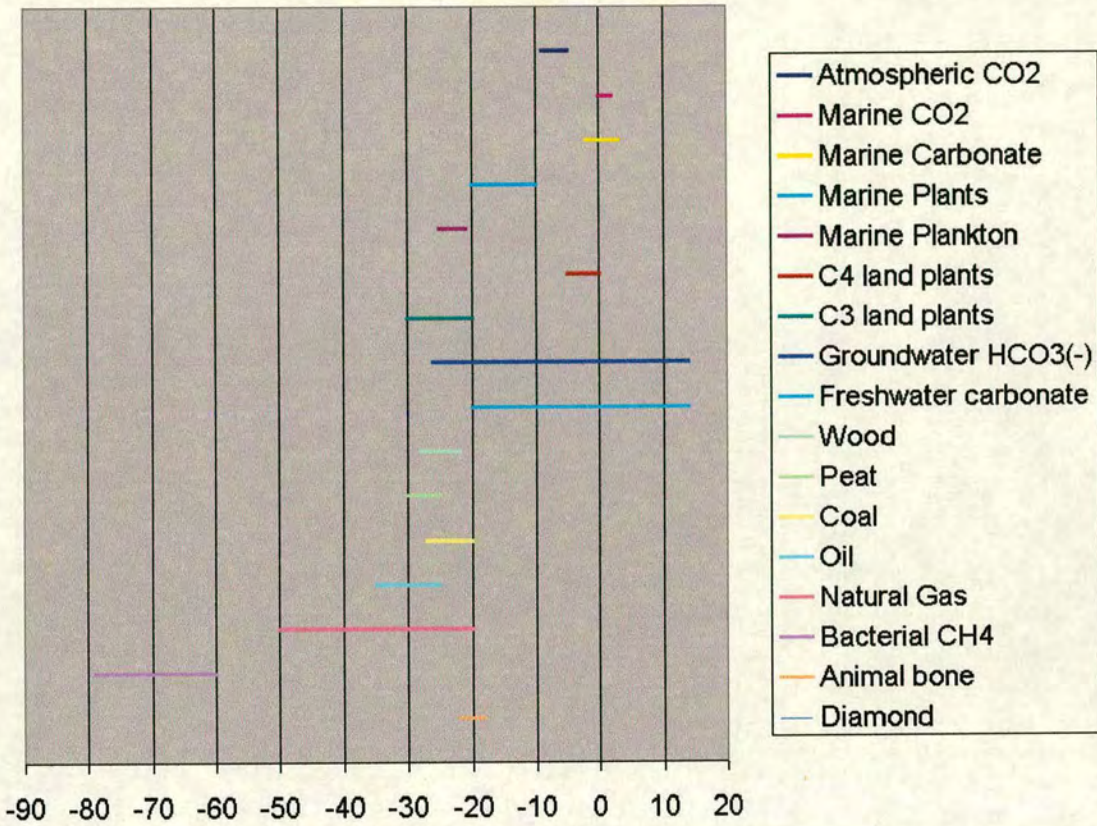


Figure 27 - Carbon Isotope Ratios of natural, terrestrial, carbon sources. [37]

8.7 Using Stable Isotope Ratios for Drug Source Region Identification

The sections above have shown that isotopic fractionations vary across the surface of the earth. In addition, the spreading of fertilisers for example can alter the stable isotope ratio of those elements concerned locally. Therefore, by measuring isotopic fractionations, natural and synthetic, and comparing them with a library of the ratios of samples of known origin, one might be able to identify the source region, or conditions, of an unknown sample.



This philosophy has been successfully applied to a variety of applications including wine [39;40], olive oil [41], honey [42;43], caffeine [44], cocaine [45;46], heroin [46;47], and most recently, cannabis [48].

The cannabis study was carried out by the Department of Botany at the University of Queensland using marijuana style samples. The published results, presented here in Figure 28, show the range of $\delta^{13}\text{C}$ and $\delta^{15}\text{N}$ seen in cannabis across a large area of Queensland. (A map showing where these Australian samples originated is given in Figure 32).

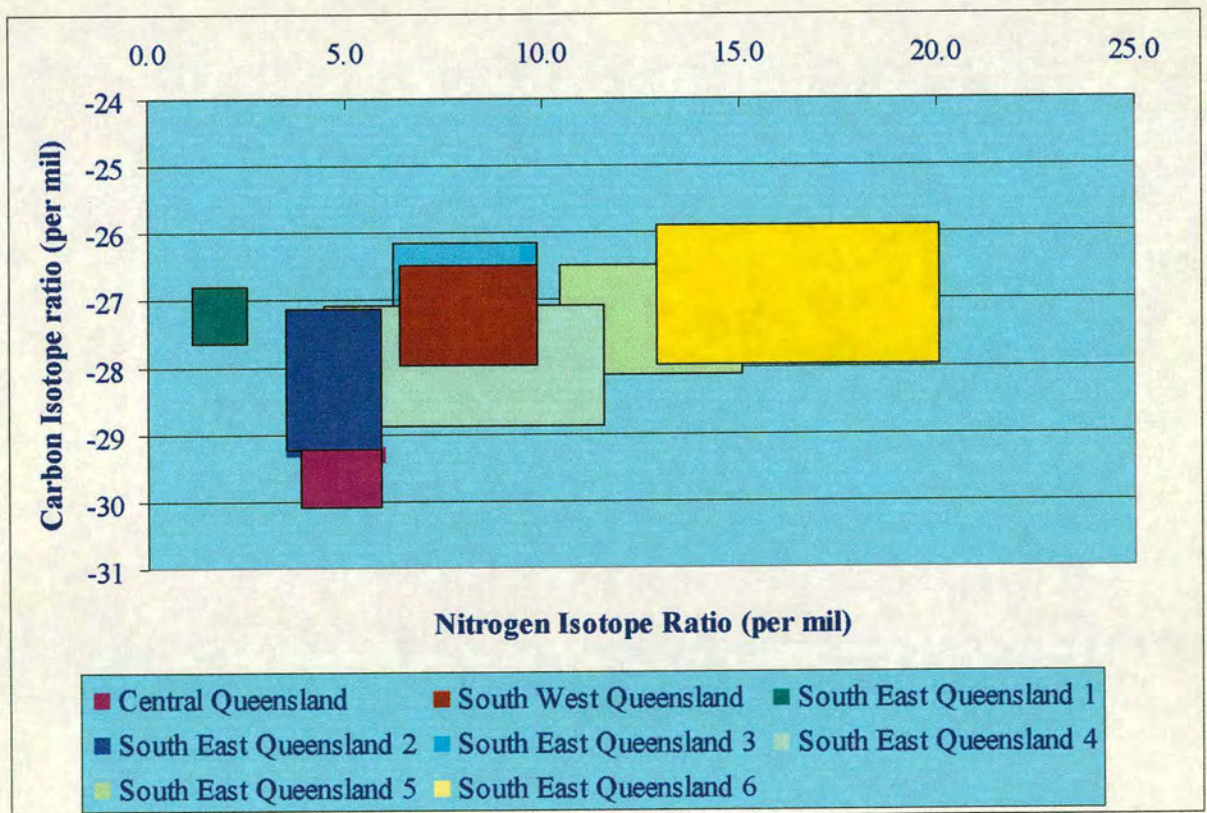


Figure 28 - Denton results



It is extremely unlikely that the resin samples seized by the Police in Scotland, and analysed in this study, came from Queensland. The advice given to us by the Lothian and Borders Police and HM Custom's and Excise was that the vast majority of hashish in the UK originates in Morocco. Therefore, what is the spread of ratios might one expect to see from drug samples originating on different continents?

Of particular relevance to this question is the work carried out by James Ehleringer of the University of Utah, on determining the source of cocaine and heroin [46].

In this paper he describes an attempt to identify the source of heroin and morphine derived from the heroin by displaying samples according to their $\delta^{13}\text{C}$ and $\delta^{15}\text{N}$ ratios. The results of this work are shown in Figure 29. (The error bars indicate 99% confidence.)

The four growth regions which were considered in this study were:

- 1) Mexico
- 2) Southwest Asia (the "Golden Crescent")
- 3) Southeast Asia (the "Golden Triangle")
- 4) South America

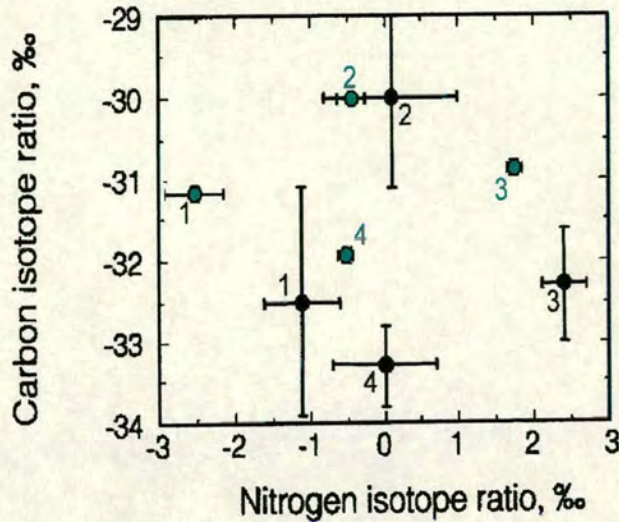


Figure 29 - Carbon and nitrogen Isotope ratios of heroin (black circles) and associated morphine samples (green circles) originating from the main growing regions (1) Mexico, (2) Southwest Asia, (3) Southeast Asia and (4) South America. After (Ehleringer et al 1999, For Sci Int)

Consider the results for Heroin in Figure 29. The data shows a slight overlap for the sample groups from Mexico and South America, but all other groups are completely distinct. For the Morphine experiments, the results of all the groups are distinct, and well spread.

Unfortunately, we don't know the size of the areas from which these samples were collected, and it is, of course, possible that each of these sample groups comes from one single plantation. However, the Ehleringer data does show the expected continental differences in isotopic ratios.

The question therefore being asked of our samples, with this analysis technique, was - did they all come from the same source continent?



8.8 Experimental Method

To allow the results from this study to be compared with those from the studies described above, it was decided that our samples should also be analysed for $\delta^2\text{H}$, $\delta^{13}\text{C}$ and $\delta^{15}\text{N}$. In all cases, the whole resin was analysed.

The $\delta^2\text{H}$ analysis was carried out with the kind assistance of John Morrison at Micromass UK, while the $\delta^{13}\text{C}$ and $\delta^{15}\text{N}$ analyses were completed at the Scottish Universities' Research and Reactor Centre, in East Kilbride with Dr Johannes Barth.

8.8.1 $\delta^2\text{H}$ Analysis

The analyses were carried out on a Micromass Isoprime instrument.

8.8.2 $\delta^{13}\text{C}$ and $\delta^{15}\text{N}$ Analyses

The analyses were carried out on a Finnegan TracerMAT instrument fitted with an automatic sampler, "flash" oxygen combustion chamber with continuous flow analyser. For a basic description of stable isotope mass spectrometers, see Appendix A.

6mg and 0.4mg of each sample were taken for nitrogen and carbon analyses. The pulverised samples were sealed in 8x5mm tin foil thimbles.

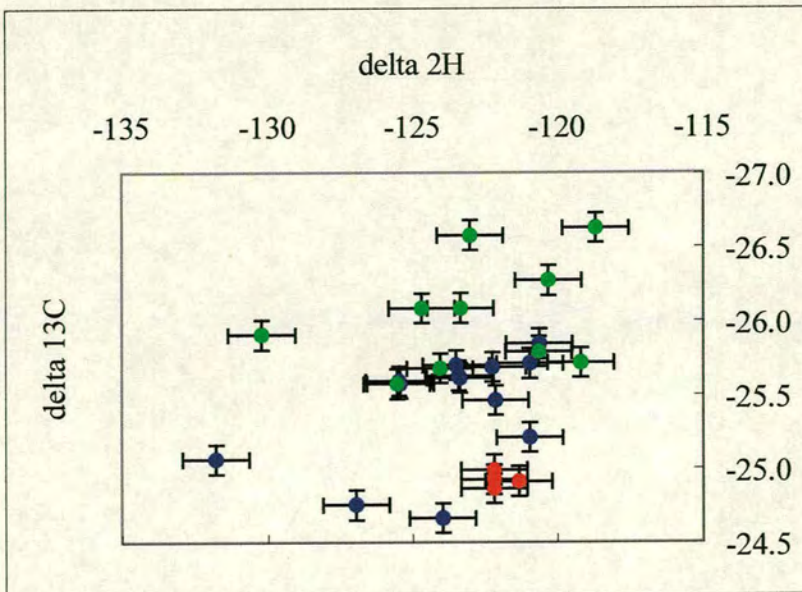
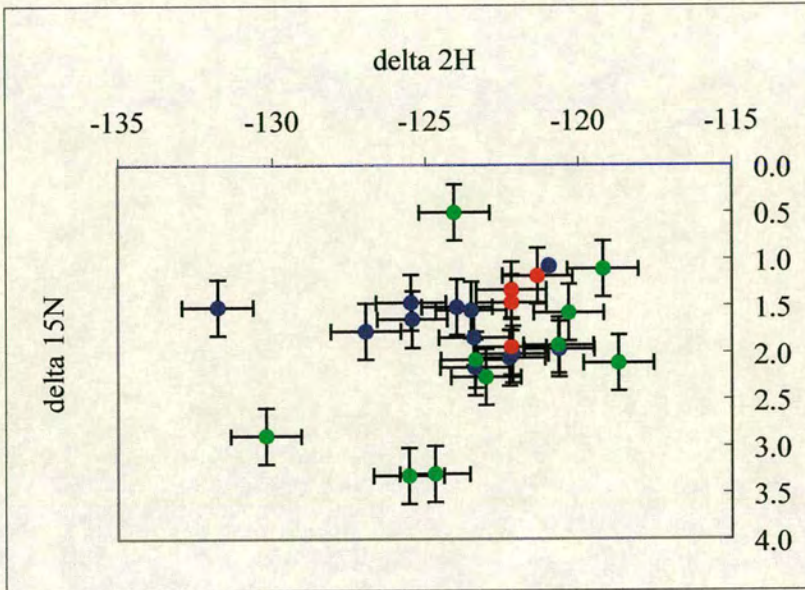


During the analysis runs, the samples were interleaved with a variety of standards to monitor the instrument's performance. Out of 50 analyses, only 22 were our samples, the rest being standards or duplicates/triplicates of samples, again to monitor the performance of the instrument.



8.9 Results

Figure 30 shows the results of the stable isotope analyses of the whole resin from our samples.



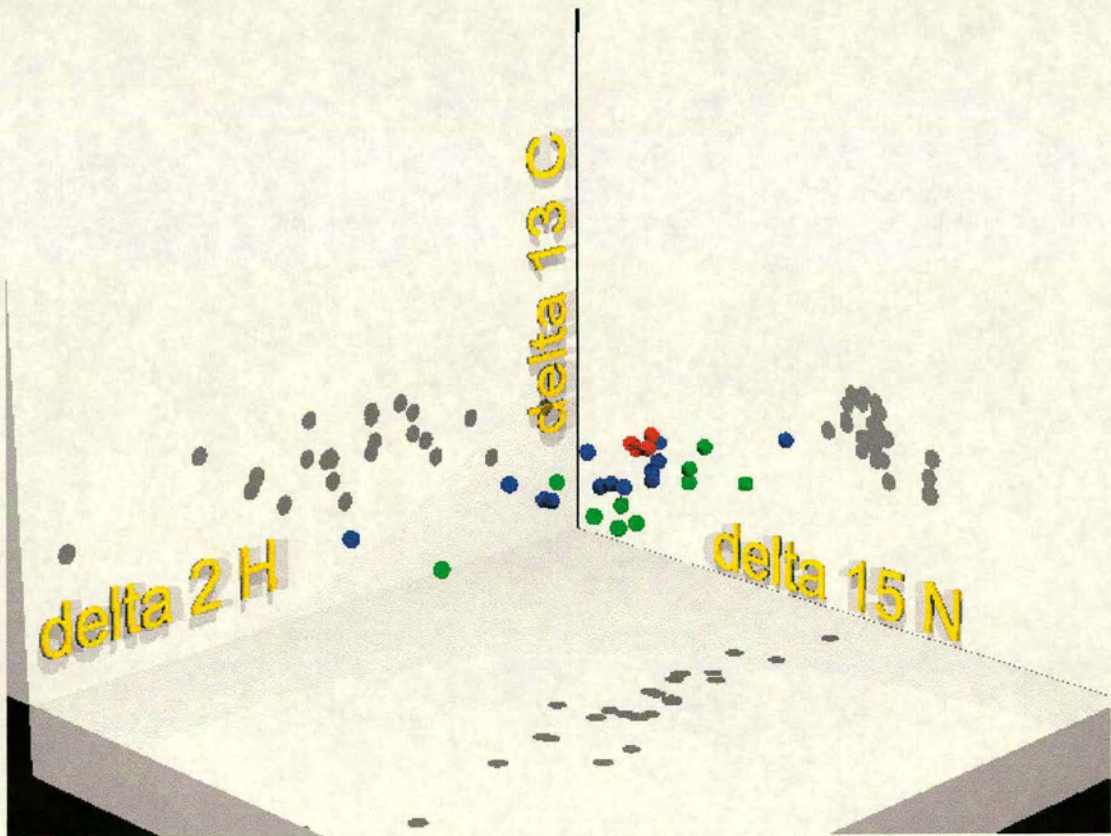
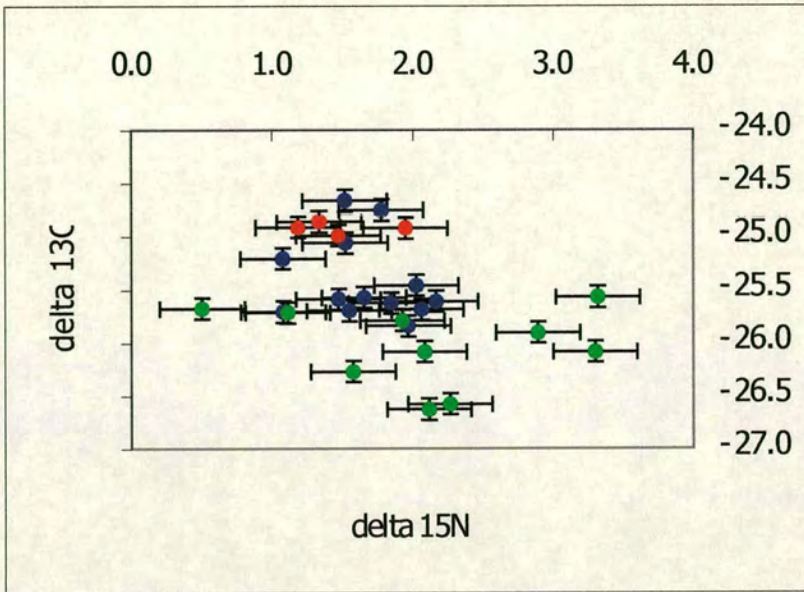


Figure 30 - Key for all - **Old Bar**, **New Bar**, **K Bars**. Error bars show standard deviation. Top - $\delta^2\text{H}$ vs. $\delta^{15}\text{N}$. Second Top - $\delta^2\text{H}$ vs. $\delta^{13}\text{C}$. Second Bottom - $\delta^{13}\text{C}$ vs. $\delta^{15}\text{N}$. Bottom - 3D projection of all series.



In reference to the errors; those for the $\delta^{15}\text{N}$ ratios in this experiment were commensurate with those of the Ehleringer paper, but the $\delta^{13}\text{C}$ errors were much lower in this study. (3 standard deviations contain 98% of the population).

8.10 Discussion

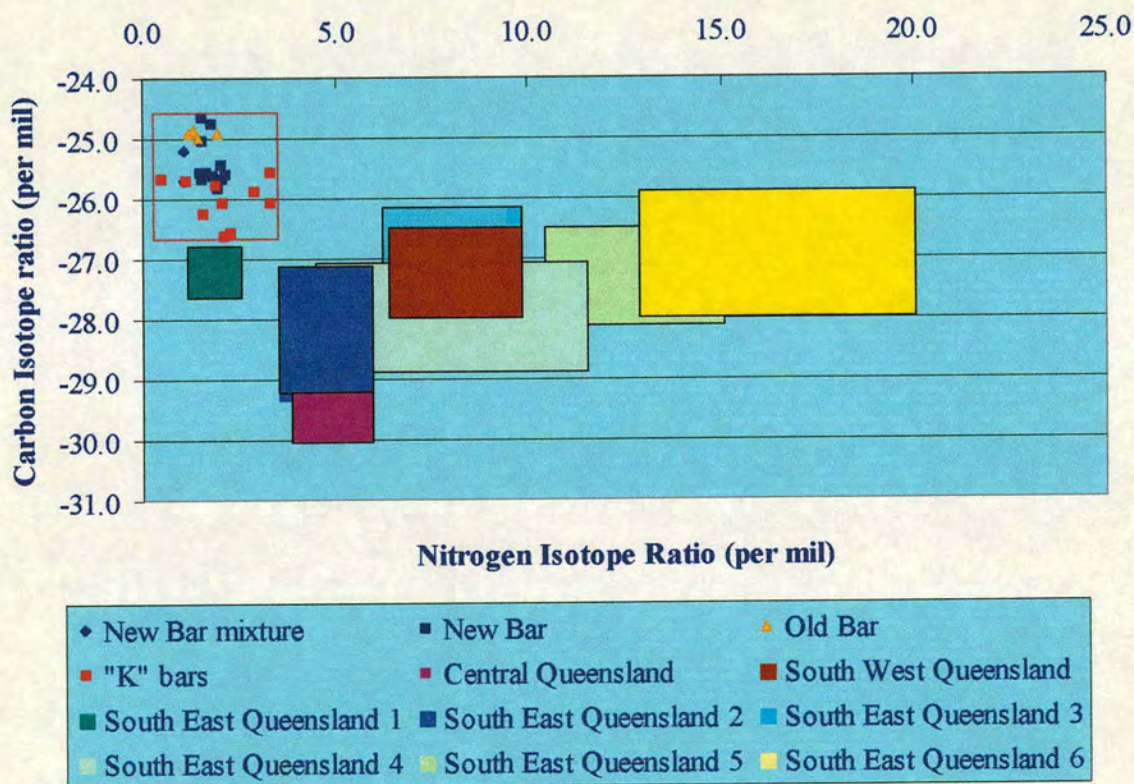


Figure 31 - Graph showing data from this project (grouped in red outline) compared with data from the Denton project.

First, the carbon and nitrogen data from this project was compared with that of the only recent published work on cannabis isotope ratios, known hereafter as the Denton project [48]. (See Figure 32). All the Denton samples in Figure 32 are from

Determining the Origin of Cannabis Resin



Queensland, Australia; and, it is immediately apparent that they plot quite distinctly from our samples. Indeed, the trend in the Denton data (from (low $\delta^{15}\text{N}$, high $-\delta^{13}\text{C}$) to (high $\delta^{15}\text{N}$, low $-\delta^{13}\text{C}$) appears lead the data groups further apart. (This was, of course, with the exception of one outlier group, (South East Queensland 1)!) It was therefore concluded that our samples did not originate from Queensland.

Additionally, the spread of points from our data is similar in size to individual sites in the Denton Project (in fact, it is smaller than some). This is taken to indicate that our samples came from a defined geographical area, considerably smaller than the areas covered in the Queensland study (See Figure 33).



Figure 32 - Map showing approximate sources of the Denton samples.



Therefore, combined with the information that the vast majority of hashish in the UK is thought to come from Morocco, the placement of our data and the Denton data would tend to support Ehleringer's hypothesis that it is possible to differentiate between different continents as sources of illegal drugs, and indeed to extend it from cocaine and heroin to include cannabis -as well.

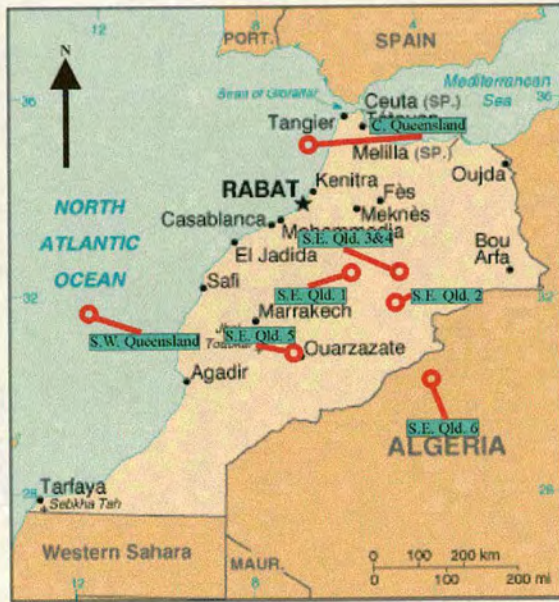


Figure 33 - Map of Morocco showing relative spread of sites samples in Queensland (to same scale).

Figure 33 shows the site distribution from the Denton study superimposed upon a map of Morocco, to the same scale. While it would be dangerous to make any quantitative predictions about the area of Morocco sampled in our experiments, it may be possible to draw some qualitative conclusions. From comparing the spread of $\delta^{13}\text{C}$ and $\delta^{15}\text{N}$ results from the Denton project with those from this study, combined with the geographic spread of the Denton sampling points compared with the size of Morocco, it seems reasonable to hypothesise that a small area of Morocco was responsible for



the hashish samples analysed in this study. Furthermore, this hypothesis is supported by the $\delta^2\text{H}$ results. By analysing precipitation data from Midway Island ($28^\circ 11'' \text{ N}$), Valencia, Spain ($39^\circ 30'' \text{ N}$) and Vienna ($48^\circ 12'' \text{ N}$), it is possible to estimate that the 11‰ spread of the $\delta^2\text{H}$ results from our samples would result from an area with a north south axis of approximately 350 miles length. This figure is calculated ignoring any seasonal temperature effects (remembering that it is temperature, not simply latitude, that affects isotope fractionation of hydrogen). These seasonal effects mean that the 350 mile north-south limit is somewhat over estimated.

In conclusion, the stable isotope analysis has shown that there is a large probability that all the hashish samples analysed in this study came from one country, and more, that they probably came from a small part of that country. Without access to more samples of known origin, it is impossible say more. Further studies should reveal what geographic resolution is attainable, and perhaps even lead to a data base of supply countries and their stable isotope ranges, allowing the origin of cannabis seizures to be monitored.

Once the stable isotope analyses had been completed, it was decided that more information was extractable from the samples. It is known that selective cultivation can have a large effect on the composition of marihuana and hashish. [49]. Therefore, although areas may be geographically close, the strain of cannabis grown may differ, leading to a chemical difference in the product. We decided to attempt to develop a method of identifying these differences and detecting them.



9 Advanced Biosynthesis Monitoring

9.1 Introduction

When the Lothian and Borders Police planned, and carried out, their chemical fingerprinting project on the cannabis samples (see Previous Work: Chemical Fingerprinting), with the aim of identifying differences in the ratios of different cannabinoids between different sample batches, they concentrated their work on the major cannabinoids; tetrahydrocannabinol, cannabinoil and cannabidiol. One possible reason why this restriction was imposed is that these three are the only cannabinoids that are available as commercial standards.

While they had little success in attempting to group samples using absolute measurements of these compounds, we perceived a to improve this situation by analysing for as many cannabinoids as possible. This was to be achieved by GC-MS (gas chromatography-mass spectrometry), and because standards were unavailable, it was proposed that the compounds be identified by mass spectrometry and quantified by internal normalisation against other compounds in the same spectrum.



9.2 Previous Work

The only applicable work showing this biosynthetic route approach appears to be that of James Ehleringer et al. at the University of Utah, on cocaine [45]. (Ehleringer was also of the heroin project described in the stable isotope section above.)

This project concerned the analysis of some 200 coca samples collected from five different growing regions in three South American Countries:

- 1) Columbia – Guaviare and Putumayo-Caqueta regions.
- 2) Peru – the Huallaga and Ucayali Valleys and the Apurimac Valley.
- 3) Bolivia – the Chapare Valley.

The Ehleringer team extracted cocaine from these raw plant samples and analysed the extracts for their $\delta^{13}\text{C}$ and $\delta^{15}\text{N}$. The raw data from these experiments was not presented, but the results were described:

“Over the entire geographical distribution, $\delta^{13}\text{C}$ and $\delta^{15}\text{N}$ values for coca leaves vary from -32.4% to -25.3% for $\delta^{13}\text{C}$, and from 0.19% to 13.0% for $\delta^{15}\text{N}$. Leaves from the Putamayo and Caqueta regions of Colombia are distinguishable from each other by their $\delta^{13}\text{C}$ content as are those from the Huallaga and Ucayali Valleys- from the Apurimac Valley of Peru. Coca leaf from Bolivia has consistently less ^{15}N than material from Peru. There is more ^{15}N in



coca leaves from Colombia and least in coca grown in the Chapare Valley of Bolivia.” [45].

By analysing this data statistically, it was calculated that 90% of the 200 samples could be grouped by their stable isotope ratios alone.

In addition, the Ehleringer team also analysed the samples for their total truxilline and trimethoxycocaine (*) concentrations. (See Figure 34)

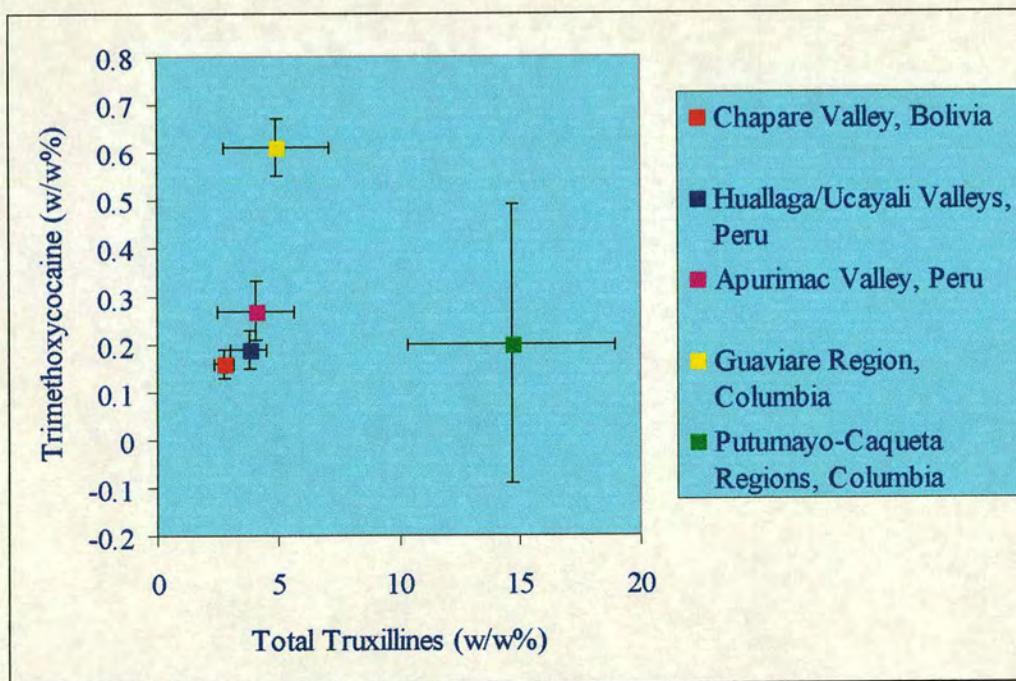


Figure 34 - Graph of Total Truxilline (w/w%) vs. Trimethoxycocaine (w/w%) for Ehleringer cocaine samples. (After [45])

With the trace alkaloids alone, it was possible to separate those samples from the Putumayo-Caqueta and Guaviare Regions of Columbia. It was not possible to



separate the other samples by this method alone. This is, perhaps, a reflection of the different degrees of selective cultivation that have occurred in these production areas and that the populations of coca grown in Peru and Bolivia are biochemically more closely related to each other than either of the populations grown in Columbia.

However, a combination of the Stable Isotope Ratio results and the Trace Alkaloid data was able to separate 96% of the samples into their individual groups (See Figure 35).

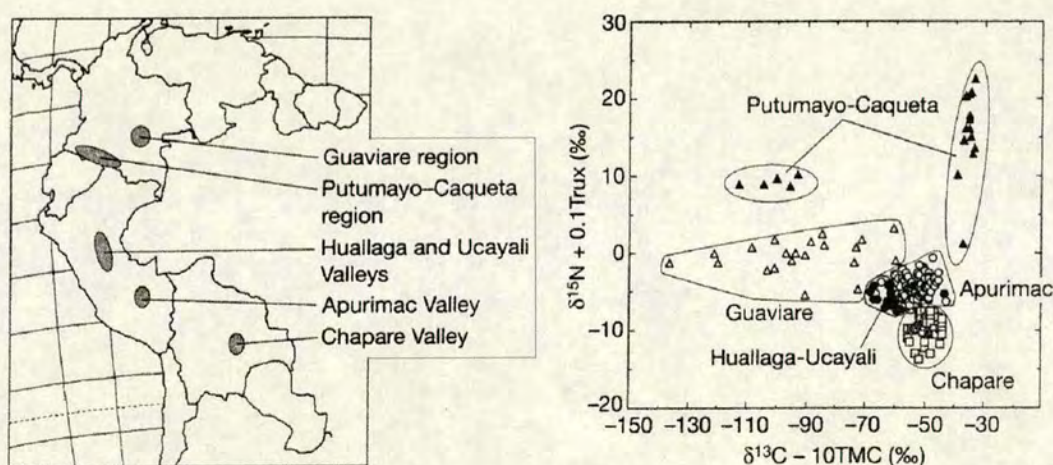


Figure 35 - Identification of geographic regions in South America where cocaine is commonly grown. Left - regions from which samples were taken. Right - plot of results of stable isotope and chemical analyses, grouped by sampling region. X-axis - $\delta^{13}\text{C} - (10 \times [\text{trimethoxycocaine}])$. Y-axis - $\delta^{15}\text{N} + (0.1 \times [\text{truxilline}])$. (After [45])

This work showed the potential of using biochemical information in combination with stable isotope ratio analysis. While the Ehleringer technique had been applied

* Trimethoxycocaine and the truxillines are trace alkaloids found in coca.



successfully to coca, to apply this idea to cannabis required development of a new method.

9.3 Experimental Method: Gas Chromatography-Mass Spectrometry

9.3.1 Sample Preparation

Approximately 0.1mg of the pulverised cannabis resin was ultra-sonically extracted with 2ml low boiling (40-60 °C) petroleum ether. This ether extract contained many of the cannabinoids.

The extract was then concentrated to around 200µl in a heated, low pressure centrifuge.

9.3.2 Analysis Method

The concentrated extract was analysed by gas chromatography-mass spectrometry (HP 6890 GC with auto-sampler and HP 5973 MSD). The injection and oven parameters were:

1µl injection

Oven start temp – 120 °C

Hold for 5 minutes.

Ramp oven temp 10° per minute until 290 °C.



Hold at 290 °C for 8 minutes.

The spectra and chromatogram were analysed using Finnigan Navigator 1.2 software. Components of the chromatogram were identified by their mass spectra and by using The Eight Peak Index of Mass Spectra [50].

Petroleum ether was used as the extractant because the resultant solution is known to contain the psychoactive components of cannabis as well as other cannabinoids[51].



9.4 Results

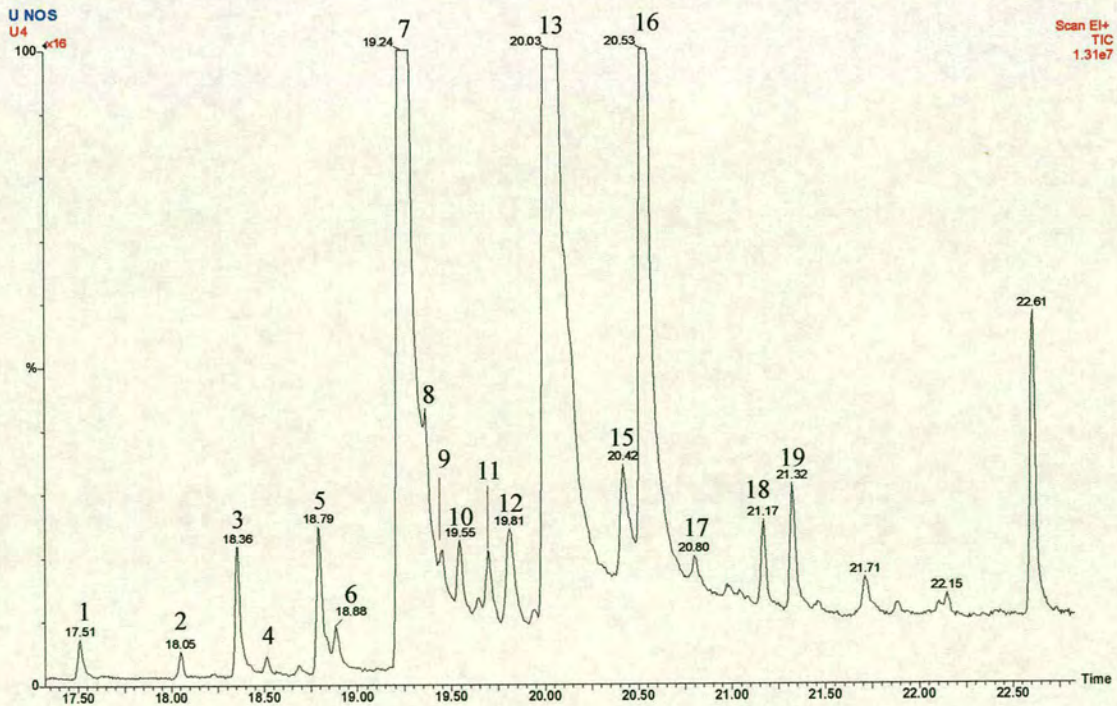
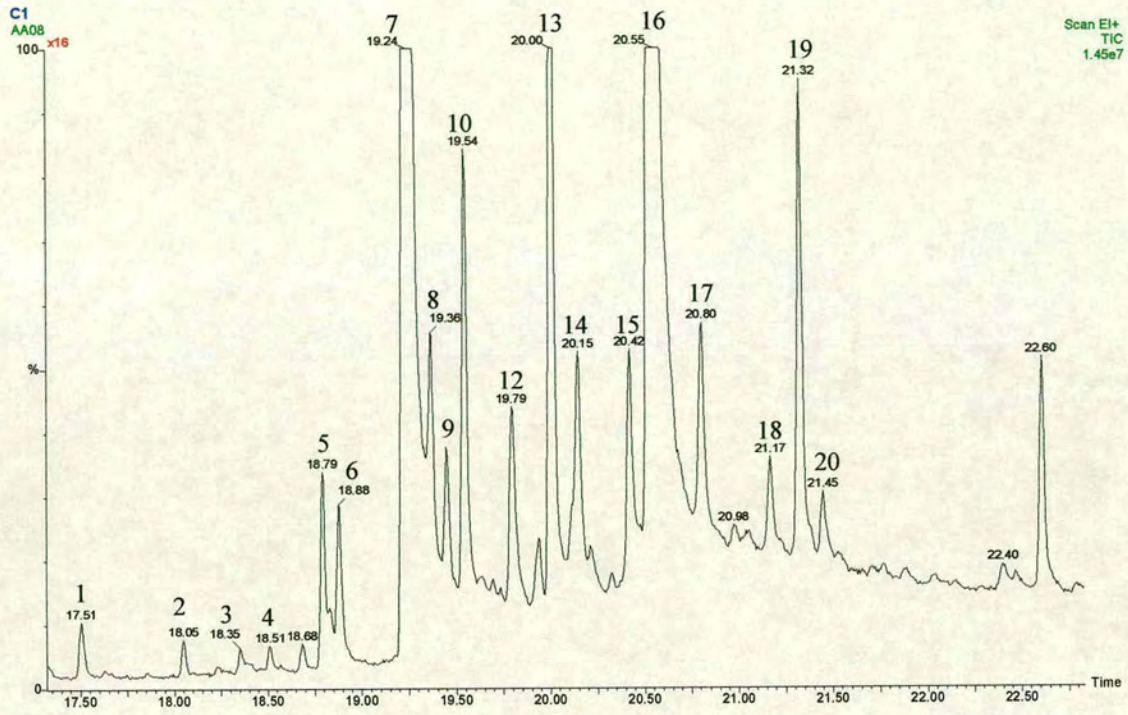


Figure 36 - Example Chromatogram showing results of a GC-MS analysis of hashish. Peaks corresponding to cannabinoid components are numbered. Two chromatograms are shown as not all components were expressed in all chromatograms.



Only three of the cannabinoids are commercially available as standards: cannabidiol, cannabinol and tetrahydrocannabinol (Peaks 7, 16 and 13 in Figure 36 above). It was outwith the scope of this project to positively identify the majority of the components detected by GC-MS (See Figure 36) or to absolutely quantify them. (It was considered that this work could constitute an entire project in its own right. (See Appendix B).

In answer to the first problem, it is possible to confirm, by the mass spectra of the chromatographic peaks, that the same components are being identified as the same peaks in all chromatograms; and therefore can be compared from sample to sample. Additionally, careful examination of the mass spectra, combined with comparison to library data[32;50], has led us to tentatively identify some of the compounds by name. Cannabinoids often show characteristic fragments in their mass spectra, so even the unnamed components are considered to be cannabinoids.

The second problem, the inability to absolutely quantify the various components, was overcome by the use of internal normalisation.

9.4.1 Detected Compounds

In the following table, the peaks corresponding to the detected compounds as shown, as numbered in Figure 36, are named and the molecular ion of the compound is given

Determining the Origin of Cannabis Resin



(taken from the mass spectra of the peaks). Additionally, the possible chemical formula(e) of the molecule is given.

Where a tentative assignation has been made, the peak is named after this compound, for other peaks, they are named after their elution time, in minutes.

Peak Number	Peak Name	Mass	Formula
1	17.51	286	$C_{19}H_{26}O_2$
2	18.06	314	$C_{21}H_{30}O_2$
3	18.36	286	$C_{19}H_{26}O_2$
4	18.51	314	$C_{21}H_{30}O_2$
5	Cannabicyclol	314	$C_{21}H_{30}O_2$
6	18.90	310	$C_{21}H_{26}O_2$
7	Cannabidiol	314	$C_{21}H_{30}O_2$
8	19.36	332	$C_{20}H_{28}O_4$
9	19.45	328	$C_{22}H_{32}O_2$
10	19.55	328	$C_{22}H_{32}O_2$
11	19.69	314	$C_{21}H_{30}O_2$
12	19.81	330	$C_{20}H_{26}O_4$ or $C_{22}H_{24}O_2$
13	Tetrahydrocannabinol	314	$C_{21}H_{30}O_2$
14	20.15	314	$C_{21}H_{30}O_2$
15	Cannabigerol	316	$C_{21}H_{32}O_2$

Determining the Origin of Cannabis Resin



Peak Number	Peak Name	Mass	Formula
16	Cannabinol	310	C ₂₁ H ₂₆ O ₂
17	Iso-Cannabinol	310	C ₂₁ H ₂₆ O ₂
18	21.17 (Long chain hydrocarbon)	Not known	
19	21.33 (Ether Molecule)	328	C ₂₂ H ₃₂ O ₂
20	Cannabitriol	346	C ₂₁ H ₃₀ O ₄

The mass spectra of all peaks were extracted from the data. In the cases where peaks occurred as shoulders on other peaks, spectral subtraction was used to minimise the influence of other components.

These mass spectra were then compared against a library [50] and against spectra supplied by the police [32] which led to the identification of Cannabicyclol, Cannabidiol, THC and Cannabinol.

Other peaks were tentatively identified by other means:

- Iso-cannabinol was assigned to peak 17 because its occurrence in all samples closely followed that of Cannabinol.
- Cannabigerol was assigned to peak 15 because it is the only 316 m.w. cannabinoid that was found in the literature.
- Peak 20 was assigned as Cannabitriol, m.w. 346, for the same reason.
- Peak 19 was assigned to a Cannabinoid alcohol methyl ether because of the loss of 15 mass units from the molecular ion at m/z 328 to give the base peak at m/z 313.

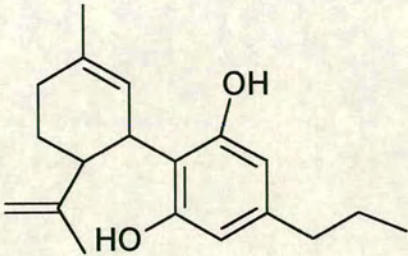
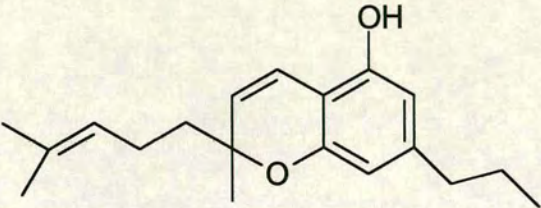
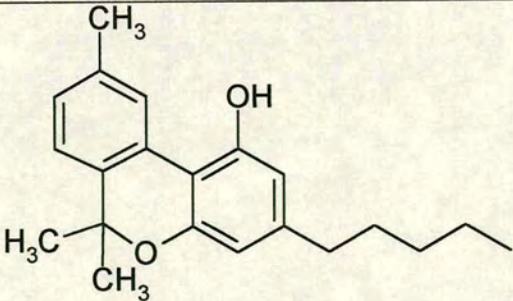
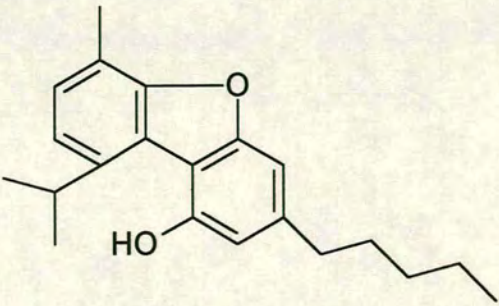


The other unassigned peaks are thought to be cannabinoids as well; as suggested by their mass spectra and the fragments therein (particularly the 231, 299 and 295 m/z fragments). It was not possible to identify them in this study, but the following rogues gallery of cannabinoids may assist future work in this area. This list is by no means comprehensive, but is instead intended to show some of the range of cannabinoids that have been characterised.

See Appendix B for more on identification of the other components found in our hashish samples.



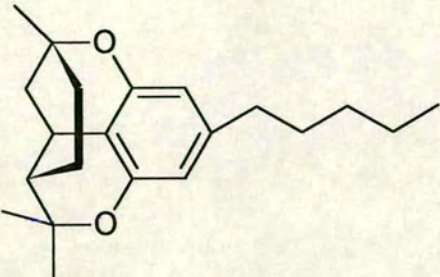
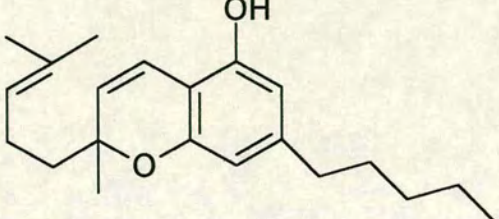
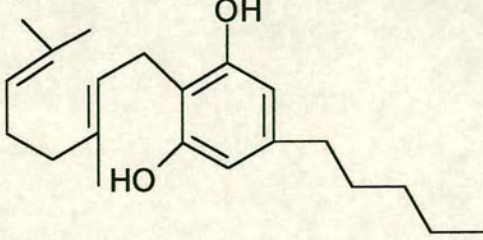
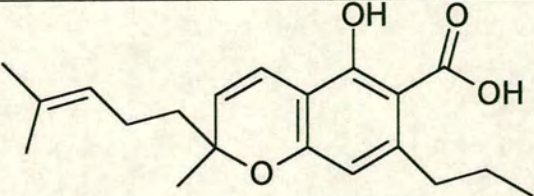
Gallery of Example Cannabinoids

Mass Compound Chemical Formula Possible Peaks	Structure
M.W. 286 Cannabidivarin $C_{19}H_{26}O_2$ Peaks – 1,3	
M.W. 286 Cannabichromevarin $C_{19}H_{26}O_2$ Peaks – 1,3	
M.W. 310 Cannabinol $C_{21}H_{26}O_2$ Peaks – 6(?), 16, 17	
M.W. 310 Cannabifuran $C_{21}H_{26}O_2$ Peaks – 6(?), 16, 17	

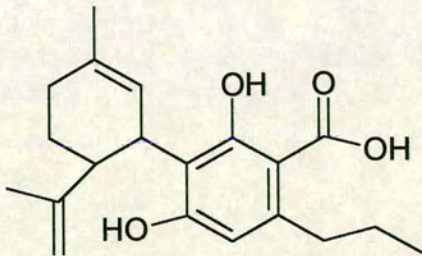
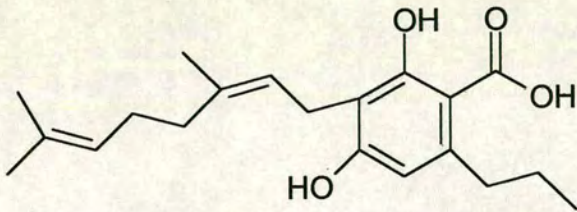
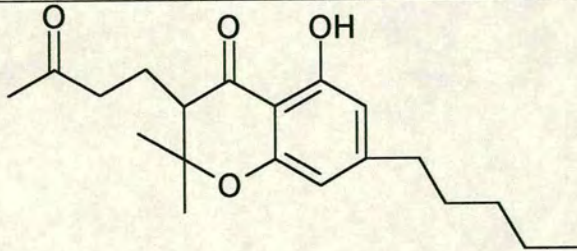
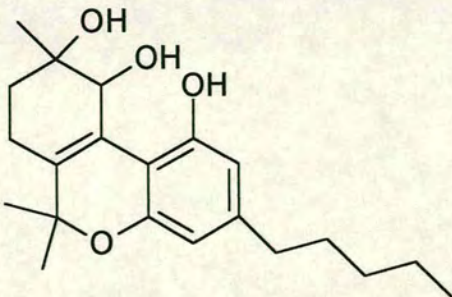


Mass Compound Chemical Formula Possible Peaks	Structure
M.W. 310 Cannabidinodiol $C_{21}H_{26}O_2$ Peaks - 6(?), 16, 17	
M.W. 314 Cannabicyclol $C_{21}H_{30}O_2$ Peaks - 2, 4, 5, 7, 11, 13, 14	
M.W. 314 Cannabidiol $C_{21}H_{30}O_2$ Peaks - 2, 4, 5, 7, 11, 13, 14	
M.W. 314 THC $C_{21}H_{30}O_2$ Peaks - 2, 4, 5, 7, 11, 13, 14	



Mass Compound Chemical Formula Possible Peaks	Structure
M.W. 314 Cannabicitran $C_{21}H_{30}O_2$ Peaks - 2, 4, 5, 7, 11, 13, 14	
M.W. 314 Cannabichromene $C_{21}H_{30}O_2$ Peaks - 2, 4, 5, 7, 11, 13, 14	
M.W. 316 Cannabigerol $C_{21}H_{32}O_2$ Peaks - 15 Also as Me ether M.W.330 $C_{22}H_{34}O_2$	
M.W. 330 Cannabichromevarinic Acid $C_{20}H_{26}O_4$	



Mass Compound Chemical Formula Possible Peaks	Structure
Peaks - 12 M.W. 330 Cannabidivarinic Acid $C_{20}H_{26}O_4$ Peaks - 12	
M.W. 332 Cannabigervarinic Acid $C_{20}H_{28}O_4$ Peaks - 8	
M.W. 332 Cannabichromanone $C_{20}H_{28}O_4$ Peaks - 8	
M.W. 346 Cannabitriol $C_{21}H_{30}O_4$ Peaks - 20	



9.4.2 Quantification of Results

Once the peaks of interest had been identified in the chromatograms, their areas were calculated using Thermo-Finnigan LCQ Navigator software. Much of the work (peak definition) had to be completed by hand because of the relatively complicated nature of the chromatograms.

As stated earlier, we intended to plot the data by normalising peaks against other peaks in the same spectra in order to identify groups of samples where certain of the cannabinoids were expressed in similar ratios. This could be the case if those samples came from plants of the same cultivar strain.

The ratio was expressed as percentage. It was calculated by this method:

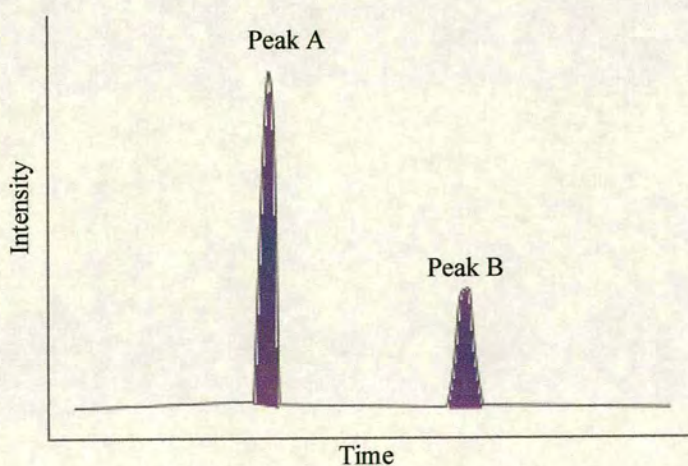


Figure 37 - Example chromatogram showing peaks A and B as used in the explanation of Peak Normalisation.



Consider peaks A and B (See Figure 37). If peak A were to be normalised against B, giving A_{AnormB} , then the area of the peaks (A_A and A_B , respectively) would be measured.

Then:

$$A_{AnormB} = 100 \left(\frac{A_A}{A_B} \right)$$

Two of these normalised peak areas would be plotted against each other. It was hoped that by finding the correct combinations, this approach would help separate out the various sample groups.

As there were 20 integrated peaks in each spectrum which could each be normalised against the other 19, there were 72,200 combinations!

It was decided that some form of automation was required, in order handle this dataset.

9.4.3 Dataminer

The program, written for this project in LabVIEW, was called Dataminer (See Figure 38). It allows the user to view any combination of normalised peaks, either with or without the isotopic data being included. In addition, as a crude absolute quantification technique, it takes the sum of all the peak integrals from each spectrum and uses these to normalise each component to aid identification of interesting components (i.e. ones where there is an obvious difference between sample groups).



The user interface of Dataminer is shown in figure 38. The four lists on the right of the screen allow the user to define the two components that are of interest (X – top left and Y bottom left) and the components against which they are to be normalised (X – top right and Y bottom right).

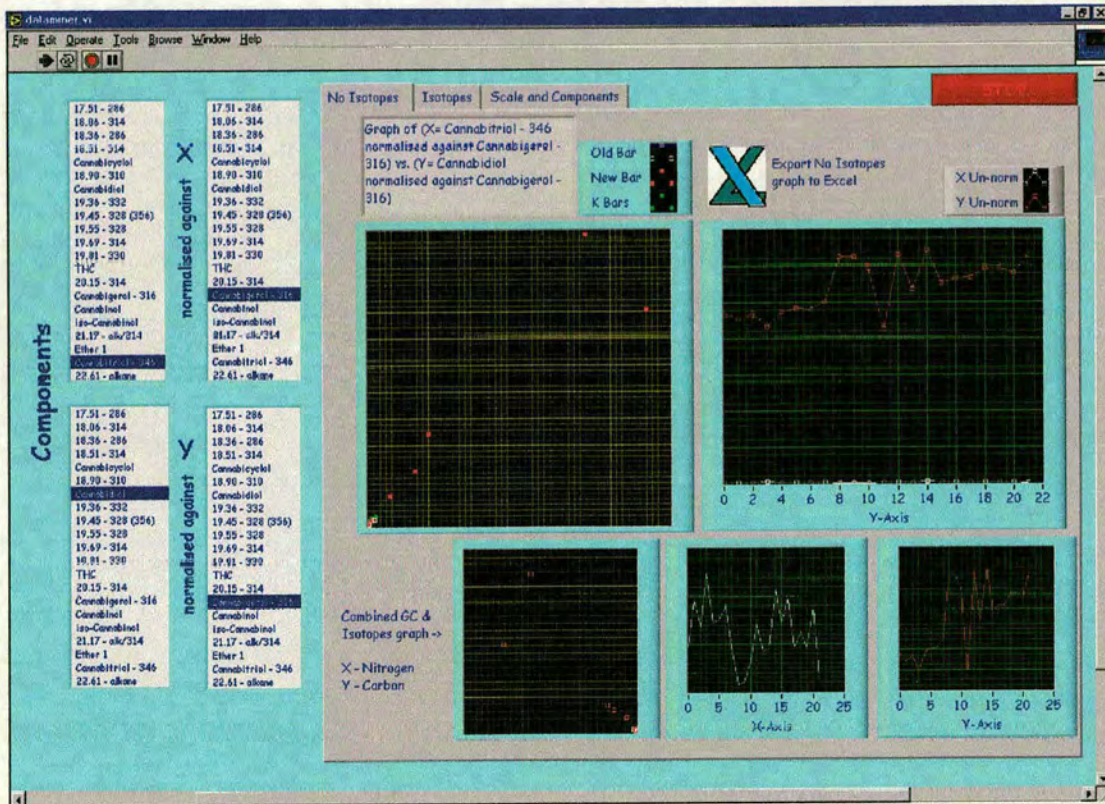


Figure 38 - Dataminer's user interface showing No Isotopes output window.

Dataminer then calculates and graphs a number of different output options on three different screen; No Isotopes, Isotopes and Scale and Components, selected by clicking on the tabs above the output window:



No Isotopes -

5 graphs on the output screen (clockwise from top left) (See Figure 38) –

- 1) Graph showing components X and Y components normalised against each one's respective Normalisation component plotted against one another for each sample.
- 2) Line Graph of each sample's X and Y (un-normalised) components. X components white, Y components red. Sample sequence – Old Bars 1 and 2, New Bar average, New Bars 1-9, K Bars 1-10.
- 3) Line Graph showing only Y data from (2) above.
- 4) Line Graph showing only x data from (2) above.
- 5) XY Graph showing Data from (1) but with X data multiplied by the carbon isotopic ratio of that sample and the Y data multiplied by the nitrogen isotopic ratio of that sample.



Isotopes -

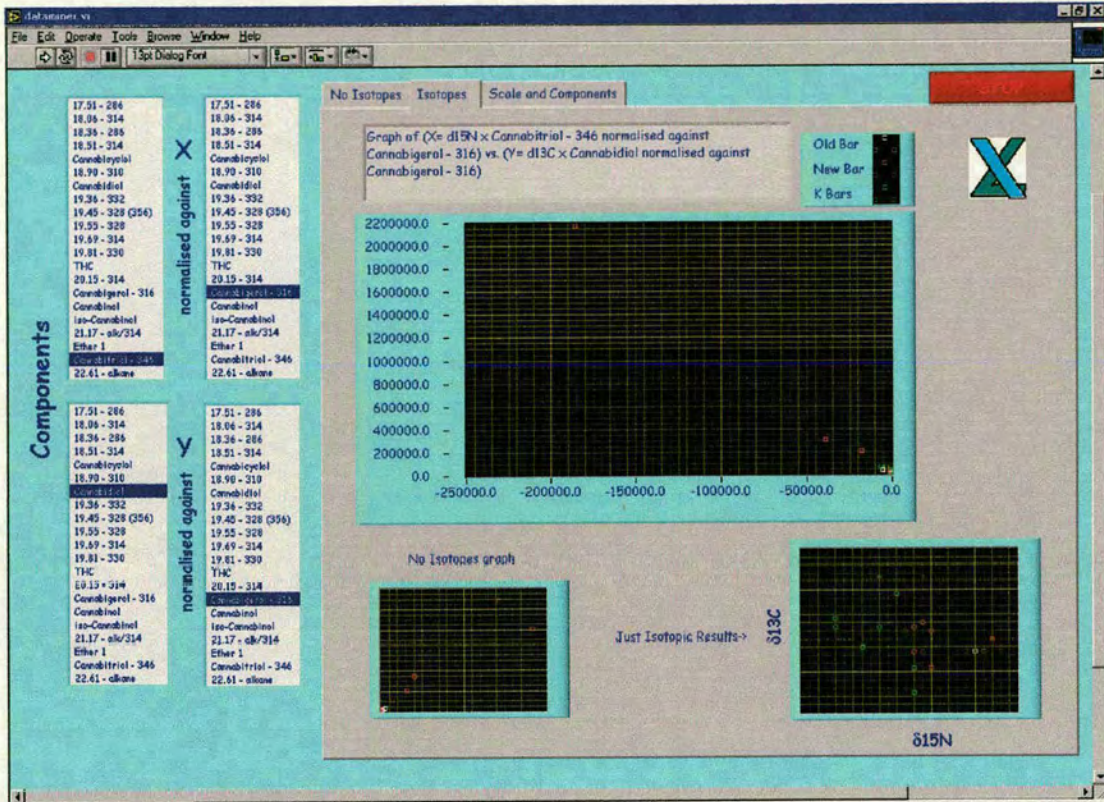


Figure 39 - Dataminer showing Isotopes output window.

3 graphs on the output screen (clockwise from top left) (See Figure 39).

- 1) Large version of No Isotopes (5) above.
- 2) XY Graph of Isotopic Data Alone
- 3) Small version of No Isotopes (1) above.



Scale and Components -

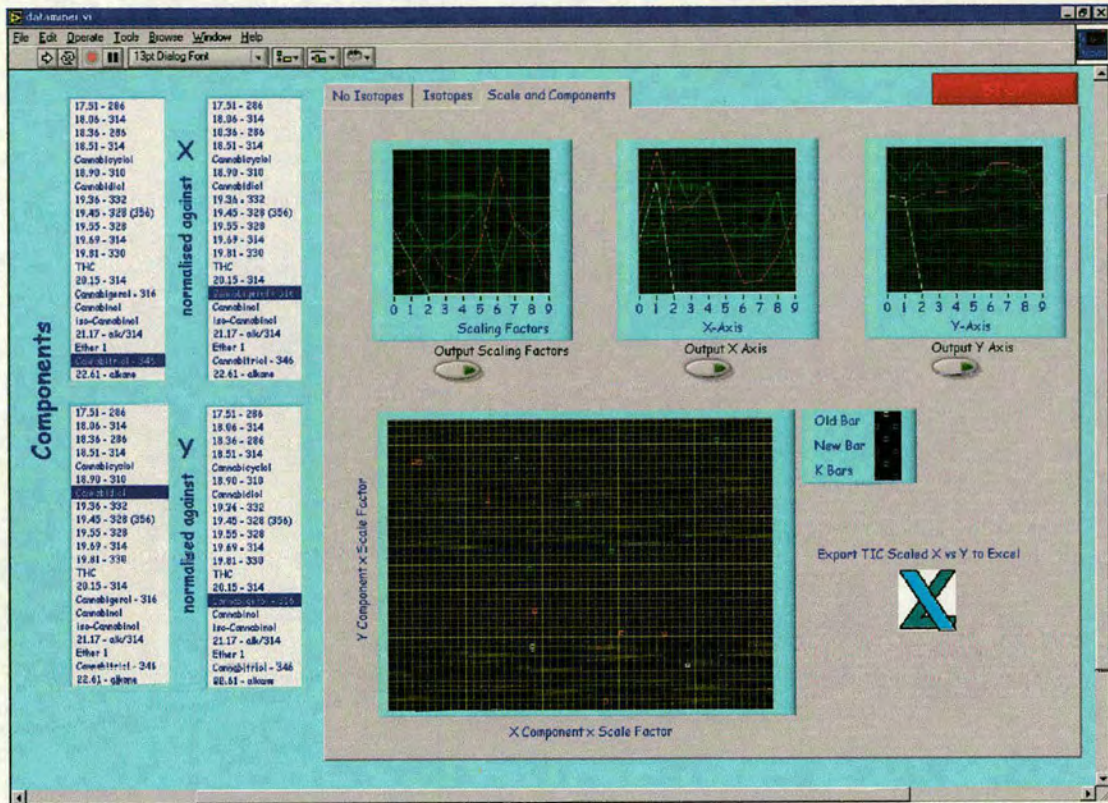


Figure 40 - Dataminer showing Scale and Components output window.

5 graphs on the output screen (See Figure 40).

- 1) Sum of all components (un-normalised) for each sample (Scale factor). Each series plotted individually: **Old Bar 1-2**, **New Bar average and 1-9**, **K Bars 1-10**.
- 2) Scaled, un-normalised X data for each sample as above.
- 3) Scaled, un-normalised Y data for each sample as in (1) above.
- 4) XY graph of Scaled X vs. Scaled Y for each sample.



Graph titles are generated automatically, and all graphs can be automatically exported to Excel for printing etc.

Dataminer made it relatively easy to compare all the different cannabinoids, and with its help, it quickly became apparent that there were dramatic differences between the K samples and the both the Old and New bars, but that the Old and New Bars looked similar. This was, however, something of a false dawn, as we had fallen into the same trap as most of the workers before us.

Specifically, the problem is that most of the cannabinoids produced naturally by cannabis (primary cannabinoids) degrade after harvesting to other cannabinoids (secondary cannabinoids). Unfortunately, the vast majority of differences we were recording were a result of the different ages of the samples that were being analysed. No published work seems to have been done on the mechanisms of these degradations, and very little on the quantitative measurement of them.

Therefore, the aim of this section of the project was to identify cannabinoids in our resin that had low degradation rates.

9.4.3 Degradation Rate Estimation

The degradation rates of all the detected cannabinoids were estimated by the Camp method [52]. The scaled quantities of the cannabinoids were averaged for each

Determining the Origin of Cannabis Resin



sample group (Old Bar – 20 years old, New bar - 4 years old and K Bars – 1 year old).

These were then plotted against their ages.

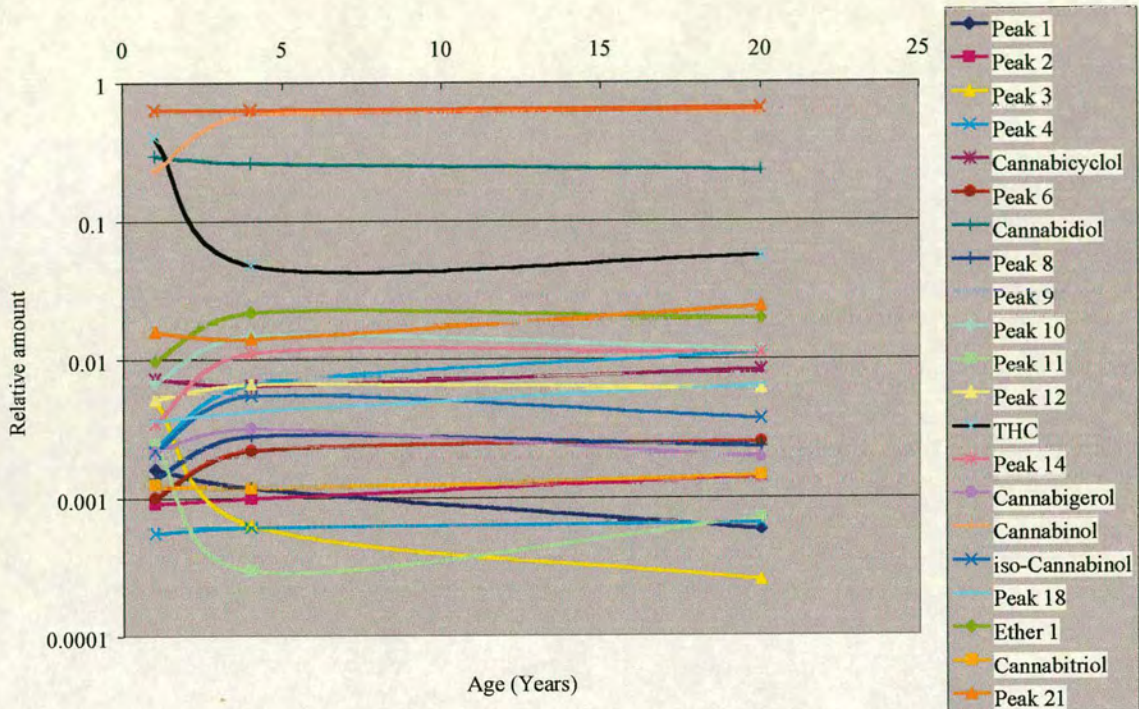


Figure 41 - Graph showing amounts of cannabinoids in resin after different time periods.

As well as the single cannabinoids shown in Figure 40, the sum of the tetrahydrocannabinol and cannabinol values is shown as well. Cannabinol is known to be the major degradation product of tetrahydrocannabinol, and therefore, the sum of the two is thought to be a good estimate of the initial tetrahydrocannabinol value. It is labelled as THC+CBN on the graph. THC and CBN are commonly used three letter codes for these cannabinoids. Others that are widely used include CBD (cannabidiol) and CBG (cannabigerol).

Determining the Origin of Cannabis Resin



The equations of the decay curves were calculated by exponential regression in Excel, and this information was used to rank the cannabinoids as primary or secondary (depending on the sign of the gradient) and also in order of reaction rate. With this information, it was possible to concentrate on low degradation rate, primary cannabinoids as these would give the most reliable information on the source plants.

Table 4 - Table of cannabinoids showing those which have relatively low degradation rates. Key

Primary Cannabinoids, Secondary Cannabinoids

Peak	Peak Name	Mass	Formula
1	17.51	286	$C_{19}H_{26}O_2$
2	18.06	314	$C_{21}H_{30}O_2$
3	18.36	286	$C_{19}H_{26}O_2$
4	18.51	314	$C_{21}H_{30}O_2$
5	Cannabicyclol	314	$C_{21}H_{30}O_2$
6	18.9	310	$C_{21}H_{26}O_2$
7	Cannabidiol	314	$C_{21}H_{30}O_2$
8	Cannabichromanone	332	$C_{20}H_{28}O_4$
9	19.45	328	$C_{22}H_{32}O_2$
10	19.55	328	$C_{22}H_{32}O_2$
11	19.69	314	$C_{21}H_{30}O_2$
12	19.81	330	$C_{20}H_{26}O_4$
13	Tetrahydrocannabinol	314	$C_{21}H_{30}O_2$
14	20.15	314	$C_{21}H_{30}O_2$
15	Cannabigerol	316	$C_{21}H_{32}O_2$
16	Cannabinol	310	$C_{21}H_{26}O_2$
17	iso-Cannabinol	310	$C_{21}H_{26}O_2$
18	21.17	Unknown	Unknown
19	21.33 (Ether)	328	$C_{22}H_{32}O_2$
20	Cannabitriol	346	$C_{21}H_{30}O_4$

The two low degradation rate primary cannabinoids were cannabidiol and cannabigerol. This was a key discovery as they are both involved in the biosynthesis of tetrahydrocannabinol (See Figure 42).



9.4.4 Identifying Differences in Biosynthesis

Analysing for cannabigerol, cannabidiol and the combined tetrahydrocannabinol and cannabinol values allows us to monitor different stages in the biosynthesis of the active ingredient of cannabis. Any differences in these stages could be a result of selective cultivation.

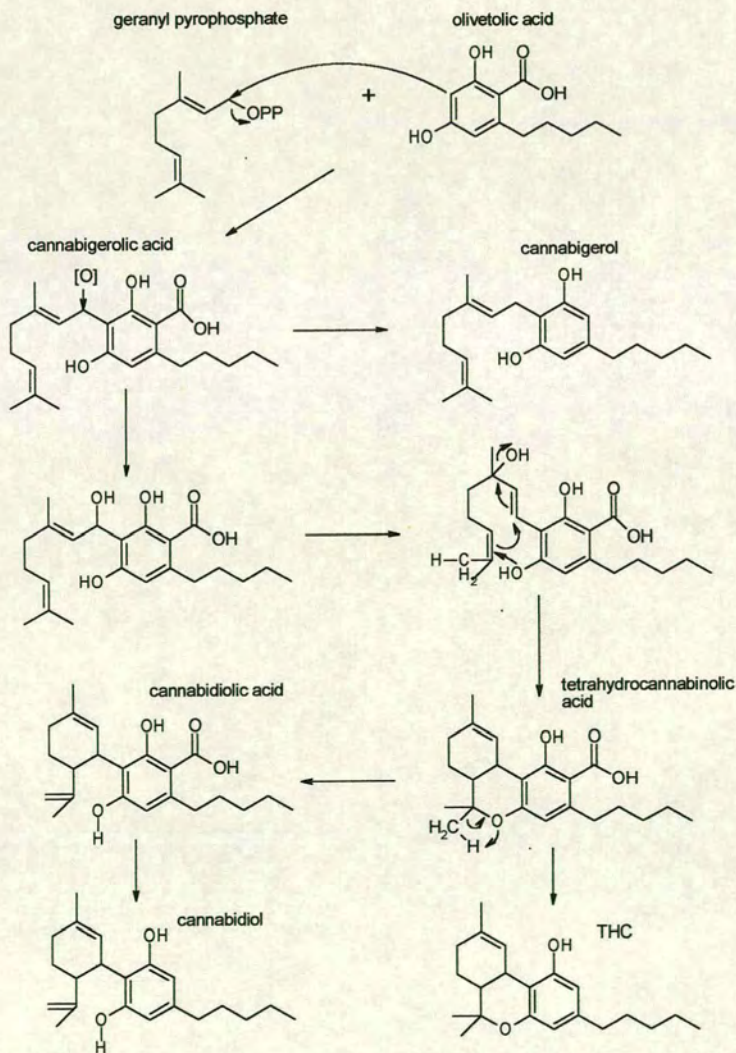


Figure 42 - Biosynthesis of THC showing relationship to cannabigerol and cannabidiol. (Copy of

Figure 11).



The rationale behind this conclusion is as follows. There are two possible aims for a hashish producer: either to produce a high quality, potent product which can be marketed at a premium, or to produce a higher volume, lower quality, lower value product. The type of plant required for the high volume low quality resin production will be selectively cultivated to produce a large volume of resin per plant, but that it need not have a particularly high potency, whereas the opposite is true for the low volume, high quality resin. Obviously, the perfect combination would be a variety that produced high volumes of high quality resin, but this has not yet been attained.

Cannabis is very susceptible to selective cultivation [49]. Therefore, as different characteristics are required for different styles of producer; over a period of time, it is expected that some enhancement of these beneficial characteristics should be evident as a result of selective cultivation. In the case of the low quantity, high quality crop, it would be expected that the THC content might increase over time, whereas in the high quantity crop, the amount of resin might increase and the potency might not be affected. Whatever the desired outcome of the selection, the growers measure its success unscientifically. If potency is required, which is related to the THC content [53], then this can be detected by taking the drug. What is not understood by the growers are the biochemical changes in the plant that have brought about this change.

Providing that the increased production of THC, or of absolute volume of resin, is not caused by the linear promotion of all stages of the biosynthesis pathway, relative differences in the amounts of the various compounds in the path will result. Indeed,



when we looked for these differences in our samples, some were apparent. (See Figure 43).

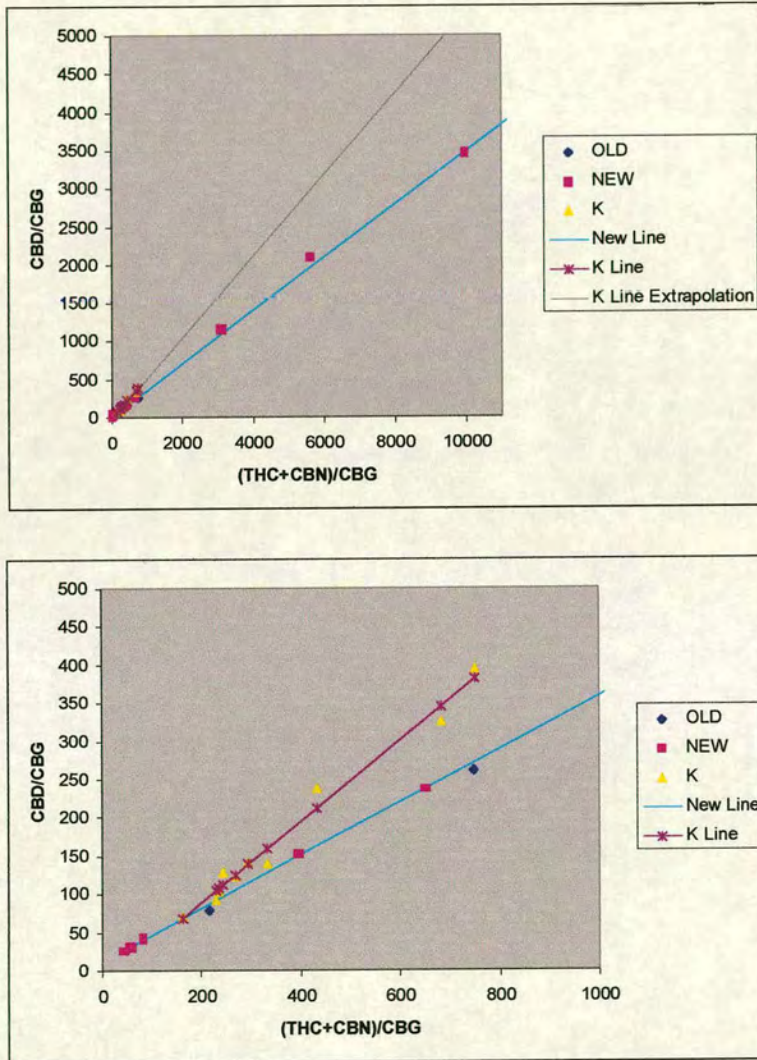


Figure 43 - Both graphs show total original THC content (THC+CBN) normalised against CBG vs. CBD normalised against CBG. Bottom graph is a magnification of the upper graph to show detail.

The graphs (Figure 43) show at least two different lines of plants (there is little difference between the Old and New Bars). Relative to cannabigerol, the recent K bar plants were producing more cannabidiol then the older plants, for the same relative amount of THC. It is interesting to note that the amount of original THC in the resin



has actually decreased over the 20 year period. This is probably because the producers are supplying a lower quality product which is cheaper to produce.

In any case, there is a clear difference in the relative importance of different stages in the biosynthesis of THC in the 2 sets (the Old and New bars being grouped).

In fact, when the cannabidiol content is plotted directly against the total THC, two parallel groups result (see Figure 44). These groups show conclusively that the newer K samples come from plants, which produce more THC initially, but that more of this is converted on to cannabidiol.

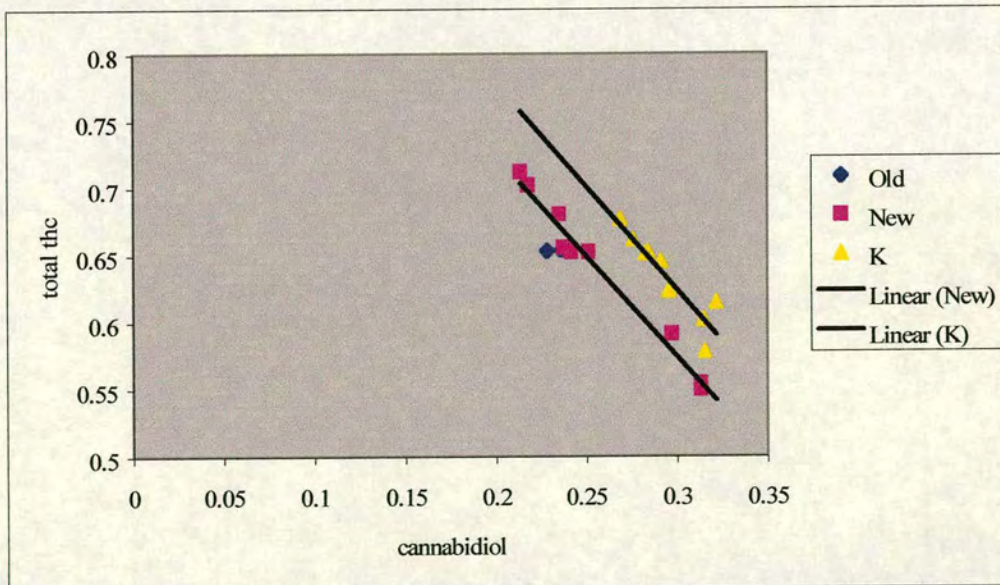


Figure 44 - Graph of cannabidiol vs total THC showing two parallel groups.



9.4.5 Conclusions

The THC concentration within the resin appears to have decreased of the last 20 years, suggesting that the goal of the producers of this hashish was not the low volume high potency product, but rather high volume low quality.

The 20 year old and 4 year old samples are too similar to separate by this means. There does, however, appear to have been a change in the source plants of the hashish analysed, sometime in the last 4 years. This could either be because a new plant strain has been introduced into the original growth area, managed by the same growers; or because a new area, where a slightly different variety is grown, became the supply region. Both hypotheses are plausible; however, if the second is the case, then we already know from the stable isotope results that the new source region cannot be far removed from the original region.

Whichever is true, both the stable isotope and biochemical data suggests that there have been no dramatic changes in the source of cannabis resin supplied to Edinburgh over the last 20 years.

Future Work

The most important work to be done in the future will be to collect cannabis resin samples from all the known growth areas, and analyse for the three isotopic ratios,



$\delta^{13}\text{C}$, $\delta^2\text{H}$ and $\delta^{15}\text{N}$. This data would then be used to build up a global database against which future finds could be measured. Following contact with the United Nations Office of Drug Control and Crime Prevention, in Vienna, this work is already at an early stage. Attempts are being made, on our behalf, to arrange for the Moroccan authorities to supply us with resin from known source regions in Morocco. Various diplomatic problems are causing a stumbling block at present, but it is hoped these will be overcome.

Analysis of the Moroccan samples should help indicate what geographic resolution that is attainable with stable isotopic analysis, and with this information, it would be possible to plan a global scheme along the same lines.

Where marijuana is concerned, the situation is much simpler. As the same biochemical processes are responsible for the production of generic compounds, such as chlorophyll and cellulose, in all plants, the same isotopic fractionation is seen in all plants. Hence, the isotopic ratio seen in chlorophyll from cannabis will be the same as the isotopic ratio in the chlorophyll from other plants grown in the same area. Therefore, it is not necessary to collect cannabis plant samples from all growth regions, as non-drug producing plants from those regions will offer the same information. Indeed, if a systematic isotopic fractionation could be established between some generic chemical found in cannabis plants and the resin they produce, then the global collection of cannabis resin may be completely avoided in the future. With this in mind, we have begun a collaboration with the Department of Pharmacognosy and Phytotherapy at the University of London. They have a licence



to grow cannabis for research purposes, and we have arranged for their licence to be amended such that they may supply us with samples for analysis.



10 Project Conclusions

This project has been the most advanced forensic drug study of its type. Despite its limited sample set it has shown the potential of the techniques developed to answer real questions.

Additionally, many of these techniques could be applied to other illegal drugs such as cocaine or heroin.

Beneficiaries of this work include the UN, H.M. Customs and Excise and local Police Forces in that it will offer them more information on the demographics of the drug trade and highlight the results of any campaigns designed to affect it.



Appendix A - Stable Isotope Ratio Measurement Mass Spectrometers

The most common type of conventional SIRMS is shown in figure 45.

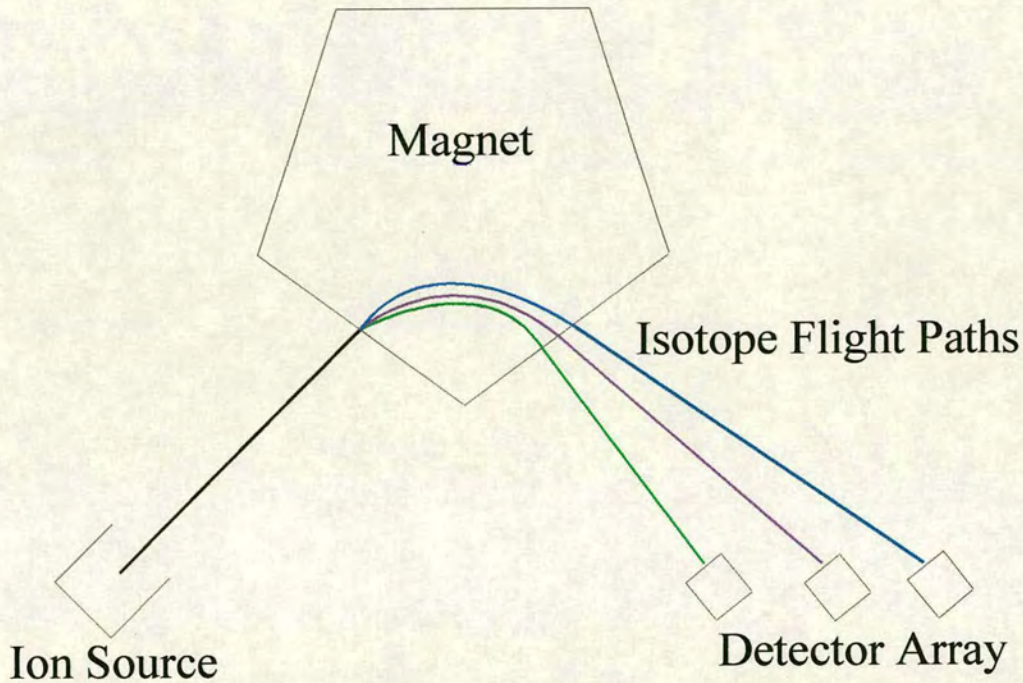


Figure 45 - Schematic of the main components of an isotope ratio mass spectrometer.

Small molecules, containing the elements of interest (in this application, these molecules are usually oxides e.g. H_2O , CO_2 and SO_2 ; or N_2) are ionised in the ion source and are accelerated towards a region of high magnetic field. The magnetic field affects the ions and forces them to follow a curved path. As the magnetic field seen by all ions is constant and assuming that the ions are equally charged, any difference in the radius of the curvature of the flight path can be ascribed to their momentum (which is proportional to their mass). Lighter ions are more affected by



the magnetic field than heavier ions. This is true whether the difference in mass is a result of a different chemical formula or because there are different isotopes being incorporated in the same molecule.

In SIRMS instruments, the detector array is usually restricted to three faraday cups. The positions of these cups are set so that they capture the ions of 1 amu higher than the last. For example, if the isotopic ratio of carbon was to be measured, then the left most detector in Figure 45, collecting the green ion beam, would be set to collect ions at m/z 44, being a singly charged CO_2 molecule where the carbon is ^{12}C and both the oxygens are ^{16}O ; the next detector, collecting the purple ion beam, would detect the isotopomer of 45 Da, where the ^{12}C has been replaced with a ^{13}C (See Figure 45).

As an ion strikes the collector electrode in a faraday cup detector, one electron is lost from the electrode. This relationship remains very constant, regardless of the ion beam intensity. This is not the case for other types of detector, and is the reason why faraday cup detectors are used in SIRMS instruments.

As many ions hit the electrode, and the same number of electrons are lost by it, a current is created between the electrode and ground:

$$Q = I.t = n.F.e \quad (1)$$

e (the number of electrons removed per molecule) = 1, so it can be ignored

$$\Rightarrow I = (n.F)/t \quad (2)$$



Let ϕ be the ion beam intensity, expressed as the number of ions passing (x), in moles per second, or:

$$\phi = x/(L.t), \text{ so}$$

$$\phi = n/t \quad (3)$$

Then (from (2) and (3)),

$$I = \phi.F \quad (4)$$

where Q is the charge in coulombs, I is the current in amps, t is the time in seconds, n is the number of moles of ions and electrons, F is Faraday's constant, x is the number of ions passing and L is Avogadro's number.

This current, and the attendant voltage, are very small. The voltage is amplified according to Ohm's law (5) by the addition of a very large resistor into the circuit (See Figure 46):

$$V=I.R \quad (5)$$

In SIRMS instruments, the ion beam voltages are not measured absolutely. Instead, the voltages of two electrodes are compared, using a differential amplifier, and the output of this is taken as the reading. This differential voltage is calibrated to an



isotope ratio by comparing it to the readings taken from a series of calibration standards.

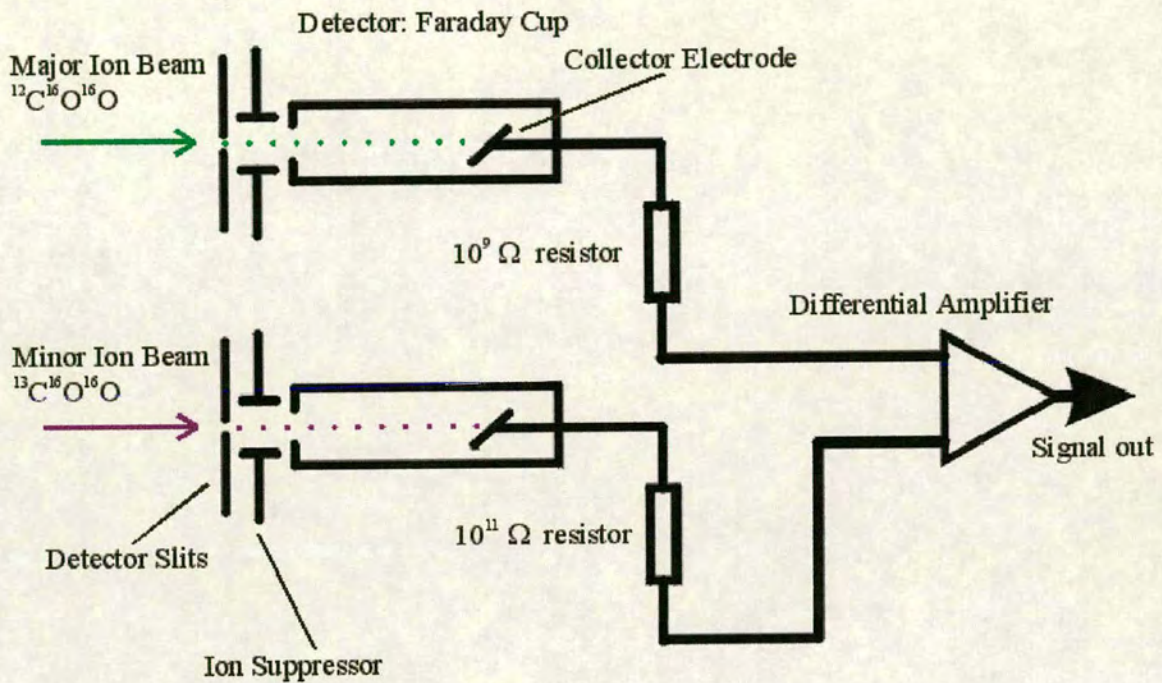


Figure 46 - Diagram of detector array and circuitry in a conventional SIMS instrument.

The measured ratio is not exactly equal to the actual ratio:

$$R_{\text{meas}} \neq R_{\text{true}}$$

But the measured ratio is proportional to the true ratio:

$$R_{\text{meas}} = k \cdot R_{\text{true}}$$

k is impossible to measure, so it is cancelled out by comparing the measured and true ratios of the standard with those of the sample:



$$\left(\frac{\text{sample } R_{\text{meas}}}{\text{standard } R_{\text{meas}}}\right) = \left(\frac{k \cdot \text{sample } R_{\text{true}}}{k \cdot \text{standard } R_{\text{true}}}\right) \quad (5)$$

During the time of an analytical run, various instrumental characteristics can fluctuate, altering k . Therefore, the instrument must be restandardised regularly so that k may be cancelled out successfully.



Appendix B – Proposed Identification of Components in Hashish GC-MS Analysis.

There are two possible routes to determine the structures of the components discerned in the GC-MS analysis of hashish: Synthesis and Extraction

The Synthetic route would advance by synthesising molecules which could match these in the GC-MS trace of hashish and analysing them by GC-MS to confirm that they are identical. If the synthesised molecule was found to be different from any of the hashish components, its structure would be adjusted and the new molecule tested – and so on until a match was found for all components.

The Extractive route would entail a large scale chromatographic separation of hashish with collection of the extracted components. Once enough had been extracted, the samples could be analysed by NMR combined with GC-MS to confirm the structure.

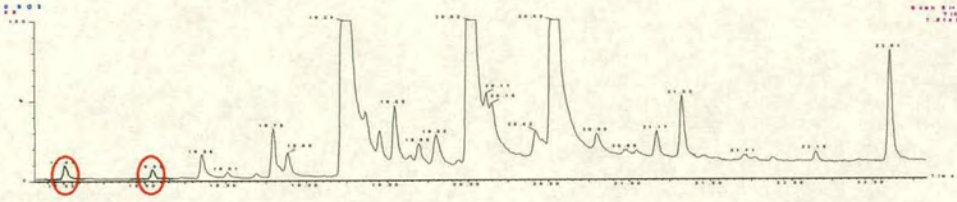
In fact, in the case of these samples, a combination of these two methods may be the more effective. For the more abundant components, extraction may show faster confirmation, whereas for the less abundant components, where very large amount of raw hashish would be required to generate a suitable mass of extract, synthesis may be more practicable.



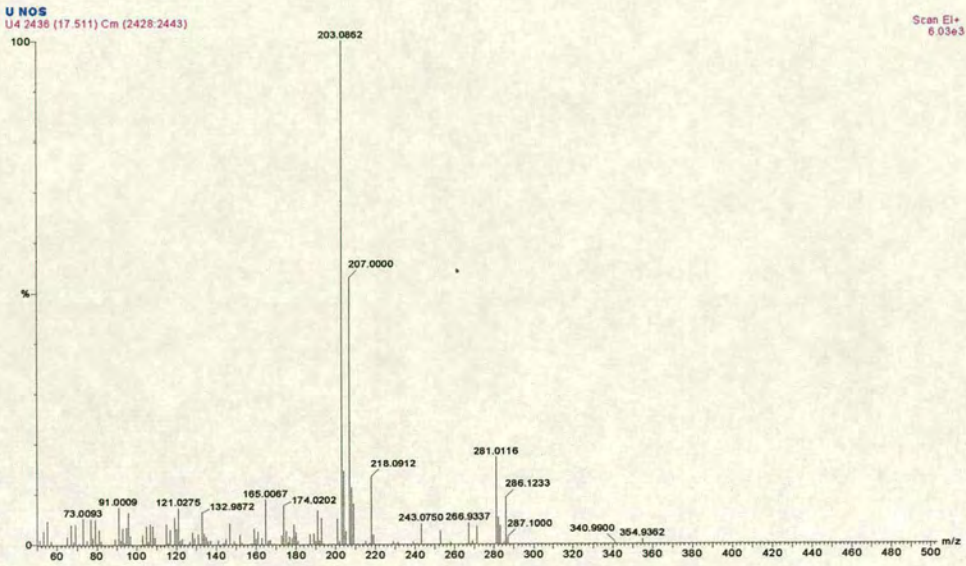
Appendix C – Mass Spectra of all Quantified Components of GC-MS analysis of Cannabis.

The following pages contain example mass spectra of all the measured components of the cannabis resin. At the top of each page is an example with two peaks highlighted. The mass spectra of these peaks are presented beneath them. Where the identity of the cannabinoid is known, it is given, otherwise, the spectra is named by the elution time of the compound in the chromatogram.

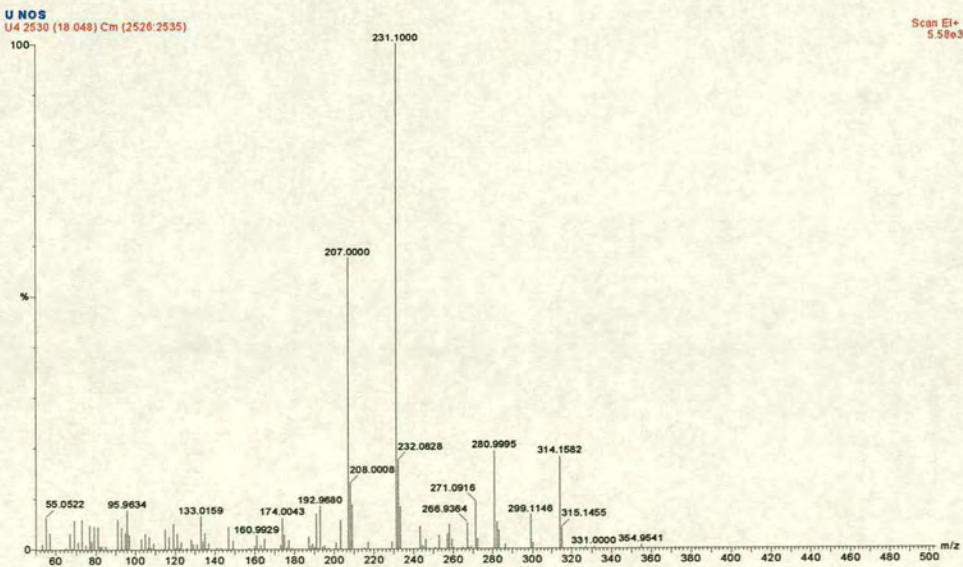
Determining the Origin of Cannabis Resin



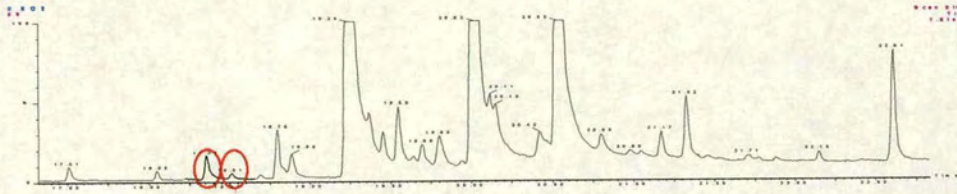
17.51



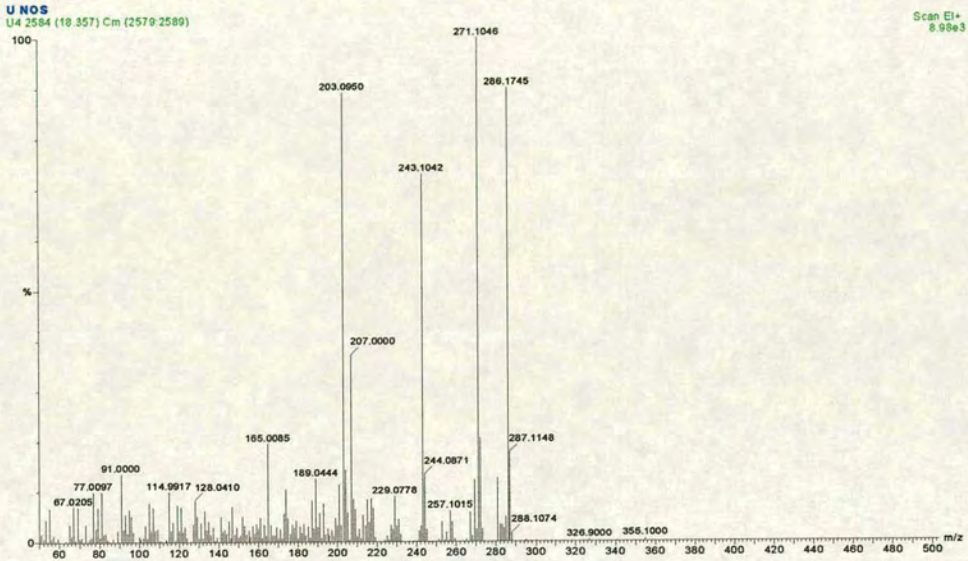
18.05



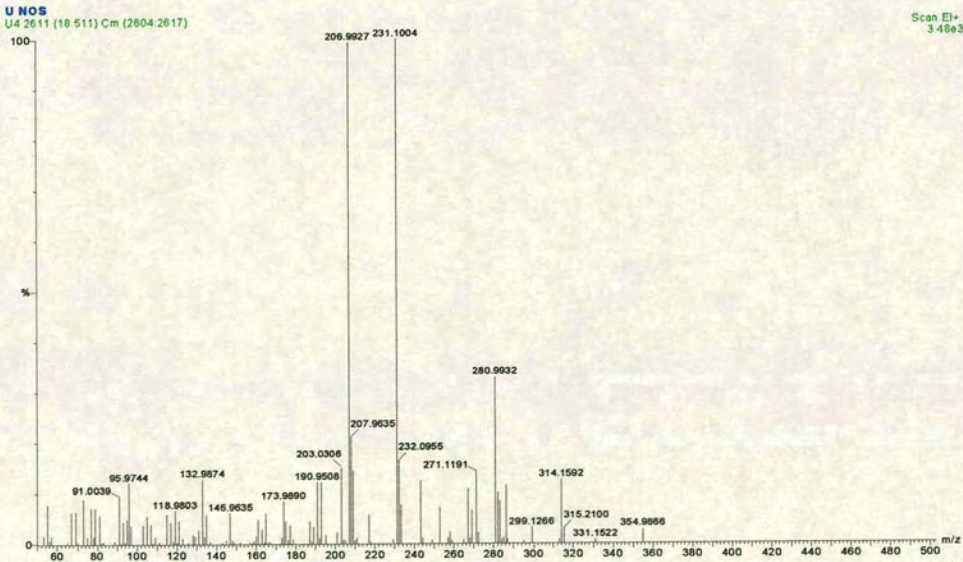
Determining the Origin of Cannabis Resin



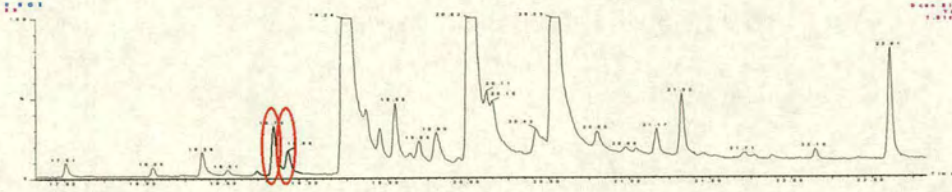
18.36



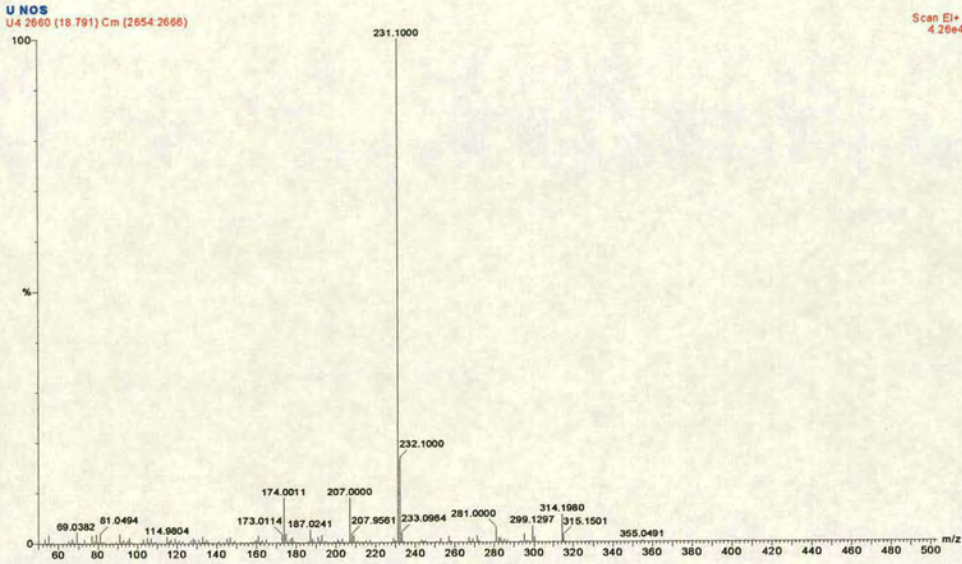
18.51



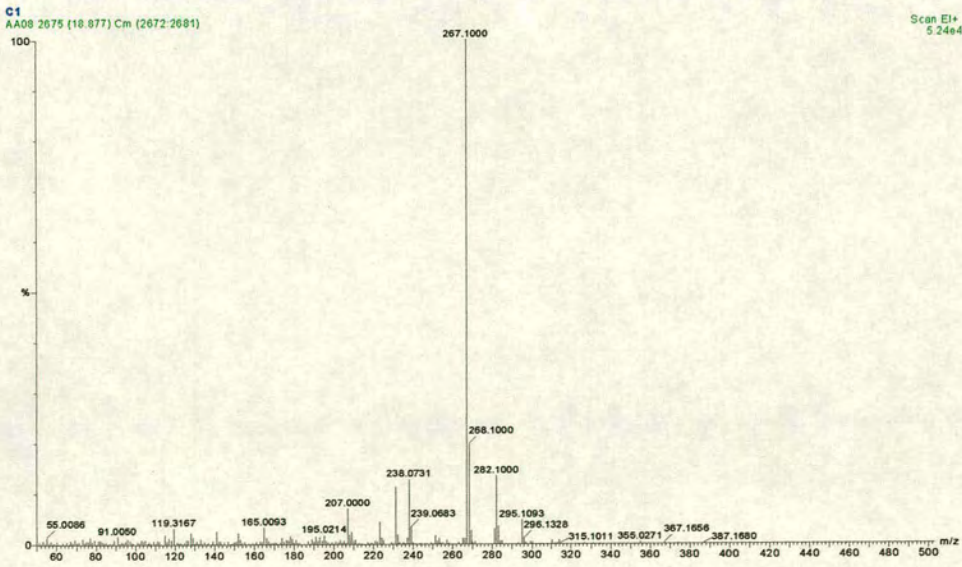
Determining the Origin of Cannabis Resin



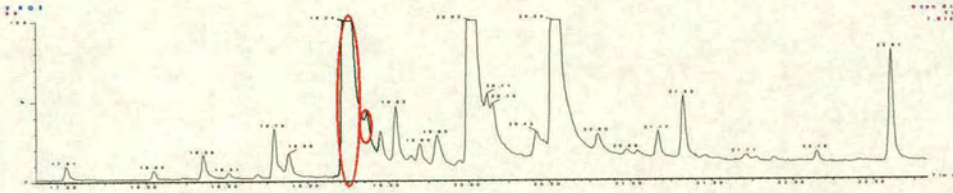
Cannabicyclol



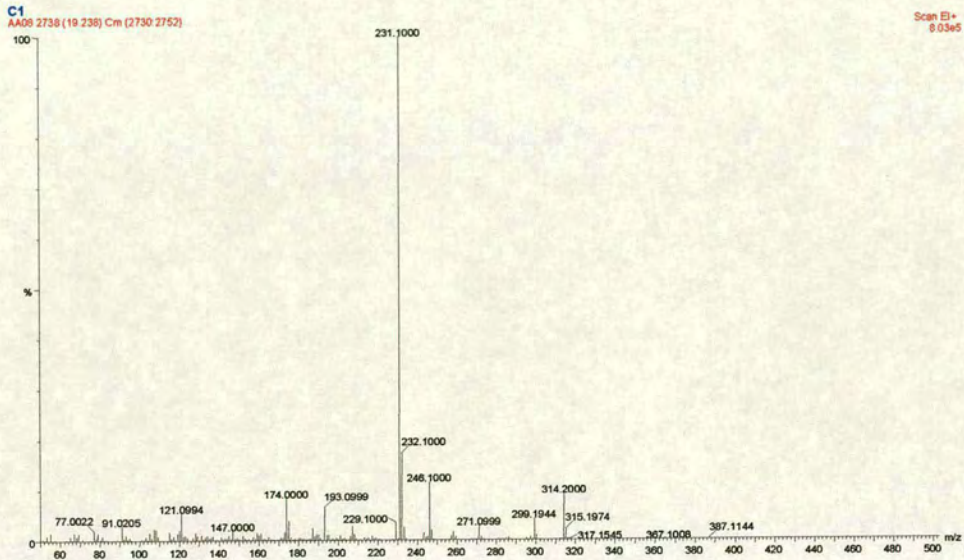
18.88



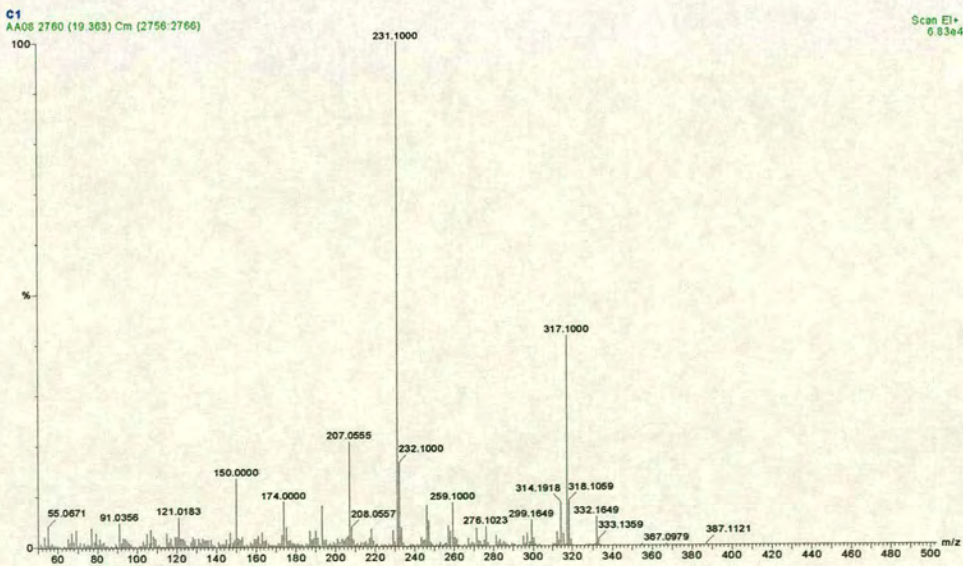
Determining the Origin of Cannabis Resin



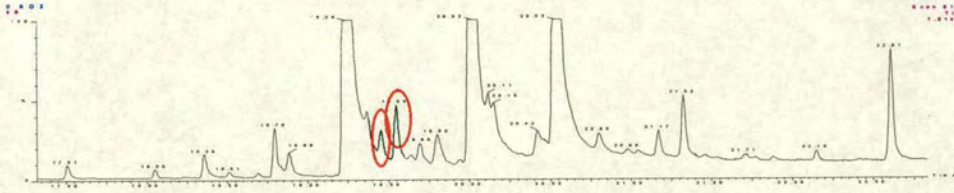
Cannabidiol



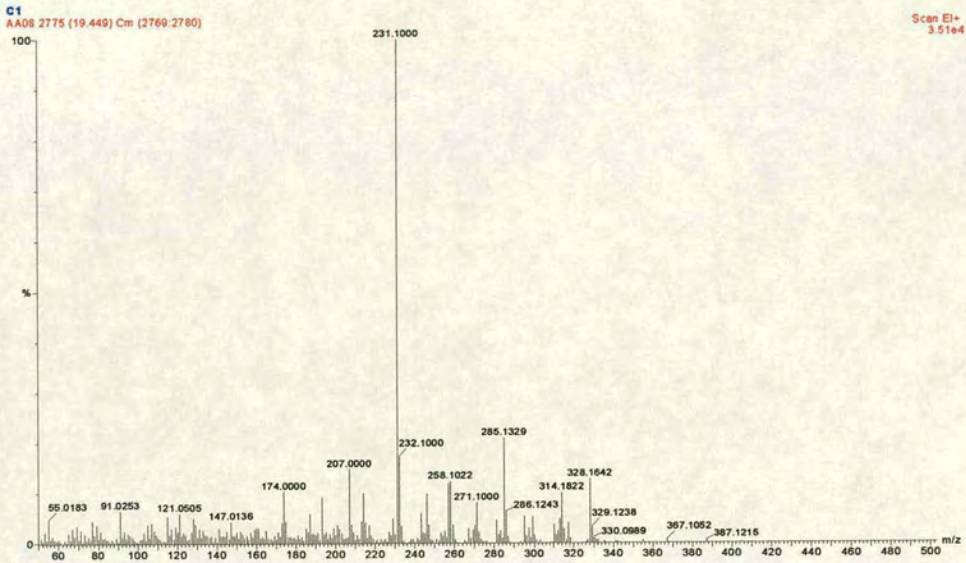
19.36



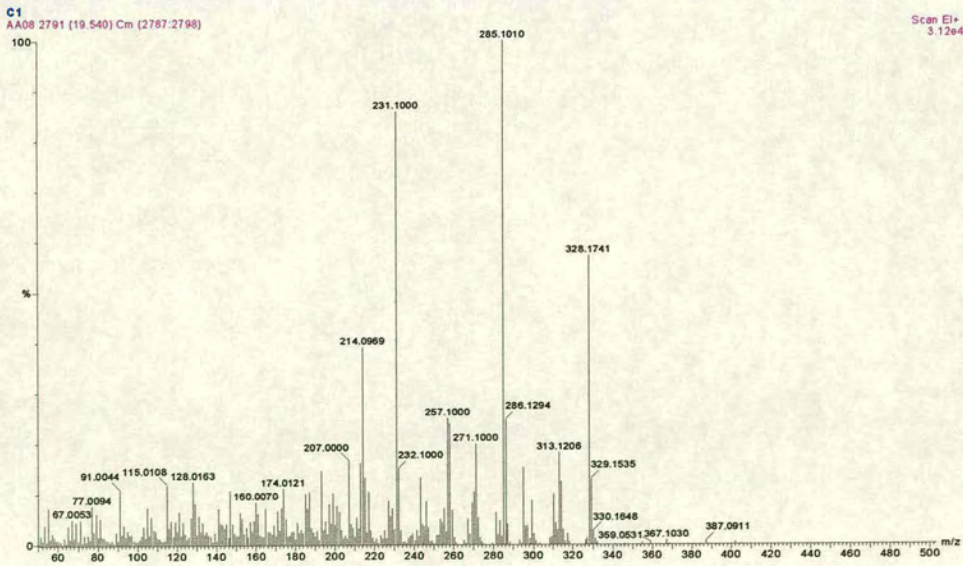
Determining the Origin of Cannabis Resin



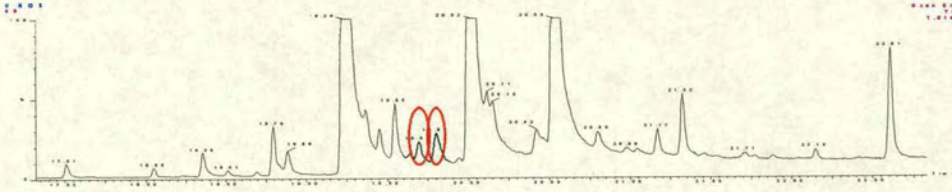
19.45



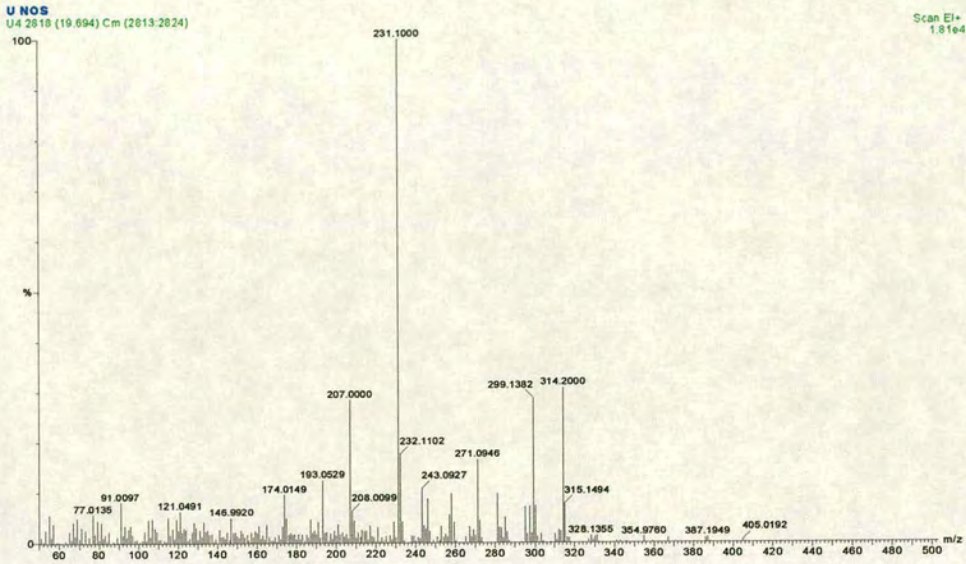
19.55



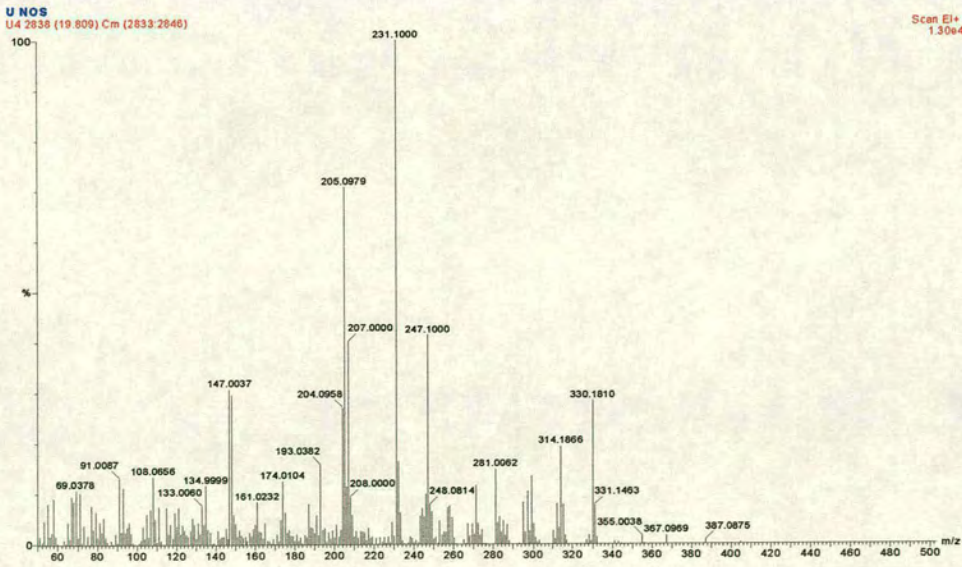
Determining the Origin of Cannabis Resin



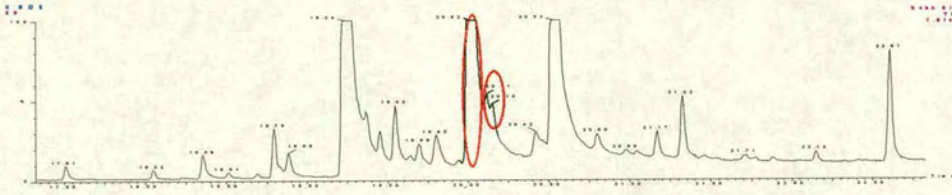
19.69



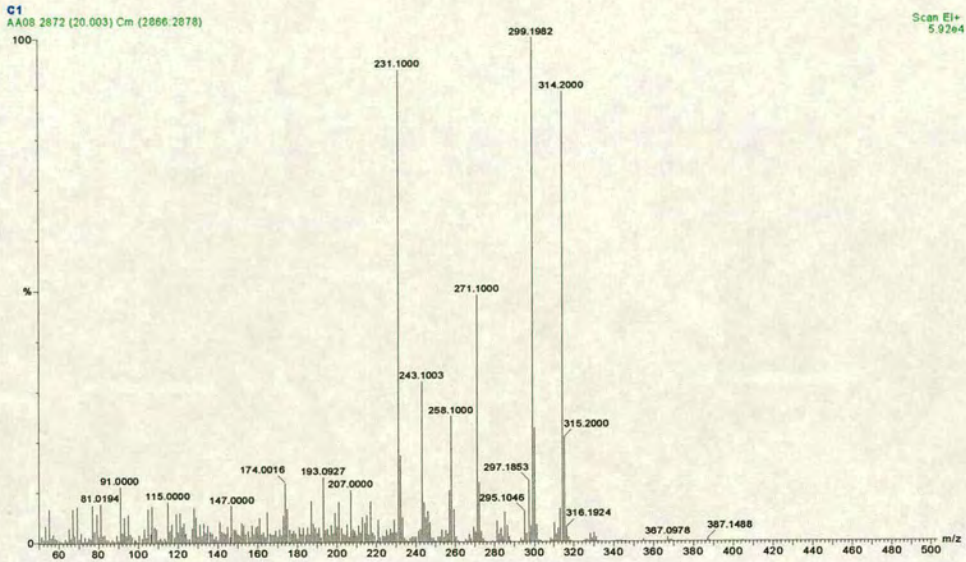
19.81



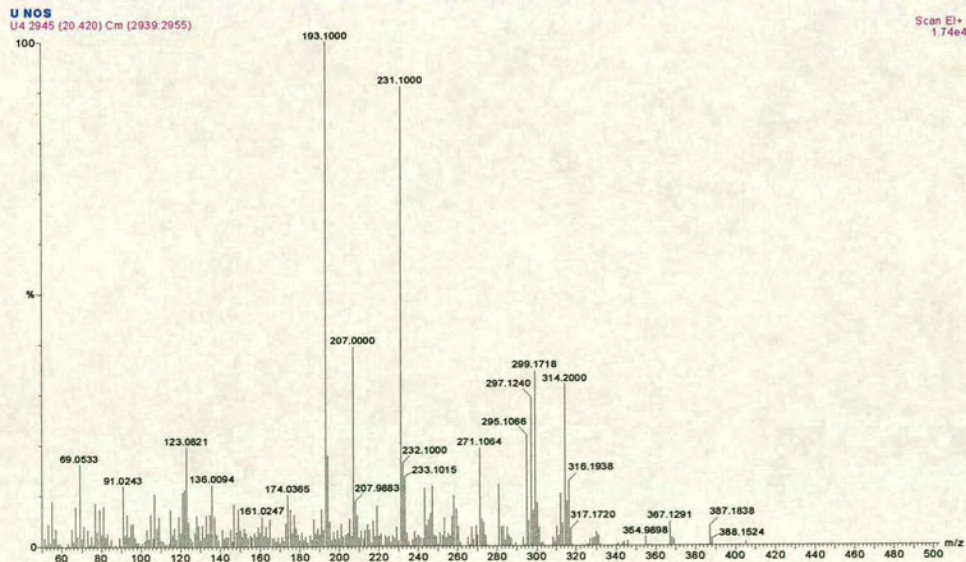
Determining the Origin of Cannabis Resin



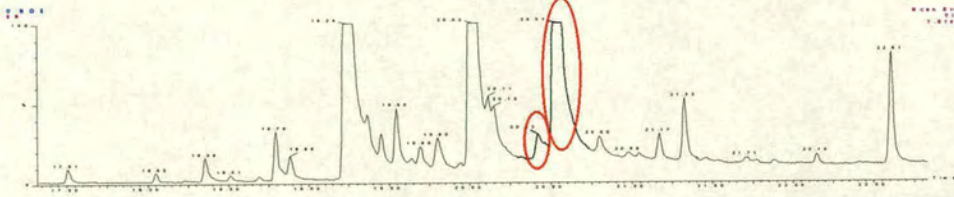
Tetrahydrocannabinol



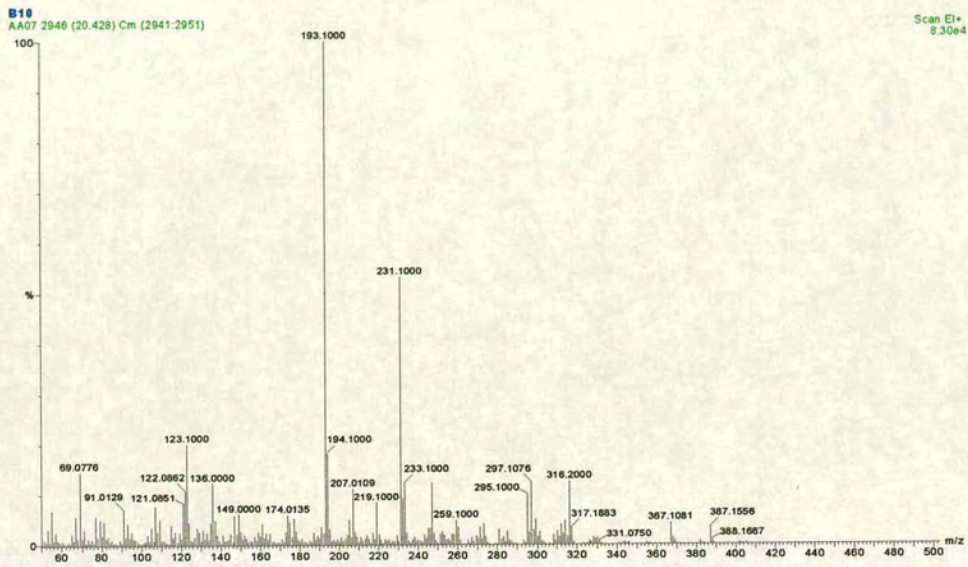
20.15



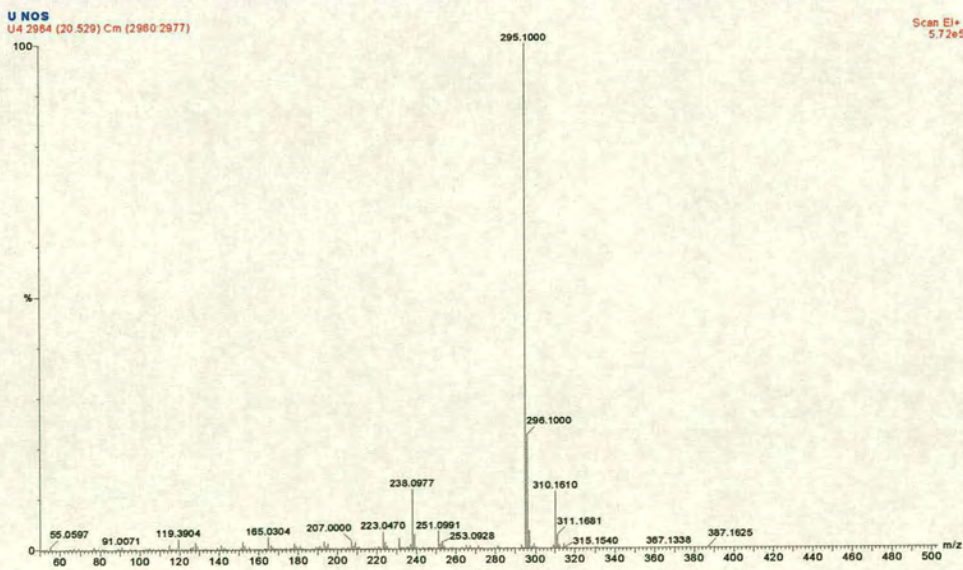
Determining the Origin of Cannabis Resin



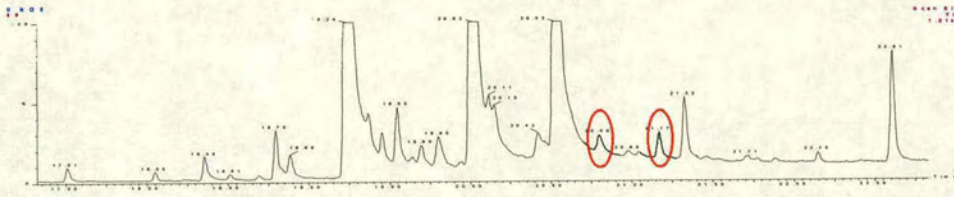
Cannabigerol



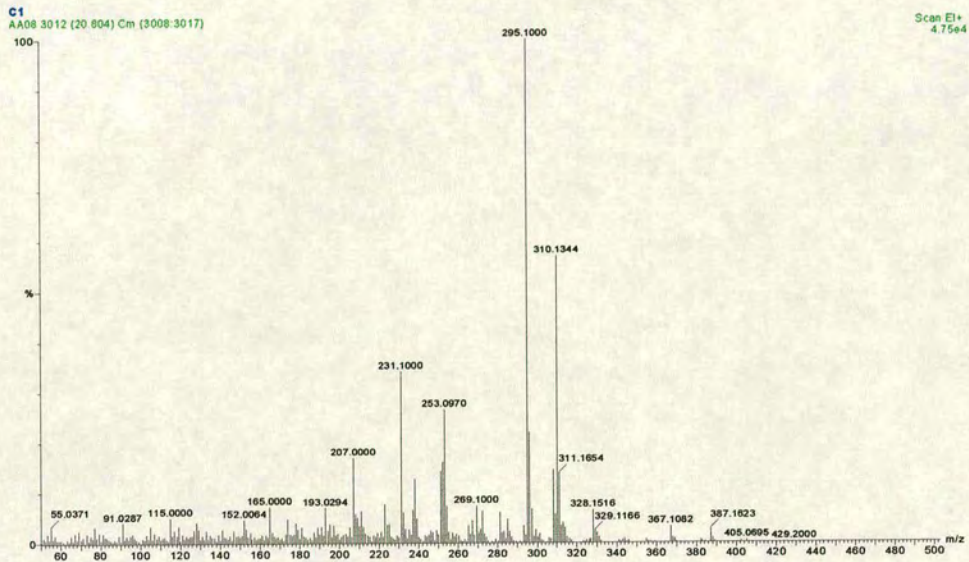
Cannabinol



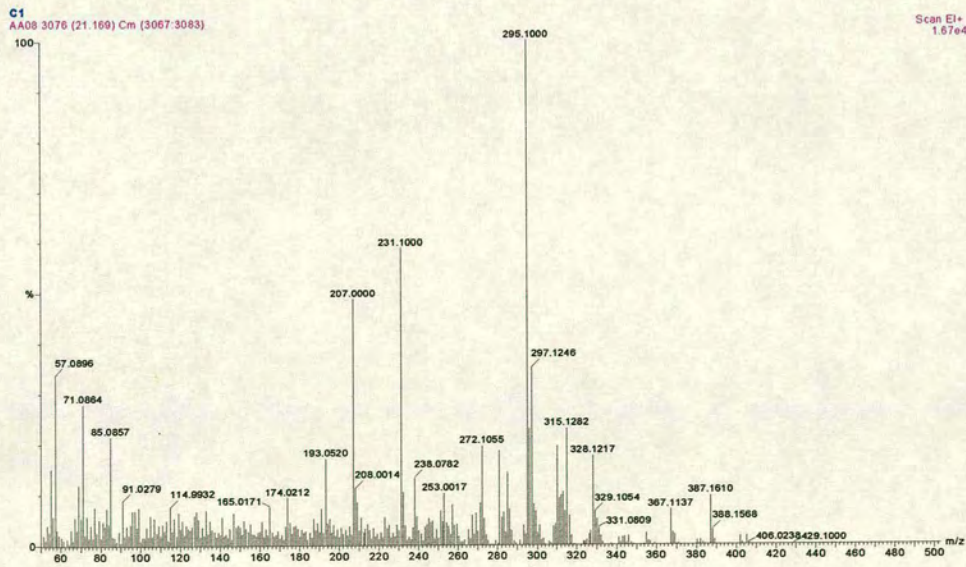
Determining the Origin of Cannabis Resin



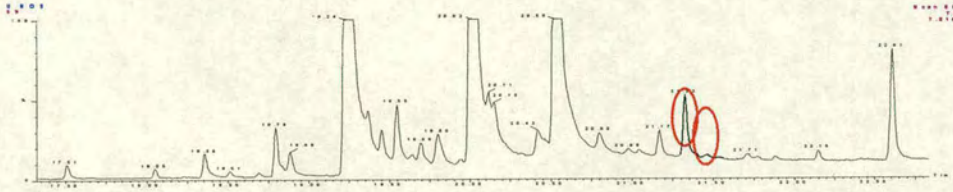
Iso-cannabinol



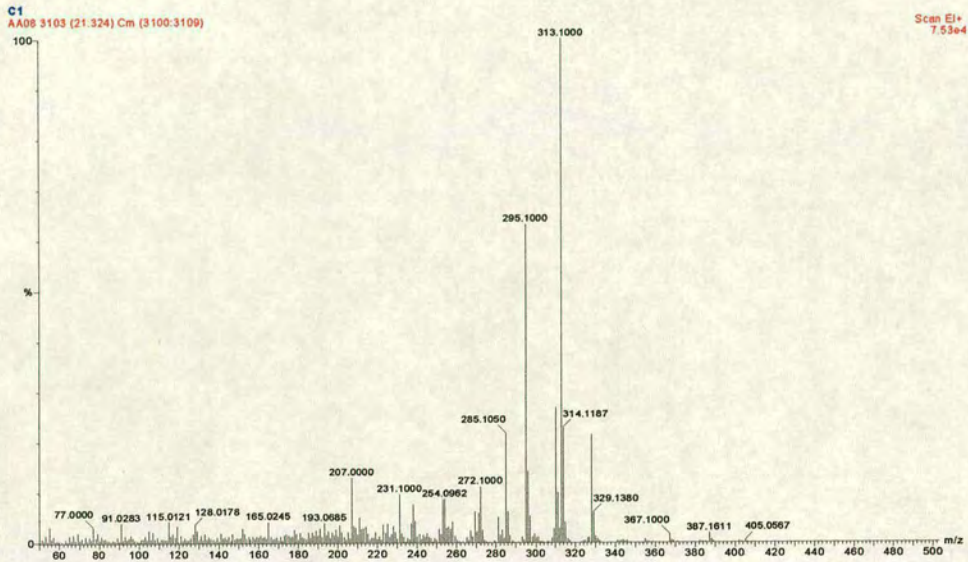
21.17



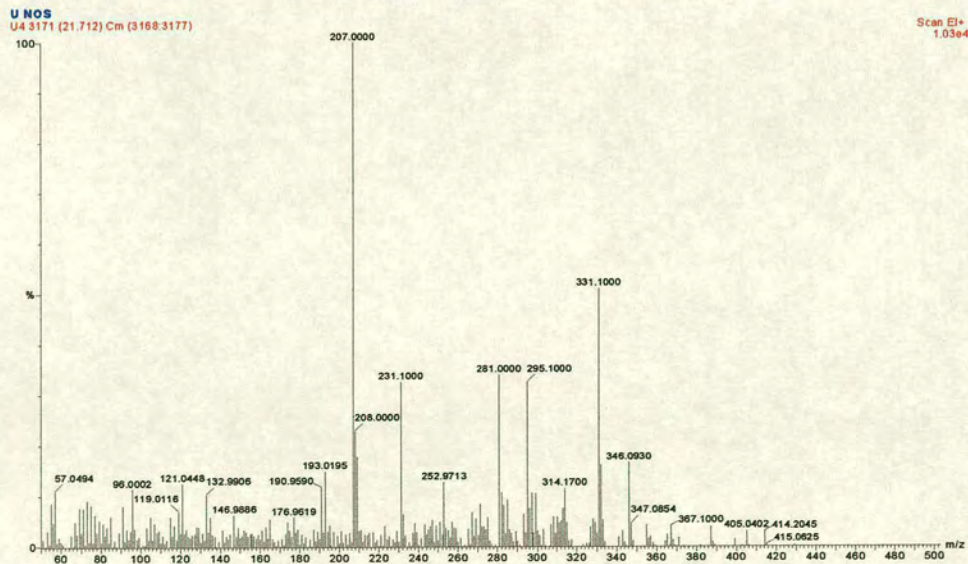
Determining the Origin of Cannabis Resin



Ether molecule



Cannabitriol





Appendix D – Dataminer Program

This information is to be found on the accompanying CD.



Reference List

1. HM Government. The Security Service Act 1989. 1989.
2. NCIS: 2000 UK Threat Assessment. National Criminal Intelligence Service, 2000;
3. Hutchinson, A. Let's Not Punt on The Third Down. 12-2-2002. US Drug Enforcement Agency.
4. Obseratoire Geopolitique des Drogues: Atlas mondial des drogues. Paris: Presses Universitaires de France, 1997;
5. Central Intelligence Agency. World Factbook 2001. <http://www.cia.gov/cia/publications/factbook/index.html> . 2001
6. Sweeney, J. DEA boosts its role in Paraguay. The Washington Post . 21-8-2001.
7. International Intellectual Property Alliance. Special 301 Recommendations: Paraguay. 20-2-1996. International Intellectual Property Alliance
8. Taylor, F. X. Narco-Terror: The Worldwide Connection Between Drugs and Terror. 13-3-2002. Washington DC, US Department of State.
9. Reuters. After attacks, spies scour for clues in So. America. The Boston Herald . 1-10-2002. Boston, Mass.
10. Office of the Coordinator for Counterterrorism. Patterns of Global Terrorism 2000. 30-4-2001. Washington DC, US Department of State.
11. Perelman, M. Argentina Set To Accuse Iran of Masterminding A Fatal 1994 Bombing. Forward . 24-8-2001. Washington DC.
12. Subcommittee On The Western Hemishpere Of The Committee On International Relations House Of Representatives. The Western Hemishpere's Response To The September 11, 2001 Terrorist Attack On The United States. 107-43. 1-10-2001. Washington DC, U.S. Government Printing Office.
13. AP and Reuters. Operativos en Brasil y Paraguay en busca de células islámicas: 17 arrestos. La Capital . 22-9-2001. Rosario.
14. Bach, W. The Taliban, Terrorism, and Drug Trade. 3-10-2001. Washington DC, US Department of State.
15. UNODCCP. UNDCP opium poppy survey in Afghanistan. ODCCP Update . 2000. United Nation Office of Drug Control and Crime Prevention.
16. CNN. Afghanistan: il bando anti oppio non funziona. CNNitalia.it . 26-1-2002. Italy, Cable News Network.



17. Perl, R. F. Taliban and the Drug Trade. 5-10-2001. Washington DC, Congressional Research Service, The Library of Congress. CRS Reports for Congress.
18. NDAB: Economic and Social Consequences of Drug Abuse and Illicit Trafficking. UNODCCP, 1998;
19. Cohen, W. S. Secretary of Defense. Annual Report to the President and the Congress. 2000. United States Department of Defense.
20. Small E, Jui PY, Lefkovitch LP: A numerical taxonomic analysis of Cannabis (marijuana) with special reference to species delimitation. Syst.Bot. 1976; 1: 67-84.
21. Mann J: Metabolites of mixed biosynthetic origin. In: Secondary Metabolism. Holker JSE, ed. New York: Oxford University Press, 1987; 261-301.
22. Fellermeier M, Eisenreich W, Bacher A, Zenk MH: Biosynthesis of Cannabinoids. European Journal of Biochemistry 2001; 268: 1596-1604.
23. ElSohly MA, Ross SA, ehmedic Z, afat R, B, nahan BF: Potency trends of D9-THC and other cannabinoids in confiscated marijuana from 1980-1997. Journal of Forensic Sciences 2000; 45: 24-30.
24. Atha, M. J. and Independant Drug Monitoring Unit. Types of Cannabis Available in the UK. The Case for Change. 2001. Release Publications.
25. Bouquet RJ: Cannabis. Bulletin on Narcotics 1950; 14-30.
26. Flashback Media Group AB. Harvesting hashish. 1998. Sweden, Flashback Media Group AB. Ref Type: Audiovisual Material
27. Carliño. 1/4 kilogram bar of Moroccan hashish in Ireland. 2001. Grass Valley, California, Erowid.
28. Gold D: Cannabis Alchemy: The Art of Modern Hashmaking: Methods for Preparation of Extremely Potent Cannabis Products. Berkeley, CA, USA: Ronin Publishing, 1990;
29. Drug Enforcement Agency. Hashish Oil. 2001. Washington DC, US Department of Justice.
30. Jenkins RW, Patterson DA: The relationship between chemical composition and geographical origin of cannabis. Forensic Science 1973; 2: 59-66.
31. Ward, S. Characterisation of cannabis resin using mass spectrometric techniques. 1998. Ref Type: Thesis/Dissertation
32. Lewis, Robert. Lothian and Borders Police Forensic Labs. 2001. Personal Communication.



33. Ferioli V, Rustichelli C, Pavesi G, Gamberini G: Analytical characterisation of hashish samples. *Chromatographia* 2000; 52: 39-44.
34. Global Network of Isotopes in Precipitation. Volumes of water involved in various stages of the water cycle per year. 2001. Vienna, IAEA/WMO.
35. Chorley RJ: Introduction to Physical Hydrology. London: Methuen & Co. Ltd., 1969;
36. Yurtsever Y, Gat JR: Atmospheric waters. In: Stable Isotope Hydrology. Gat JR, Confiantini R, eds. Vienna: IAEA, 1981; 103-142.
37. Mook WG: Environmental Isotopes in the Hydrological Cycle Principles and Applications. Vienna/Paris: UNESCO/IAEA, 2000;
38. O'Leary, MH, Madhavan, S, Paneth, P: Physical and chemical basis of carbon isotope fractionation in plants. *Plant Cell And Environment* 1992; 15: 1099-1104.
39. Ogrinc N, Kosir IJ, Kocjancic M, Kidric J: Determination of authenticity, regional origin, and vintage of Slovenian wines using a combination of IRMS and SNIF-NMR analyses. *Journal Of Agricultural And Food Chemistry* 1901; 49: 1432-1440.
40. Gimenez-Miralles JE, Salazar DM, Solana I: Regional origin assignment of red wines from Valencia (Spain) by H-2 NMR and C-13 IRMS stable isotope analysis of fermentative ethanol. *Journal Of Agricultural And Food Chemistry* 1999; 47: 2645-2652.
41. Angerosa F, Breas O, Contento S, Guillou C, Reniero F, Sada E: Application of stable isotope ratio analysis to the characterisation of the geographical origin of olive oils. *Journal Of Agricultural And Food Chemistry* 1999; 47: 1013-1017.
42. White JW: Isotope ratio testing of honey: Demystifying the internal standard test. *American Bee Journal* 2000; 140: 318-321.
43. Cienfuegos E, Casar I, Morales P: Carbon isotopic composition of Mexican honey. *Journal Of Apicultural Research* 1997; 36: 169-179.
44. DUNBAR J, WILSON AT: DETERMINATION OF GEOGRAPHIC ORIGIN OF CAFFEINE BY STABLE ISOTOPE ANALYSIS. *Analytical Chemistry* 1982; 54: 590-592.
45. Ehleringer JR, Casale JF, Lott MJ, Ford VL: Tracing the geographical origin of cocaine. *Nature* 2000; 408: 311-312.
46. Ehleringer JR, Cooper DA, Lott MJ, Cook CS: Geo-location of heroin and cocaine by stable isotope ratios. *Forensic Science International* 1999; 106: 27-35.



47. Desage M, Guilluy R, Brazier JL, et al: Gas-chromatography with mass-spectrometry or isotope-ratio mass-spectrometry in studying the geographical origin of Heroin. *Analytica Chimica Acta* 1991; 247: 249-254.
48. Denton TM, Schmidt S, Critchley C, Stewart GR: Natural abundance of stable carbon and nitrogen isotopes in *Cannabis sativa* reflects growth conditions. *Australian Journal Of Plant Physiology* 1991; 28: 1005-1012.
49. Szendrei K: Cannabis as an illicit crop: recent developments in cultivation and product quality. *Bulletin on Narcotics* 1997; 2
50. Multiple Contributors: Eight Peak Index of Mass Spectra. The Royal society of Chemistry, 1986;
51. Gaoni Y, Mechoulam R: The isolation and structure of d1-Tetrahydrocannabinol and other neutral cannabinoids from hashish. *Journal of the American Chemical Society* 1971; 93: 217-224.
52. Camp, P. University of Edinburgh, Department of Chemistry. 2002. Personal Communication
53. Marshman JA, Popham RE, Yawney CD: A note on the cannabinoid content of Jamaican ganja. *Bulletin on Narcotics* 1976; 63-68.





Section 3:

Software.

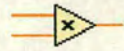


Table of Contents:

Table of Contents:	210
Table of Figures	211
1 Computers in Research	212
2 Programs Written for this Project	212
3 Introduction to LabVIEW	212
4 Programs	215
4.1 Laser Induced Fluorescence Project	215
4.2 Laser Induced Fluorescence or LIF	215
4.3 Experimental setup	216
4.4 Extracting Data	217
4.5 The Pretty Picture Integrator	218
4.6 pretty picture integrator (logan).vi Diagrams	219
5 SCRAM 97 PC Interface	222
6 Dataminer	222
7 Contents of the CD	222
8 Conclusions	223



Table of Figures

Figure 1 - Comparison of similar programs written in BASIC and G, using a simple example.....	213
Figure 2 - Showing front panel and diagram of a simple VI.....	213
Figure 3 - Comparison of BASIC and LabVIEW showing the 3D nature of diagrams when structures are involved.....	214
Figure 4 - Fluorescence diagram.....	216
Figure 5 - Photograph of glass slide containing orthogonal 50 μ m capillaries.	216
Figure 6 - LIF CE experimental setup.....	217
Figure 7 - 3 frames from a recording of a run showing the passing of an analyte band. Approximately 0.5s between shots.....	217
Figure 8 - Screenshot of the Pretty Picture Integrator frontpanel.	219



1 Computers in Research

In modern research, as experiments become more complicated or faster, and the volume of data produced increases, the computers and the software used for experimental control and data processing assume an ever more important role. It is a testament to this inexorable trend that not only have bespoke computer solutions been required to complete both sections of this project, but they have also been required by most of the other workers in the group.

The programs described here have been written using National Instruments LabVIEW[®], and fulfil a role that would have, at the least, been impractical and immensely time consuming to complete by hand; and at the most, impossible.

2 Programs Written for this Project

The following programs were written during this project as an aid to experimental control or subsequent data analysis:

	Program	Associated Section	Use
i)	Picture Integrator	Described below	Post-processes laser induced fluorescence chromatograms.
ii)	SCRAM97 PC Interface	Cement	Shell program for SCRAM97.exe thermodynamic modelling software.
iii)	Dataminer	Cannabis	Data handling and visualisation program.

3 Introduction to LabVIEW

LabVIEW is a computer programming package built around the programming language G; a general purpose programming language. LabVIEW differs from normal text based languages (e.g. BASIC, FORTRAN or C) in that it is a graphical language, where the program appears not as a list of instructions, but as a **diagram**. (See Figure 1). Programs written in LabVIEW are known as “Virtual Instruments” or VI’s.



BASIC	G
<pre> 10 PRINT "Enter X": INPUT X 20 PRINT "Enter Y": INPUT Y 30 PRINT X*Y 40 END </pre>	

Figure 1 - Comparison of similar programs written in BASIC and G, using a simple example.

The diagram is one half of a VI. The other half is the graphical user interface, or GUI, which is called the **front panel**. Normally, the front panel is the only part of a G program that a user would see (See Figure 2).

Front Panel	Diagram

Figure 2 - Showing front panel and diagram of a simple VI.

Another important distinction between G and many other languages is the manner in which it moves through a program. Most text based languages are sequential; i.e. they complete the program from the top, down, initiating each command in turn. G programs run broadly non-sequentially; i.e. they begin from all inputs simultaneously and work towards all outputs. (However, G does have in-built data dependency – i.e. the program will wait at a node until all inputs are filled.) This non-sequentiality of LabVIEW makes it difficult to describe the operations of a program in writing as prose is inherently sequential.

As an added complication, the VI diagrams, the programs, are often too large to be printed out, particularly so when they contain many *if-then-else* (case) structures or other similar structures or loops which appear in diagrams as 3D stacks of frames. For example, imagine a program which asks the user for 2 inputs, X and Y. If X is greater than, or equal to, Y then the program will display the product, otherwise it will display the sum. Two versions of this program are displayed below – once in BASIC and once in G - (See Figure 3).



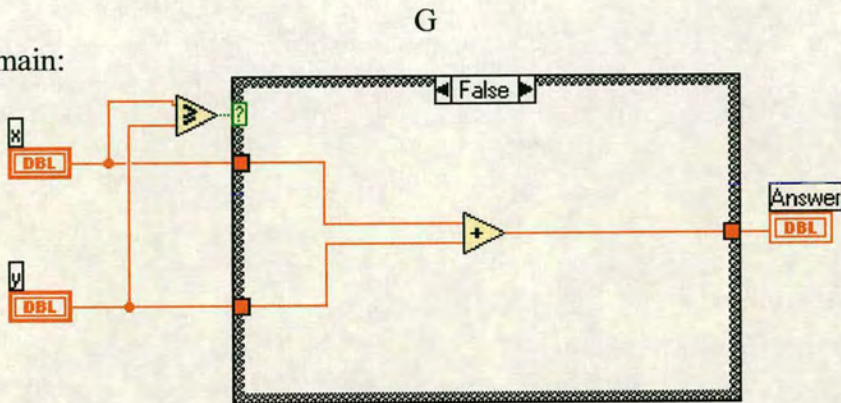
Basic

```

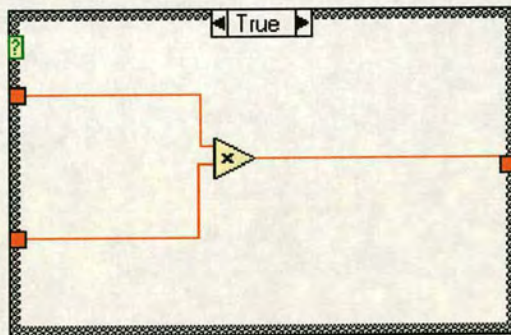
10 PRINT "ENTER X" : INPUT X
20 PRINT "ENTER Y" : INPUT Y
30 IF X>=Y THEN
40PRINT X*Y
50 ELSE
60 PRINT X+Y
70 END

```

Diagram main:



Alternate case structure stack:



This would display vertically above the case structure in the main diagram, on the screen.

Front Panel:

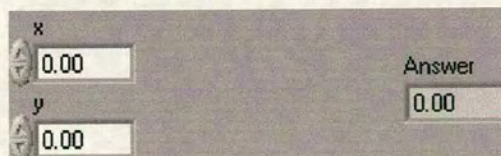


Figure 3 - Comparison of BASIC and LabVIEW showing the 3D nature of diagrams when structures are involved.

The above example (see Figure 3) is fairly simple, but it should be apparent that if two or more structures were nested, it could quickly become difficult to understand the program, when displayed in this way.



It is for these reasons that, although the programs written during this project will be displayed within the sections with which they were used, little description of the actual programmatical machinery will be entered. Instead, the programs will be described from a user's point of view.

4 Programs

This section contains the diagrams of the software packages written during this project.

4.1 Laser Induced Fluorescence Project

The "Pretty Picture Integrator" package had a pivotal role in the project with which it was connected. The aim was to design and build a low cost, reliable Laser Induced Fluorescence (LIF) detector for an on-chip capillary electrophoretic separator.

4.2 Laser Induced Fluorescence or LIF

LIF is the emission of a photon by a molecule, as it relaxes to ground after excitation by a higher energy photon and a small, internal, non-emissive energy loss due to internal rotational or vibrational energy uptake. Because of this internal energy loss, the wavelength of the emitted photon is always longer than that of the absorbed photon.

$$E_a = h \times (c/\lambda_a)$$

&

$$E_e = h \times (c/\lambda_e) \quad [1]$$

where E_a and E_e are the energies of the absorbed and emitted photons respectively and λ_a and λ_e are their wavelengths. (See Figure 4).

Also

$$E_a = E_e + E_i \quad [2]$$

where E_i is the internal, non-radiative loss to rotational or vibrational energy.

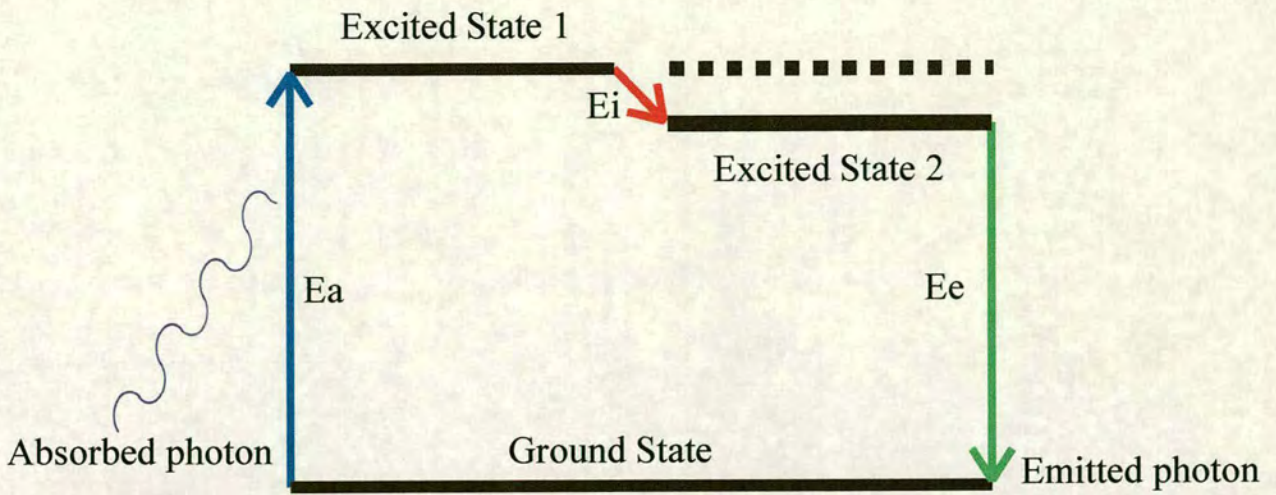


Figure 4 - Fluorescence diagram.

4.3 Experimental setup

The chip (a glass slide containing the capillaries) (see Figure 5) was positioned below a microscope objective (Prior Scientific). The objective carried out the dual task of focusing the laser beam (488nm) onto the capillary and collecting the emitted light.

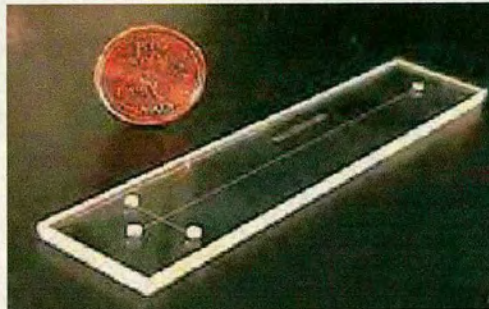


Figure 5 - Photograph of glass slide containing orthogonal 50 μ m capillaries.

The capillary was imaged by a Pulnix PE2015 CCD camera connected to a monitor and a video. A glass filter (Schott, OG550, 3mm thick), between the objective and the camera, filtered the excitation out of the detected signal. (See figure 6).

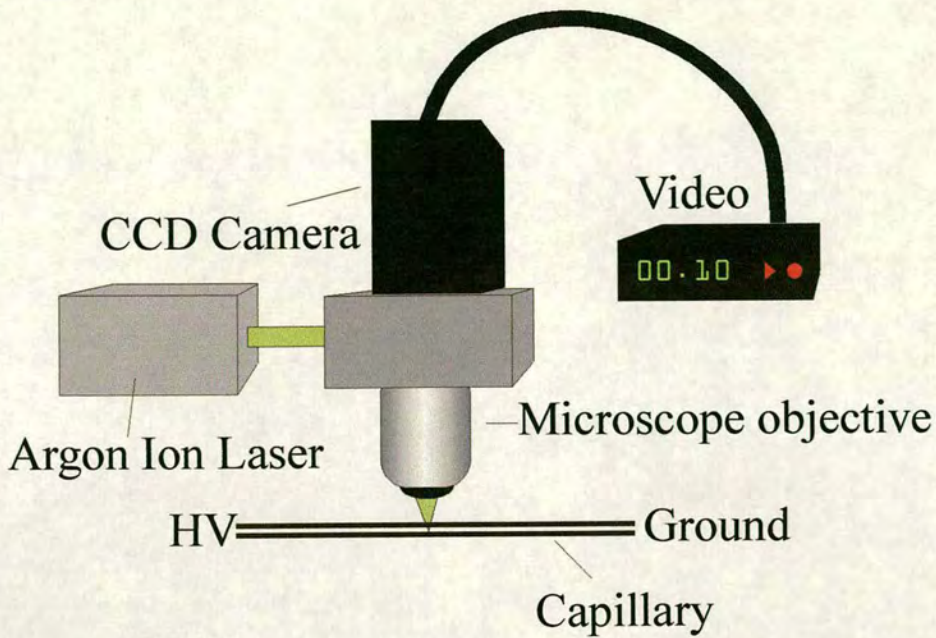


Figure 6 - LIF CE experimental setup.

As analytes containing fluorophors pass through the field of view of the objective and the excitation area, they fluoresce and the emitted light is detected by the CCD camera and recorded onto video. (See Figure 7).

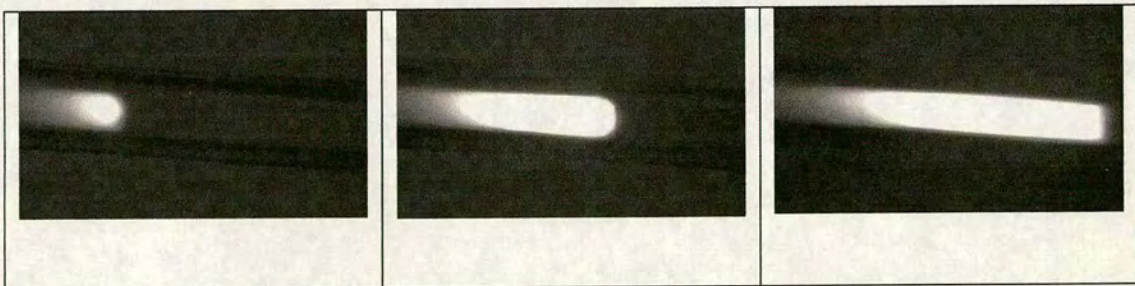


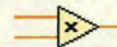
Figure 7 - 3 frames from a recording of a run showing the passing of an analyte band. Approximately 0.5s between shots.

Video was chosen as the recording medium as it is designed for recording large volumes of visual information.

4.4 Extracting Data

It proved relatively simple to record LIF chromatograms onto video, but there was a problem in extracting the data. The Pretty Picture Integrator was written to overcome this hurdle.

First, the video was converted to individual frames and saved onto the computer as sequential bitmap files.



Secondly, these files were analysed by the Pretty Picture Integrator to produce the chromatogram.

4.5 The Pretty Picture Integrator

Upon starting the Pretty Picture Integrator (the name and the interface design were developed in concert with the end user, and hence the author assumes no responsibility for any aesthetic inferences drawn from them) the program asks the user to identify the first of the sequential image files to be identified (using a standard file dialog box). The filename of this image must be comprised of a base name, a sequential number and the file extension.

e.g. **image124.bmp** – “**image**” is the **base name**, “**124**” is the **number in the sequence** and “**.bmp**” is the **extension**.

The filename of the selected image file will appear in the “Identify Base Name” box and the user should remove the numerical and extension sections to leave only the base name. The number of files to be processed should be entered into the “No of files to be read” box and the “Base name identified” button should be clicked (this button begins to blink at the appropriate time to indicate this).

The program now loads the picture files sequentially, starting at the one identified by the user initially and continuing for the required number. For each file, the program records the sum of the intensity information of each pixel and builds a graph of the file position vs. the integrated intensity. This graph is displayed as it is created in the “Progress Chart” box, and in two ways once processing is complete:

- i) Chromatogram – Frame number vs. Amplitude
- ii) Intensity Graph – The same information displayed as Frame Number vs. Intensity where the intensity is displayed visually rather than graphically.

During the processing run, the “No of files to be read” counts down as each frame is processed. The Progress bar follows the progress and each frame is displayed in the “Captured Image” box. (See Figure 8)

Finally, the chromatogram is saved as a spreadsheet readable text file.

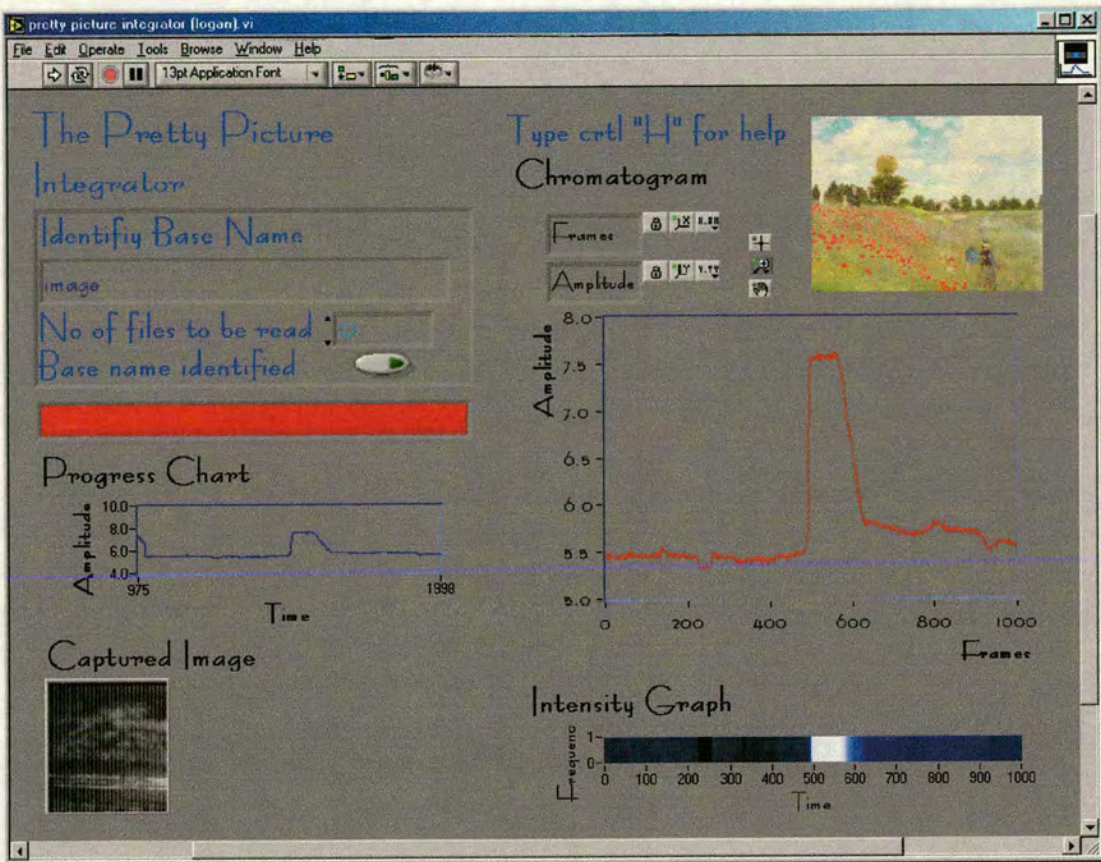


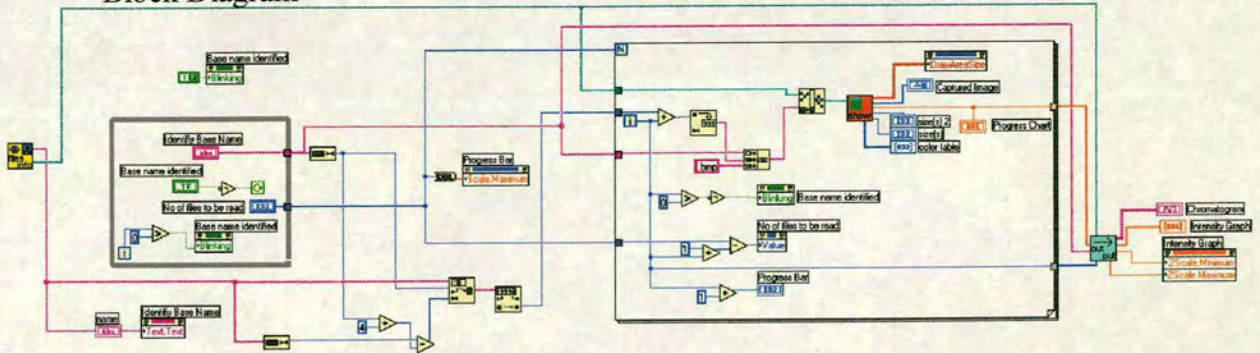
Figure 8 - Screenshot of the Pretty Picture Integrator frontpanel.

4.6 pretty picture integrator (logan).vi Diagrams

Connector Pane



Block Diagram

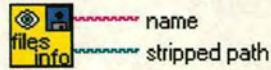




files info.vi

This sub-VI gathers the information on the image files to be processed. It outputs the name of the first image file to be read and the full path of the directory of that file.

Connector Pane



Block Diagram

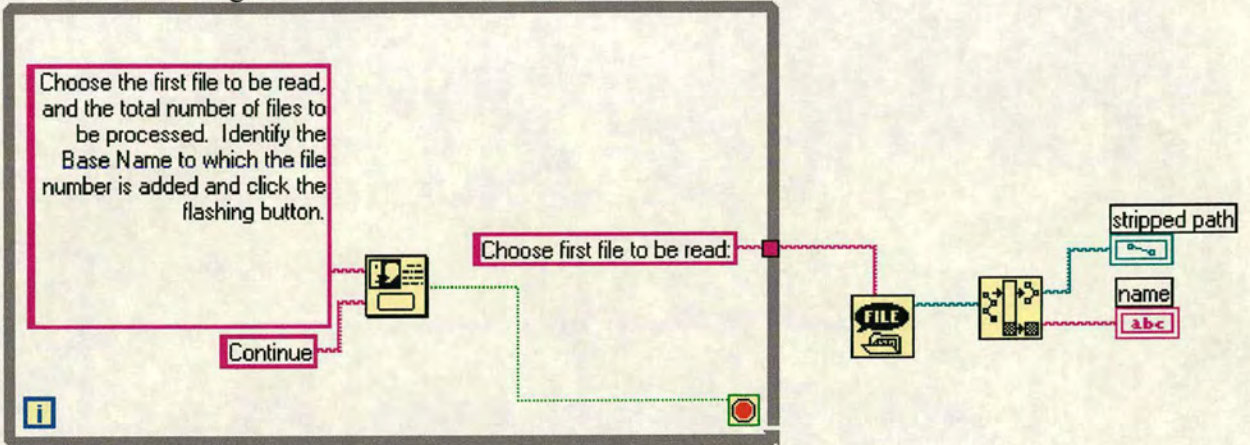
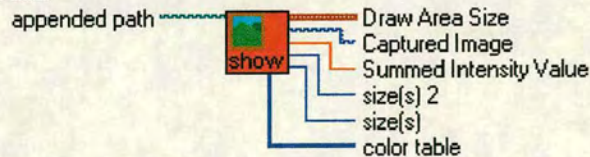


image displayer.vi

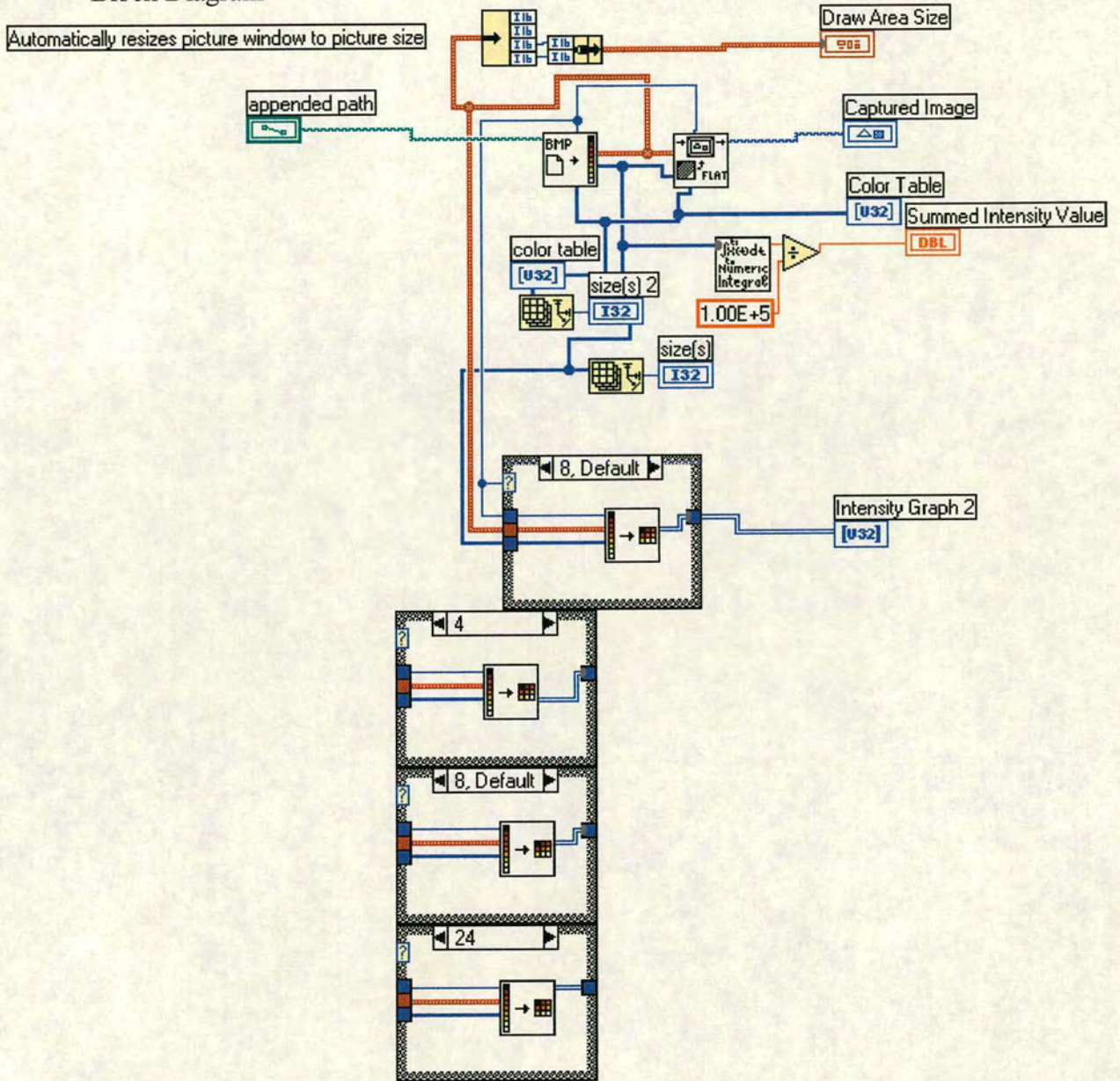
This sub-VI displays the current image file on the main PPI screen. It also sums the intensity of the pixels in the image. This value is used to create the chromatogram the outputs.vi

Connector Pane





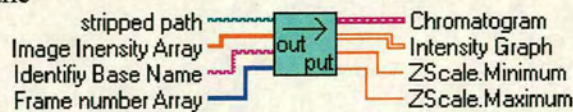
Block Diagram

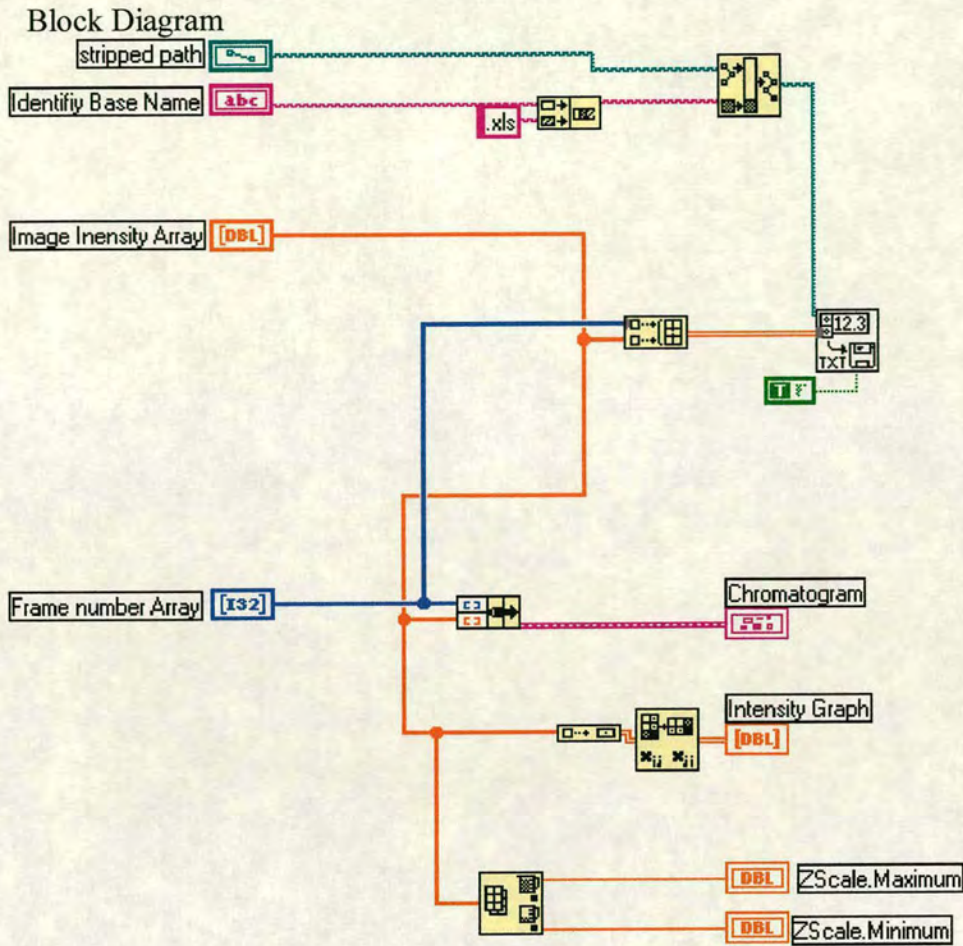
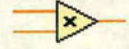


outputs.vi

This sub-VI collates the data to produce the Chromatogram and the Intensity Chart and offers the possibility of saving the chromatogram as a spreadsheet file.

Connector Pane





5 SCRAM 97 PC Interface

This program was completed during the Schlumberger cement research project. The SCRAM 97 PC Interface is described in Section 1 of this thesis, and its documentation is included on the CD.

6 Dataminer

This program was completed as part of the Cannabis analysis project. Dataminer is described in Section 2, and its documentation is also included on the CD.

7 Contents of the CD

The CD contains compiled versions of all three programs with their accompanying datafiles. Additionally, there are copies of the LabVIEW documentation which



contains the diagrams. Finally, there are uncompiled LabVIEW versions of the programs that can be accessed only by a computer that has LabVIEW 6.02, or later, loaded on it.

8 Conclusions

In conclusion, the production of data processing software proved to be an integral and essential part of this project. Without this, the volume of data produced by the projects would have precluded success.

Courses and Conferences Attended

In accordance with the regulations of the Department of Chemistry, University of Edinburgh, I have attended the following courses, conferences, seminars and colloquia:

1. X-ray Diffraction. (Postgraduate lecture course.)
2. Human Computer Interaction.
3. Research Grant Applications.
4. Information Resources - Searching Research Literature.
5. Introduction to Entrepreneurship.
6. Commercialisation & Business Start-up.
7. Twenty-third Meeting of the British Mass Spectrometry Society, Reading, 1999 – Poster presentation.
8. Twenty-fifth Meeting of the British Mass Spectrometry Society, Southampton, 2001 – Poster presentation.
9. Chemistry Departmental Physical Colloquia.
10. Physical Chemistry Seminars.